MODULATION OF ENDOTHELIAL CELL ADHESION TO SYNTHETIC VASCULAR GRAFTS USING BIOTINYLATED FIBRONECTIN IN A DUAL LIGAND PROTEIN SYSTEM

by

Charles Chibuzor Anamelechi
Department of Biomedical Engineering
Duke University

Date_____

Approved:

_____
W. Monty Reichert, Chair

_____
George A. Truskey

_____
Ashutosh Chilkoti

_____
Bruce Klitzman

_____
Marian G. McCord

Dissertation submitted in partial fulfillment of the requirements for the degree of Doctor of Philosophy in the Department of Biomedical Engineering in the Graduate School of Duke University
2008

ABSTRACT

MODULATION OF ENDOTHELIAL CELL ADHESION TO SYNTHETIC VASCULAR GRAFTS USING BIOTINYLATED FIBRONECTIN IN A DUAL LIGAND PROTEIN SYSTEM

by

Charles Chibuzor Anamelechi
Department of Biomedical Engineering
Duke University

Date_____

Approved:

_____
W. Monty Reichert, Chair

_____
George A. Truskey

_____
Ashutosh Chilkoti

_____
Bruce Klitzman

_____
Marian G. McCord

Dissertation submitted in partial fulfillment of the requirements for the degree of Doctor of Philosophy in the Department of Biomedical Engineering in the Graduate School of Duke University
2008

ABSTRACT

Over half a million coronary artery bypass operations are performed annually in the US yielding an annual health care cost of over 16 billion dollars. Only five percent of bypasses are repeat operations in spite of the procedures prevalence. Patients facing repeat coronary artery bypass operations often lack transplantable autologous arteries or veins, necessitating the use of substitutes. Unfortunately, synthetic small diameter vascular grafts have unacceptable patency rates, primarily due to lumenal thrombus formation and intimal thickening. Endothelial cells (EC) mediate the anti-thrombotic activity in healthy blood vessels, and due to the scarcity of suitable autologous vascular replacement, EC-seeded small diameter synthetic vascular grafts represent a clear, immediate, and practical solution. The fundamental goal of this project was to optimize the dual ligand (DL) system on synthetic vascular graft (SVG) surrogates to show enhanced cell adhesion, retention, and native functionality compared to fibronectin alone. Initially, two SVG surrogates were identified through characterization by x-ray photoelectron spectroscopy (XPS), atomic force microscopy (AFM), and ^{125}I radiolabeling. The first modification to the DL system involved direct biotinylation of fibronectin (bFN) as a replacement for co-adsorption of FN with biotinylated bovine serum albumin (bBSA). This was analyzed with a Langmuir model using surface plasmon resonance (SPR) spectroscopy to verify the binding affinity of bFN and ELISA to detect the availability of the RGD binding motif post biotinylation. The second major change in this project examined cell binding and formation of focal adhesion after shifting from direct incubation of HUVECs with RGD-SA to sequentially adsorbing

bFN(9) and RGD-SA prior to introducing unmodified HUVECs. These experiments were conducted under static seeding conditions. Next, dynamic cell seeding onto the sequentially adsorbed protein surface was examined as a function of surface immobilized protein and Trypsin/EDTA concentration. SPR results showed statistical differences in $\alpha_5\beta_1$ and $\alpha_v\beta_3$ integrin binding to RGD cell binding motifs introduced by bFN(9) and RGD-SA. Increase in binding specificity through these integrins lead to rapid cell binding and retention on Teflon-AF surfaces adsorbed with this protein formulation. This system appears to be the nexus at which the DL has proven its value. These results could have broader implications in augmenting EC attachment to SVG prior to implantation.

TABLE OF CONTENTS

LIST OF FIGURES

LIST OF TABLES

ACKNOWLEDGEMENTS

I dedicate this thesis to Gervase and Juliana. Any success that I have is because of you!

I would like to thank my family for their continued support and unwavering belief in me. I extend my sincere gratitude to all those who have helped me through this process either by counsel or by deed. In particular, cheers to my committee for their guidance and support through this process and especially Monty for constantly challenging me to become a better researcher. Thanks to the many fine undergraduate students that have helped usher this project along most notably Miao Wang, Lorenna Lee-Houghton, and Ed Clermont. I am also indebted to the members of the Reichert lab, Truskey lab, Chilkoti lab, Katz lab, "the hallway" people, loose cannons, and all other avocations that were necessarily escapes from lab. As I complete this process, I would like to most graciously thank my dear friends, past and present, whom have been there to support me through the ups and downs of this degree. I am eternally grateful!!

Chapter 1. Research objectives

1.1 Significance of Research

Clinical Impact

Over half a million coronary artery bypass operations are performed annually in the United States according to 2003 estimates generating 209.3 billion dollars in direct healthcare care costs and an additional 94.1 billion dollars in "in-hospital" costs[1]. The replacement vessels of choice are the internal mammary artery and saphenous veins. However, once these replacements fail, the patient often lacks sufficient and suitable autologous options. Unfortunately, small diameter (id <6mm) synthetic vascular grafts (SVG) have unacceptable patency rates, primarily due to lumenal thrombus formation, intimal thickening, and leukocyte adhesion[4]. Endothelial cells (EC) mediate the anti-thrombotic activity in healthy blood vessels, and due to the scarcity of suitable autologous vascular replacement, autologous EC-seeded small diameter synthetic vascular grafts represent an obvious and practical solution to improving SVG blood compatibility[5,6]. However, successfully growing a layer of EC in the lumen of a small diameter graft does not ensure graft patency in humans because of numerous unresolved issues concerning cell seeding efficiency, cell retention under flow, and achieving a quiescent, non-thrombotic phenotype that resists thrombosis, hyperplasia, and leukocyte adhesion[4,7-9].

Research problem

The majority of approaches used to improve vascular graft endothelialization have employed integrin-dependent surface conditioning to strengthen lumenal EC adhesion and retention [10,11]. All of these approaches have been unsuccessful owing to the lack of formation of stable, adherent, and quiescent endothelium in the graft lumen. The hypothesis for this project is that any method to improve *in vitro* endothelialization and formation of mature focal contacts must employ a mechanism that augments the intrinsic integrin binding with higher affinity interactions that (1) increase the rapidity of binding by constraining binding sites, and that (2) in turn facilitates downstream affects that lead to formation of mature focal contacts at a short time point.

Approach

A previously developed "dual ligand" (DL) system that combined high affinity integrin-independent ligands with low affinity integrin-dependent ligands was shown to promote rapid EC attachment and spreading on glass. However, when employed *in vivo* using a rat femoral artery model the results were not consistent with results seen on glass[12]. Possibly *in vitro* testing is a poor predictor of *in vivo* performance and/or glass is a poor substrate for optimizing attachment to synthetic vascular graft (SVG) materials. Addressing the latter issue, this project aims to optimize the DL system using modified protein formulations that better approximate results on SVG surrogates, promote rapid cell binding and formation of mature focal adhesions at short time points, and enhance the amenability of the system to *in vivo* experimentation. Figure 1.1 shows the layout of

the current system compared to standard cell adhesion on grafts using single ligand treatments.

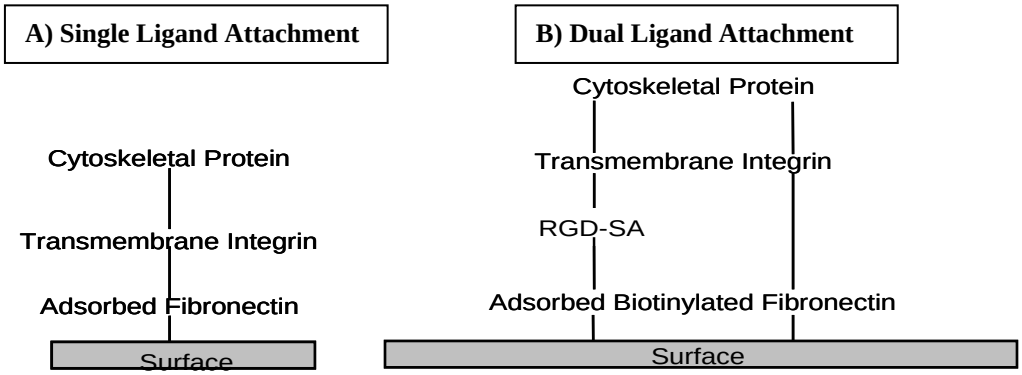

Figure 1.1. Schematic illustration of the linkage for adhesion via single ligand (A) and dual ligand system (B)

1.2 Specific Aims

Specific Aim 1. Validation of Mylar and Teflon-AF as suitable *in vitro* SVG surrogates for studying binding of Human Umbilical Vein Endothelial Cells (HUVECs)

In vitro experiments on glass showed benefits using the dual ligand system to promote firm cell adhesion and biofunctionality. These results were not conserved in initial *in vivo* results[12] leading to the conclusion that glass, though suitable for some approximations, was a poor predictor of *in vivo* performance. The motivation for the current study was that better *in vivo* performance can be achieved by optimizing cell seeding and retention on polymers that better mimic the chemistry of commercial Dacron and Goretex. Dacron and Goretex, due to their opacity and highly textured surfaces, present challenges in *in vitro* experiments. The materials examined for comparison were Mylar, a film version of Dacron, and Teflon-AF, a fluorinated copolymer. First, detailed surface characterization was done by AFM, XPS, and contact angle analysis. Second, protein adsorption and strength of attachment on glass, Mylar, and Teflon-AF was quantified by I^{125} radiolabeling. Last, pilot cell adhesion studies determined the amenability of the current system to standard *in vitro* microscopic techniques

Specific Aim 2. Characterization and Kinetic Analysis of Biotin Functionalized Fibronectin.

The goal of these studies was to characterize the experimental utility of bFN and to determine the effect that varying levels of biotinylation had on binding kinetics. The DL system was modified to include bFN. The hypothesis was that biotinylation of fibronectin would enhance the DL system by elimination of the bulky BSA protein, thus limiting competition for binding sites on the graft surface. The dual ligand system with bFN was characterized by Enzyme Linked Immuno-Sorbent Assay (ELISA) and surface plasmon resonance (SPR) spectroscopy to determine the availability the RGD cell binding motif post biotinylation compared to native protein. Binding kinetics for wild type streptavidin (WT-SA) and mutant streptavidin (RGD-SA) bound to immobilized bFN with levels ranging from 2-21 biotins per FN were measured using a Langmuir model. Fluorescence activated cell sorting (FACS) was used to determine RGD-SA binding specificity to transmembrane integrins. SPR kinetic binding verified that affinity of bound biotin was the same for WT-SA as well as RGD-SA. No improved kinetic effect was observed with increasing biotin levels underscoring the lack of cooperativity in the system. FACS analysis confirmed the specificity of RGD-SA binding to transmembrane integrins. These results highlight the benefit of using biotinylated fibronectin in the dual ligand model.

Specific Aim 3. Sequentially adsorbed bFN(9) with RGD-SA gives enhanced cell functionality over cells incubated with RGD-SA prior to seeding .

Based on results from specific aim 2, these studies used biotinylated fibronectin with 9 biotins per FN (bFN9). This biotinylation level was determined to be the best for cell binding due its high affinity interaction with RGD-SA and due to observed steric effects above this biotinylation level in Specific Aim 2. The goal of this study was to determine the utility of co-adsorbing bFN(9) and RGD-SA on the surface prior to incubation with untreated HUVECS. This analysis involved rate of spreading studies, cell retention studies, and immunohistochemistry. The advantage conferred in cell spreading was demonstrated by comparison to old DL procedure. The modified system formed focal adhesions at short time points as was observed by confocal microscopy. The number of focal adhesions was quantified by LSM software version 4.2.0.121. The strong adhesion strength means that this system can be used to enhance cell adhesion and presents a new strategy for promoting rapid cell attachment and spreading. Biotinylated fibronectin in the DL system also showed enhanced effects in promoting formation of focal contacts over FN alone.

Specific Aim 4. Examination of cell adhesion under dynamic seeding conditions as a function of surface adsorbed protein and Trypsin/EDTA (T/E) concentration.

In these studies, HUVECs in a well mixed solution were seeded onto Teflon-AF surfaces sequentially adsorbed with biotinylated fibronectin and RGD-SA by settling and attachment in a flowing solution at 1ml/min. Attached cells were subsequently subjected to a shear stress of 60 dynes/cm^2. Cells seeded onto the surface were isolated using two

different T/E concentrations to determine the effect of the higher concentration on cell attachment and retention under flow at short time points. Injection of cells at flow rates ranging from 1 ml/min to 40 ml/min examined the effect of injection speed on the ability of the surface to capture cells. Data were corrected for differences in settling distance under different flow conditions. SPR analysis was used to measure the amount of bound integrins to immobilized bFN compared to the co-immobilized DL in an attempt to determine the contribution of $\alpha_5\beta_1$ and $\alpha_v\beta_3$ integrins to cell adhesion. This system was also modeled to numerically quantify the contribution of each experimental parameter.

Chapter 2. Background

2.1Pathology

The lumen of a healthy artery is covered by a smooth and intact layer of endothelial cells that regulate the homeostasis of the vessel. Plaque buildup disrupts this balance by hardening and narrowing the artery walls in a process known as arteriosclerosis. Soft plaque can suddenly rupture causing the formation of thrombus. This thrombus can grow larger and inhibit the flow of blood to a region of the body. When the thrombus is localized in the coronary arteries the condition is known as coronary artery disease (CAD). Coronary artery disease caused 479,305 deaths in the US in 2003 and is the leading cause of death among Americans. This year, an estimated 1.2 million Americans will have a new or recurrent myocardial infarction[1]. About 330,000 people each year die of a sudden heart attack in an emergency department or without being hospitalized. It is estimated that 7.5 million Americans have one form of cardiovascular disease (CVD).

Current techniques to clear obstructed vessels include angioplasty, a combination of angioplasty plus stents, or coronary artery bypass graft surgery (CABG). Coronary artery bypass graft surgery involves connection of one or more vessels from the aorta to the region of the heart distal to the clot (figure 2.1) [1]. Current gold standards for graft replacements, which can be harvested from the patient, include the saphenous veins, the left and right internal mammary arteries, the radial arteries, and the gastroepilectic artery[13].

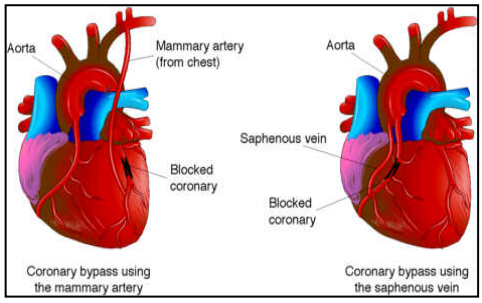

Figure 2.1. Coronary artery bypass graft (CABG) with an internal mammary artery and a saphenous vein graft.

While harvesting of autologous vessels is preferred, these procedures require additional surgery and more trauma to the body. Of all these methods, the saphenous vein is the most widely used, but there are problems associated with it. During the first post-operative year up to 15% of venous grafts occlude. By the tenth year, only 60% of grafts are still patent (figure 2.2)[14].

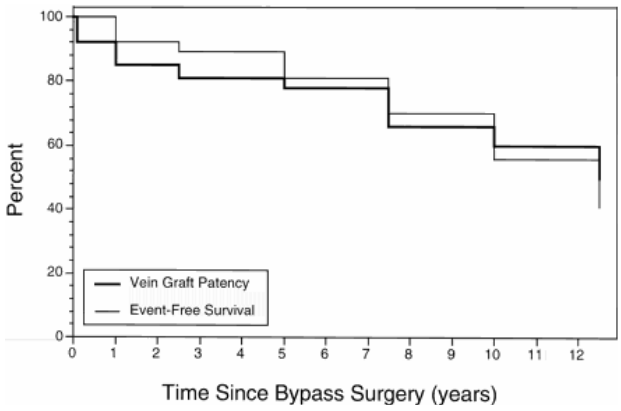

Figure 2.2. Long term graft patency and survival of saphenous vein bypass grafts.

There are several factors that can mitigate or exacerbate the rapidity of occlusion: age, quality of life, personal behavior, ethnicity, or a combination of these risk factors. Re-operative bypass surgery is required in roughly 4% of patients by year 5, 19% of patients by year 10, and 31% of patients by year 12[15]. Patients requiring repeat operations often lack autologous vessels for transplants yielding a need for an "off the shelf" substitute.

2.2 Synthetic Vascular Grafts (SVG)

For many years autologous grafts have remained the most reliable surgical remedy but autologous sources are not always available due to a lack of suitable sources or use in previous procedures[16]. Synthetic vessels have been successfully used in larger diameter vessels (id> 6mm)[17], which are able to tolerate minimal thrombus, but similar successes have not been achieved in small diameter vessels (id <6mm)[18]. The status of this work has been reviewed in the literature by Ballerman et al.[19], Zilla et al.[20], and Nerem and Seliktar[21] to name just a few. The current research has focused on two leading methods to address this problem: (1) tissue engineering of a completely biological graft and (2) synthetic vessels based on polymeric materials[22,23]. Polymeric grafts have been the most thoroughly researched and continue to represent the most active area of study[24] but tissue engineering has seen many success in animal models recently[25].

2.2.1 Tissue-Engineered Grafts

Tissue-engineered grafts attempt to recreate the layered structure of native vessels. Fabrication of these vessels involves the use all cellular/biological components[23] or a combination of a biodegradable polymer scaffold and cells[26]. These systems create 3-

dimensional structures that can better mimic native vessel structure and can mitigate compliance mismatch issues associated with primarily polymer based material. The promise of a tissue engineered graft is attractive because it represents the closest approximation to native vessels in terms of cellular and structural morphology. Current systems attempt to achieve produce a prostheses *in vitro* that resembless native grafts as closely as possible in physical proportion, cellular make-up and mechanical properties that can subsequently be implanted *in vivo*. There are three leading techniques to produce tissue-engineered biological vessels (TEBV): 1. Weinberg and Bell developed the collagen-based blood vessel model. The main advantage of this model is it is composed of a biological scaffold and induces cell-mediated remodeling of the graft[27]. They fabricated an adventitia-like layer made from fibroblasts and collagen, a media-like layer made from smooth muscle cells (SMC) and collagen, and an intima-like endothelial cell (EC) monolayer constructed into a tubular configuration (figure 2.3).

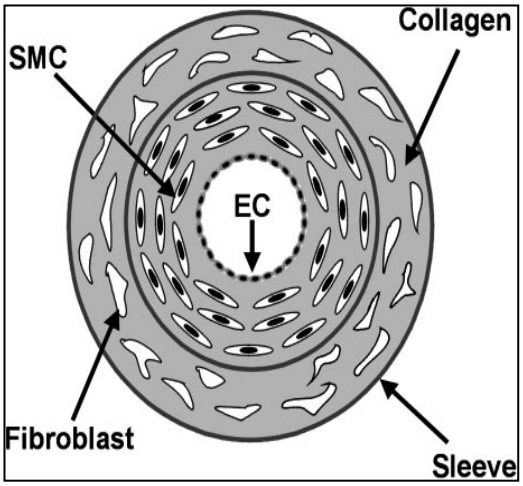

Figure 2.3. Schematic representations of a collagen-based construct. The most general configuration contains an inner monolayer of ECs, a media-like layer with SMCs and collagen, an adventia-like layer with fibroblasts and collagen, and Dacron sleeves for structural reinforcement.

The grafts required support sleeves made from Dacron. Attempts to develop the vessel without the Dacron support lead to low burst strength because the "celluralized" collagen could not withstand the load due to the hemodynamic environment. The main limitation of this approach is the necessity of a synthetic reinforcement which in turn limits the adaptability of the synthetic material to the biological environment.

The cell self-assembly model is made from intact layers of human vascular cells grown to form a sheet of cells and extracellular matrix[23](figure 2.4).

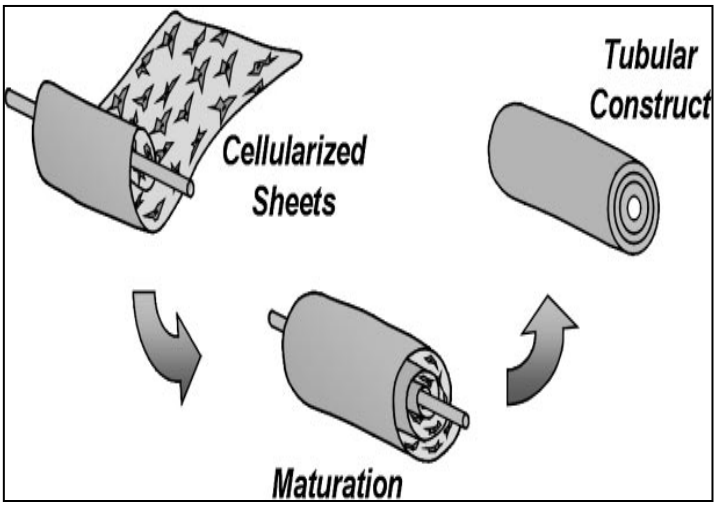

Figure 2.4 Schematic representation of the cell self-assembly model. Vascular cells are cultured to form a continuous sheet of cells and extracellular matrix and then rolled over a central mandrel.

In the initial assembly of the construct, an SMC sheet is rolled over a permeable mandrel to give a tubular structure that mimics the medial layer. A fibroblast layer is rolled over the SMC to create an adventitial layer. The tube is cultured for a period of 8 weeks during which the cells orient themselves in a circumferential manner and deposit abundant amounts of extracellular matrix (ECM). After maturation, human EC are seeded into the lumen to create a neo-intima. These vessels had burst strengths on the same order as

native arteries. This constructs' fabrication eliminates immunological mismatch but long time is an inherent limitation.

The cell-seeded polymeric scaffold approach to TEVG fabrication was pioneered by Niklason et al. [26](figure 2.5).

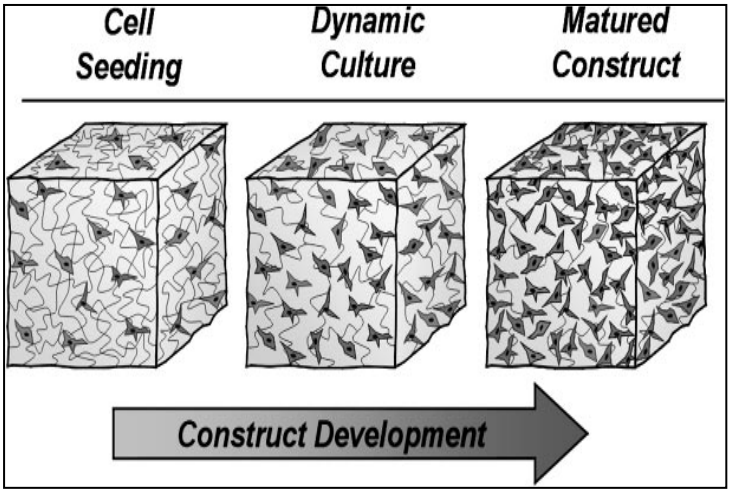

Figure 2.5 Schematic representation of a cell-seeded polymeric scaffold. Vascular cells are cultured on a woven PGA mesh. The construct is matured using dynamic culture, allowing the cells to proliferate and organize ECM as PGA degrades.

Briefly, a biodegradable scaffold, usually a polyglycolic acid (PGA) mesh, is seeded with SMC and cultured for 8 weeks in a bioreactor that produces pulsatile and radial stresses on the constructs vascular cells. After maturation, the constructs are seeded with EC to produce a confluent monolayer. These vessels also exhibited burst strengths on the same order as native arteries. Besides the length of time, another limitation of this system is the high cost needed for the development.

Tissue-engineered grafts are advantageous, because of the ability to control their structural and mechanical properties through modifications in cell seeding densities. They also represent the closest approximation to native vessels in terms of cellular morphology but, due to their extended culture time with autologous cells and lack of proven success in human clinical trials, they are not currently at the point to meet the clinical need for a readily available synthetic vascular graft replacement.

2.2.2 Synthetic Materials

There are three polymers that dominate the SVG market: expanded polytetrafluoroethylene (ePTFE) (www.gore.com), polyethylene terephthalate (Dacron) (www.DuPont.com), and polyurethane (PU). Polyurethane grafts with a Dacron support are commercially available from Corvita. While ePTFE and Dacron remained the only options for many years, PU has recently shown promise in clinical trials as a potential more compliant graft option[4]. ePTFE and Dacron are used regularly while PU is in clinical trial[24]. While these materials are manufactured differently and possess different physical characteristics, they all lack biocompatibility due to their hydrophobicity and their crystalline nature which prevent hydrolysis[28]. As will be discussed, some biodegradation issues exist with PU; these hurdles have been overcome to some degree through chemical modification of the material.

expanded Polytetrafluoroethylene (ePTFE)

ePTFE or Teflon, was first introduced as an artificial heart valve and then made microporous by extrusion to form ePTFE. The fluorocarbon is highly crystalline with a stiffness of 0.5 GPa, and a tensile strength of 14.0 MPa. ePTFE has a node-fibril structure with an internodal distance of roughly 30μm for the most popular surgical grade (figure 2.6).

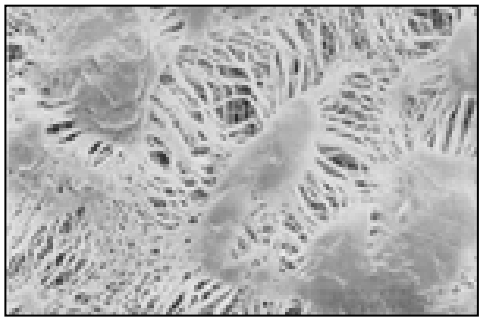

Figure 2.6. SEM image of a Goretex graft.
The porosity ranges from 30μm to 120μm.

Graft construction is achieved by stretching a PTFE tube to generate the porous structure. ePTFE is non-degradable and its purely fluorocarbon chemical composition (figure 2.7) provides an electronegative surface that prevents reaction with blood components, therefore imparting biocompatibility and reduced thrombogenicity to the inner surface[28].

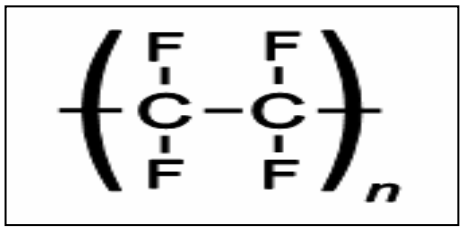

Figure 2.7. Monomer repeat of ePTFE.

Increasing porosity of the graft has been explored as a means through which tissue in-growth can be increased and subsequent transmural capillary in-growth can provide the cell source for endothelialization. While an increase in porosity of up to 90μm showed increased tissue in-growth and EC adhesion in animal studies, this was not seen in human trials[28].

Dacron

Dacron is a polyethylene terephthalate based graft. The grafts come in two forms, knitted and woven (figure 2.8).

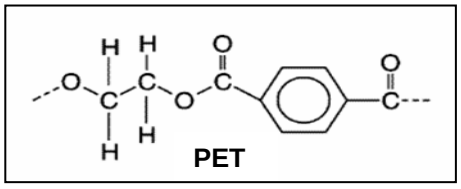

Figure 2.8. Chemical repeat unit of Dacron.

Knitted grafts possess a great deal of porosity and some radial flexibility which contributes to its compliance (figure 2.9) as opposed to woven grafts which possess very little of either.

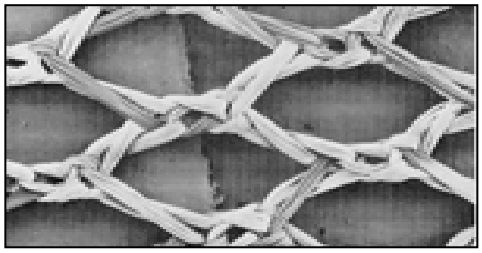

Figure 2.9. SEM of Dacron woven mesh

Despite the differences between the types of Dacron grafts, there is no major difference in the clinical patency rates between the two[29]. However, due to large pore size, grafts need to be preclotted with albumin, gelatin, or blood prior to usage to mitigate seepage, especially at high shear levels in the aorta[30]. Dacron can persist for over 10 years with good stability but knitted versions of the graft are prone to dilatation in arterial prosthesis[28]. In addition, no significant difference in patency rates in small diameter grafts has been noticed in clinical trials with Dacron and ePTFE[28].

Polyurethane

Polyurethane is a copolymer consisting of a diisocyanate derived hard domain, a main chain, containing several urethane -NH(CO)O- groups, and a soft domain that is most often a polyol (figure 2.10).

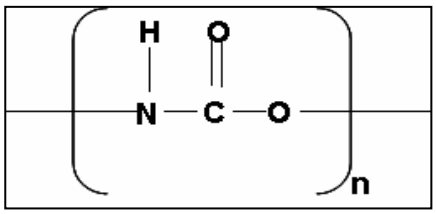

Figure 2.10. Chemical repeat unit of polyurethane.

Depending on the percentage of the individual components, tensile strength ranges between 20 MPa and 90 MPa with a tensile modulus of 5 MPa to 1150 MPa. The mixture of different material properties combine to give PU mechanical compliance (figure 2.11) and also the ability to vary flexibility and rigidity of the graft[31].

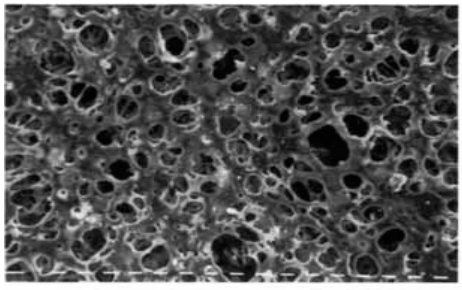

Figure 2.11. SEM of compliant polyurethane (CPU)[2,3]

Among the polymeric grafts currently in use, polyurethane (PU) grafts provide the greatest potential as a compliant graft material[32], but issues exist with their susceptibility to biodegradation[33]. While it has not been definitively proven, it is widely accepted that

compliance mismatch is a factor that disrupts flow and in turn promotes neointimal hyperplasia. When clinical patency rates were compared against viscoelastic properties it was found that patency differed by 35% between compliant grafts, including human saphenous vein and gluteraldehyde-treated umbilical cord vein, and non-compliant grafts, including Dacron and ePTFE[34]. This trend has been supported *in vivo* in dogs through the treatment of autologous carotid arteries with varying amounts of gluteraldehyde which was used to vary compliance[35]. While its compliance makes it ideal to mitigate hyperplasia, and SMC proliferation generated by turbulent flow at the anastomosis site, its tendency to be oxidatively degraded has limited the wide usage of these grafts[4]. Current PU grafts are being developed to circumvent these issues. New generations of PU grafts are polycarbonate based. This reduces the ether linkages and makes the graft more hydrolytically and oxidatively stable and more resistant to biodegradation. While PU has great mechanical properties not enough clinical successes have occurred to date to supplant Dacron and ePTFE as the first options for SVG materials[28].

All these materials, however, still lack *in vivo* patency owing to their hydrophobicity, mechanical incompliance, and post-implant biodegradation[28]. This results in thrombus formation and SMC proliferation which can lead to intimal thickening and occlusion of the graft. Neointimal hyperplasia is also a major contributor to the failure of synthetic vascular grafts. Hyperplasia results from the vascular trauma associated with graft implantation which sets off a signaling cascade that results in SMC proliferation and neointimal wall thickening. This occurs primarily at the site of anastomoses. There is considerable research to indicate that this process can be mitigated

by endothelialization of the graft surface. The end result of this process is complete coverage of the graft surface by endothelial cells that will behave in a manner similar to native endothelium. This was first attempted in 1978 by Herring et al.[36]. These polymers are poor substrates for endothelial cells necessitating the need for surface treatments prior to endothelial cell incubation.

2.2.3. Methods to Improve Graft Biocompatibility

Chemical Graft Surface Modification

Formation of neointima *in vitro* can be achieved by direct modification of the graft by coating the surface with an inert synthetic material or adsorption of ECM)proteins[37,38]. Denucleation removes trapped air that can denature plasma proteins at the air-gas interface which leads to thrombus formation[39]. ePTFE has been found to contain between 61.8% and 75.5% air by volume depending on the manufacturer[39,40]. Techniques for achieving denucleation include treatment with acetone or ethanol[39] and saline treatment followed by exposure to hydrostatic pressure[39,41,42]. These methods have been shown to decrease thrombogenicity and increase patency *in vivo* in rats. Denucleated vessels have shown increased patency in small animal models[41].

Plasma

Plasma irradiation adds charged groups to the surface of the graft material to improve EC attachment or adsorption of ECM proteins [43-45]. In glow discharge, electrons are shot into gases, causing them to ionize into positively charged groups which become

imbedded on the graft surface. These gases can include ammonia[45], argon, nitrogen[46,47], oxygen[46,48] and hydrogen [47]. These charged groups decrease the hydrophobicity of the surface increasing EC attachment and adhesion of serum proteins.

Other synthetic coatings have been used on SVG to increase EC adhesion and decrease thrombus formation. Carbon coating is used to increase surface electronegativity in order to diminish thrombus formation. Vapor deposition of pyrolitic carbon was used to make the graft more chemically benign yielding reduced protein adsorption[49], argon plasma grafted L-lactide not only enhanced EC adhesion but decreased platelet adhesion[50], and cast films of Fluoropassive reduced inflammation and thrombus formation of Dacron grafts[51].

Anticoagulants and Growth Factors

Blood plasma agents have also been successfully used to enhance EC adhesion. Albumin promotes EC adhesion to polymeric surfaces[52] but it's also commonly used as a carrier for growth factors. Albumin has been used with vascular endothelial growth factor (VEGF) and basic fibroblast growth factor (bFGF) to enhance EC proliferation and migration[53,54]. Both stimulate EC proliferation and migration and thus they are ideal for use in aiding in the endothelialization of synthetic vascular grafts [55,56].

Stone et al. used VEGF covalently linked to bovine serum albumin to stimulate proliferation and migration of ECs [53]. They used migration assays to determine how albumin linkage modulated the effect of VEGF on EC migration. Albumin-bound VEGF, in fact, had a greater effect on migration than did unbound VEGF. They also found that bound VEGF had a greater effect on proliferation as well as increased EC adhesion as measured through absorbance of the EC solution. These findings show that growth factors can improve chemotactic function and promote cell movement when bound to proteins which can be adsorbed to graft surfaces.

Bos et al. have conducted similar studies with bFGF that have gone into more depth in relation to the synthetic vascular graft applications[57,58]. They have examined the use of crosslinked albumin-heparin gels with just immobilized bFGF as well as ones to which fibronectin was adsorbed. Heparin is a molecule in the ECM that provides structural rigidity. In both studies they used polystyrene polymers, modified through CO_2 plasma treatment onto which crosslinked albumin-heparin gel was coated. bFGF was then immobilized through washing with a solution of bFGF in phosphate buffered saline

(PBS). Optimal results were obtained when all of these elements were present in the gel and that EC proliferation decreased when any one of them was removed. While the presence of heparin increased platelet adsorption, the effect of the concomitant increase in endothelialization that occurred in its presence far outweighed the negative effect of platelet adsorption. These techniques show promise as a possible coating method for the improvement of EC seeding.

Gelatin, like albumin, is used to generate a non-interactive surface but its best utility is as a carrier for other vasoactive agents, primarily anticoagulants or growth factors [59,60]. Heparin and hirudin immobilized with albumin, gelatin, fibrin glue, growth factors, cell adhesion molecules, and *in situ* chemical hybridization techniques [61-64 65] onto graft surfaces mitigate SMC proliferation and intimal hyperplasia.

There are commercially available heparin bound grafts. A heparin-bonded Dacron graft by InterVascular (LaCiotat, France) is currently available on the European market. The heparin is bound through Van der Waals forces after pretreatment of the graft with tridodecil-methyl-ammonium chloride (TdMAC)[66]. Heparin bound ePTFE grafts demonstrated reduced thrombogenicity and improved patency rates at 8 weeks compared with the standard graft in the rat infrarenal aortic position [67]. The heparin is continuously released from the graft surface after implantation. Various other bioactive substances have been integrated onto SVG by various delivery vehicles to modulate graft healing and biocompatibility. Fibrin glue (FG) was used for delivery of growth factors onto ePTFE grafts. The enmeshed growth factors are released from the glue *in vivo* while maintaining their bioactivity. ePTFE grafts impregnated with FG containing fibroblast

growth factor FGF-1 and heparin that were implanted into canine bypass graft models elicited greater endothelialization and tissue incorporation than untreated or FG/heparin (no FGF) treated grafts[68,69]. Many growth factors, such as FGF-2, platelet derived growth factor (PDGF), and vascular endothelial growth factor, have been grafted to graft surfaces using similar grafting techniques[53,70].

2.2.3 In Vitro Endothelialization

Graft materials currently in use are inherently thrombogenic and while the high flow conditions of larger diameter grafts prevent occlusion, low flow conditions that occur in small-diameter grafts promote thrombus formation and SMC proliferation leading to intimal thickening and occlusion of small vessels. Lumenal seeding of small diameter synthetic vascular grafts to produce a confluent monolayer of EC is a long sought solution to improving their *in vivo* patency[5,71]. This is because intact endothelium, the lining of all the natural blood vessels: (1) provides a structural barrier between the circulation and the surrounding tissue, (2) secretes vasodilators and vasoconstrictors which regulate vascular hemodynamics and vascular tone, (3) presents an active anti-thrombogenic surface that inhibits platelet adhesion and clotting and promotes fibrinolysis, and (4) expresses receptors and mediators that regulate the interaction of circulating leukocytes with the vessel lumen[5,72].

The greatest benefit from the generation of an intact neo-intima is to confer similar homeostasis characteristics as the endothelium to the *in vitro* seeded vessel. The biochemical activity of the neo-intima plays a pivotal role in successful treatment of

cardiovascular disorders, and ultimately in the successful endothelialization of cardiovascular implants [73]. Endothelial cells in the lumen of vessels express numerous anti-thrombotic factors that inhibit platelet adhesion/aggregation, inhibit fibrin formation, and promote fibrinolysis [72]. Platelet aggregation is prevented by production of prostacyclin (PGI_2). Nitric oxide (NO), a powerful vasodilator released by EC, also inhibits platelet adhesion, leukocyte aggregation, and limits neointimal thickening by inhibiting smooth muscle cell migration and proliferation. Thrombin, the active form of circulating prothrombin, cleaves fibrinogen to form fibrin, and promotes platelet aggregation. Thrombin activity is inhibited by binding to antithrombin III (AT III), which is catalyzed by heparin sulfate at the surface of EC, or to thrombomodulin expressed on the EC surface. Thrombomodulin-bound thrombin activates protein C, which is an inhibitor of factors preceding thrombin in the coagulation cascade. Activated protein C has been suggested to be a physiological feedback mechanism limiting thrombin coagulant activity to the site of a vessel wall injury. Tissue plasminogen activator (tPA) converts plasminogen to plasmin, which in turn converts fibrin to soluble degradation products. Elevated tPA inhibitor (PAI-1) causes impaired fibrinolytic function. Expression of tissue factor (TF) by perturbed EC dramatically accelerates the activation of factors X and XI in the coagulation cascade. Vascular endothelial injury stimulates the release of endothelins (ET), which activate macrophages, act as strong chemo-attractants for circulating monocytes, and have potent vasoconstriction activity[72].

Graft endothelialization can be accomplished two ways: pre-seeding and post-seeding. Pre-seeding requires the *in vitro* seeding of grafts prior to implantation; the goal

being to develop a neointima *in vitro*. Pre-seeding can be separated into two categories: single-stage seeding and two-stage seeding. Single-stage seeding involves the autologous cell isolation, immediate seeding onto graft surface, and subsequent implantation [24]. This is desirable for patients requiring an emergency procedure but there are issues with isolating enough cells to completely endothelialize the entire graft [20,74]. Two-stage seeding, however, involves the isolation of ECs and their expansion in culture for weeks [24]. The ECs are isolated with a protease or by scraping. The cells are seeded onto the graft prior to implantation. This technique produces more cells and is a better method for achieving total surface coverage prior to implantation [17]. The ideal system would use the single-stage seeding method. Post-seeding requires attachment of circulating ECs after graft implantation[24,75]. This method is ineffective in humans, because it relies on spontaneous or "fall-out endothelialization", which occurs in other animals, but not in humans[76].

Biological Coatings

Endothelial cells, in the absence of exogenous ECM protein, will secrete their own proteins over time to facilitate spreading. However, the availability of an exogenous protein source adsorbed to the biomaterial prior to EC incubation can increase rapidity of binding and spreading and ultimately lead to faster formation of focal contacts and confer a phenotype more resistant to shear stress [77]. Adsorbed proteins are present in the layer between the cell membrane and surface and act as anchorage points for the cell to the material surface. The majority of approaches used to improve vascular graft

endothelialization have employed solely integrin-dependent ligand models to strengthen lumenal EC adhesion and retention[10]. Of these models, fibronectin has been the most extensively studied [74,78,79]. Other extracellular matrix (ECM) proteins have been used as well, such as laminin, collagen, and mixtures of the different ECM proteins[80-82]. Additionally, grafting of peptide sequences such as RGD (Arg-Gly-Asp) and YIGSR (Tyr-IIe-Gly-Ser-Arg) to vascular graft surfaces can be done with crosslinkers as an alternative to whole protein adhesion[83,84]. Common crosslinkers and biological adhesion promoters used are glutaraldehyde, carbodiimide and succinimidyl chemistries[85], polyethylene oxide[62].

Peptide Coatings

A great deal of research has focused on coating of the graft surface with various peptide sequences such as RGD of fibronectin and YIGSR of laminin. Other sequences that have been studied to a lesser extent include CREDV (Cys-Arg-Glu-Asp-Val) and CCRRGDWLC (Cys-Cys-Arg-Arg-Gly-Asp-Trp-Leu-Cys) [77]. These peptide sequences were selected based on their ability to support cell adhesion as a result of binding to transmembrane integrins on vascular endothelial cells. These sequences are generally attached to the surface being examined, which has ranged from glass to more biomedically applicable materials such as ePTFE or Dacron. Binding occurs through their amino-termini to a hydroxyl group or similar nucleophilic group [86]. Such groups have been found to increase cell spreading and adhesion on surfaces through integrin-mediated binding interactions with ECs. These results have been comparable to these

types of interactions found with traditionally used EC binding proteins such vitronectin, laminin, and fibronectin[87].

Fibronectin

Fibronectin is a 450kD glycoprotein that couples the ECM of cells to the cytoskeleton using transmembrane integrins. It is not only found in the ECM, but also in the blood plasma at a concentration of about 300 μg/ml. The structure of the protein consists of two dimers covalently linked by two disulfide bonds found near the C-termini of each monomeric unit. In addition, each monomer is composed of homologous repeating structural components called type I, II, and III which group together into functional domains with specific biological activity[88] (figure 2.12).

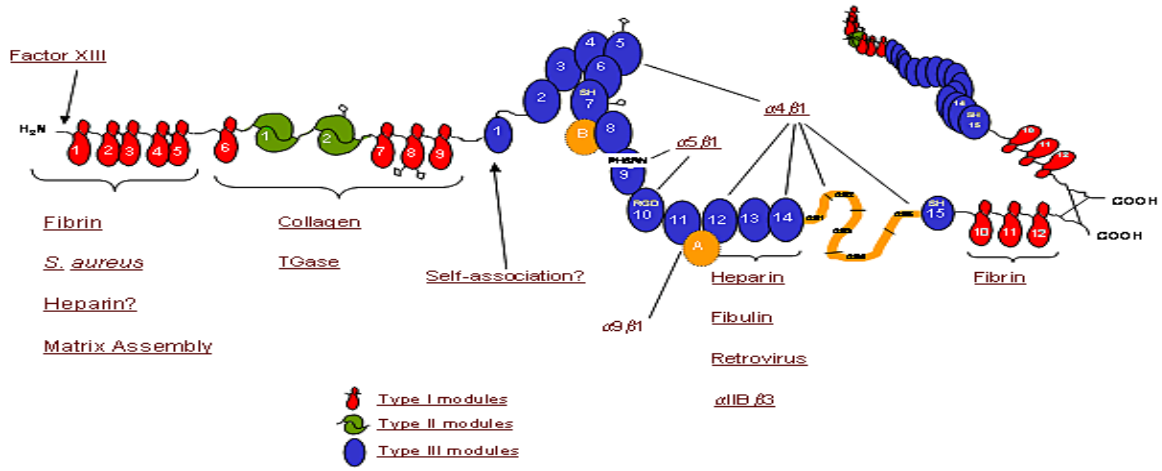

Figure 2.12. Domain structure of fibronectin. Fibronectin is a multimodular protein composed of these 3 structural motifs. The dimer is formed by two interchain disulfide bonds at the c-termini. FN main binding domains are highlighted above.

Fibronectin exists as a soluble dimer in blood and in fibrillar form in the ECM. It is this fibrillar FN that is responsible for most of the proteins biological activity including cell attachment and proliferation[89,90].

Fibronectin contains many cell recognition sites; the most widely studied and understood being the RGD peptide sequence which is recognized primarily by the $\alpha_5\beta_1$ and $\alpha_v\beta_3$ integrin receptors. This site is located on the $FNIII_{10}$ and specificity and strength of binding is enhanced over 40-fold by its synergy site located on $FNIII_9$ [91]. The integrin $\alpha_v\beta_3$ binds directly to RGD without need for the synergy site but binding by $\alpha_5\beta_1$ requires

the use of this site. We have evidence to suggest that this interaction is exploited by new changes made to the dual ligand system. Binding of RGD and its synergy site initiates downstream intracellular signaling events that are not seen with other ECM proteins [88].

When fibronectin binds to 1 of the 24 transmembrane integrin heterodimers, activation is initiated through the cytoplasmic tail. The conformational changes and the concomitant increase in binding affinity are due to clustering of integrins into focal adhesion complexes[92]. These structures occur simultaneously with actin polymerization into stress fibers that provide a mechanical link between the cell and the substrate[93]. Integrins mediate signaling from the extracellular space into the cell via adaptor molecules such as focal adhesion kinase (FAK), integrin-linked kinase (ILK), particularly interesting new cysteine-histidine rich protein (PINCH) and non-catalytic (region of) tyrosine kinase adaptor protein 2 (Nck2). Activated pathways signal a variety of processes including survival/apoptosis, proliferation, cell-cycle progression, cell shape, polarity, adhesion, migration and differentiation[94 95]. Dynamic remodeling of the adhesions at the cell-surface transduce shear stress at the onset of flow (figure 2.13).

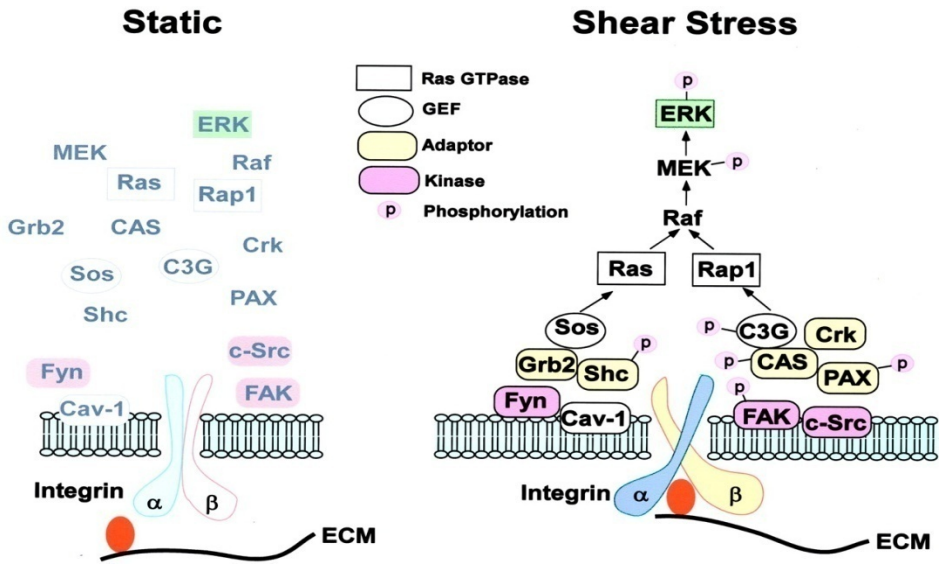

Figure 2.13. Under static conditions, the mechanosensitive integrins are in an inactive conformation, and various signaling molecules are not phosphorylated or assembled as signaling complex. Shear stress activates the integrins by switching them to an active conformation, with increases in their affinity and avidity for the cognate ECM proteins. The red ovals represent the ECM binding site for integrins.

Integrin-mediated mechanotransduction includes multiple kinases (eg, FAK, c-Src, and Fyn), adaptor molecules (eg, CAS and Shc), guanine nucleotide exchange factors (GEFs) (eg, C3G and son of sevenless [Sos]), and small GTPases (eg, Rap1 and Ras) in activating MAPKs (eg, ERK). Through specific interaction of the [alpha] and [beta] subunits of the activated integrins, the FAK/c-Src and the Cav-1/Fyn pathways are activated to elicit cascades of phosphorylation on various downstream effectors and their assembly through SH2 and SH3 interactions. The 2 pathways converge at the level of

Raf-MEK-ERK in ECs in response to shear stress. MEK indicates MAPK kinase; PAX, paxillin; and CAS, $p130^{CAS}$.

Deposition of FN onto synthetic vascular graft substrates has been necessary for proliferation under the two-stage seeding model[96]. Fibronectin has been proven to not only improve EC binding and spreading but also to enhance the strength of adhesion after the onset of blood flow[11,97]. This strength of attachment is dependent on conformation of the adsorbed protein and surface concentration of protein used[98]. Wigod and Klitzman showed that endothelial cell retention was significantly increased when fibronectin was bound to ePTFE grafted with the cationic surfactant tridodecylmethylammonium chloride[99]. The main drawback with using fibronectin, in addition to the other extracellular matrix proteins, is that they promote platelet adhesion at denuded points on the graft surface. This issue underscores the necessity for a protein system that can produce complete endothelial coverage in vitro.

Cocktail Methods

So called "cocktail methods" involve the use of multiple adhesive proteins to mediate EC adhesion. When the adhesive properties of these proteins were first being explored, several different combinations were tested. Unfortunately there is much discrepancy in these results. Anderson et al. reported that coating with combinations of laminin and fibronectin or collagen resulted in inferior EC attachment at cell saturation conditions compared to fibronectin or collagen individually[100]. They also observed that collagen and fibronectin coating resulted in slightly better EC attachment than either

individually; however, this result was not significantly different than collagen alone. Individually, they found collagen to be more effective than fibronectin, both of which were more effective than laminin. In contrast to these results, Li et al. found fibronectin to aid in EC adhesion to a greater degree than type I collagen and their combination to have an effect in between the two[101].

Kaehler et al. tested a wide variety of different combinations including collagen types I and IV with fibronectin or laminin[102]. They found that collagen I with fibronectin aided the most in EC adhesion, followed by collagen I with laminin. Collagen types I and IV in conjuction with fibronectin or laminin performed the worst. The singular proteins fell in between these two extremes. It is difficult to draw any conclusions due to the variability in the results, the inconsistencies of which can most likely be attributed to variations in protein sources and protein coating, EC seeding and incubation procedures. Due to failures of individual protein coatings to aid in producing a confluent EC layer on SVGs, successful methods will most likely stem from the fusion of multiple approaches. The dual ligand (DL) approach, discussed below, aims to exploit multiple protein functionalities to increase EC binding and retention on SVG at short times[103].

All of these approaches have been unsuccessful owing to the lack of rapid and firm initial cell attachment necessary to nucleate the formation of stable, adherent, and quiescent endothelium in the graft lumen. Recently, we reported a dual ligand approach to enhance endothelial cell attachment and spreading on vascular graft materials[104]. This technique combines high affinity integrin-independent ligands with low affinity integrin-dependent ligands to promote rapid EC attachment and spreading. The high affinity

avidin-biotin linkages bring the cell membrane in close apposition to the pre-coated surface, thus facilitating faster integrin-fibronectin linkages that lead to downstream signaling that promotes faster cell spreading and firm attachment[103]. The resulting formation of firm focal contacts is intended to increase EC retention on vascular grafts and lead to improved patency. The impetus for creating the dual ligand system was to circumvent issues with adhesion using a primarily integrin dependent single protein system[78]. This novel system was refined by the introduction of RGD-streptavidin (RGD-SA)[105]. The streptavidin mutant, RGD-SA, bridges the cell and the substrate by binding to the EC membrane via integrin receptors and to biotinylated bovine serum albumin (bBSA) on the surface. The dual ligand system has three proteins: RGD-streptavidin mutant (RGD-SA) bound to integrin receptors prior to EC seeding, and a surface conditioning film of sequentially adsorbed human fibronectin (FN) and biotinylated bovine serum albumin (b-BSA). RGD-SA not only eliminated the need for EC biotinylation, but also appears to potentiate focal contact formation, actin filament polymerization, and release of anti-thrombotic mediators[105]. All *in vitro* optimizations were done on glass. The current system simplifies the model by direct biotinylation of FN thus eliminating bBSA and also by optimizing cell functionality on SVG surrogates. The current formulation utilizes two bifunctional peptides: RGD-SA binds specifically to surface integrins while binding with high affinity to biotins on fibronectin. These additional binding sites can lead to rapid cell attachment and improved retention under flow.

2.3 Outline of Experiments

Results seen with the dual ligand system on glass were not conserved in *in vivo* experiments[12]. The first goal of this project was to identify surfaces that would better approximate *in vivo* behavior of SVG (Chapter 3). Attempts to use the same set up on Teflon-AF™ were unsuccessful; in fact the data indicated that the DL, with the current application, was similar to fibronectin in cell binding as well as cell retention under flow[104,106]. Second change from the original DL was direct biotinylation of fibronectin to eliminate the bovine serum albumin, which Grainger et al. showed to out-compete fibronectin for binding sites on fluorinated surfaces[107]. Elimination of the xenogeneic protein source also made this system more amenable to future animal experiments (Chapter 4). Using the biotin functionalized fibronectin with co-incubation of HUVEC with RGD-SA gave no discernable and repeatable enhancements over fibronectin alone. The thought was that the incubation time was too long for the protein to still be active on the surface given the dynamic nature of the cell membrane. Schraa et al. have shown that transmembrane integrin get recycled often and also internalize bound surface proteins[108]. In addition, our data suggests that RGD-SA was occupying integrin sites on the cell surface, and thus handicapping the natural cell binding mechanism. The final shift was then to incubate the surface sequentially with biotinylated fibronectin then RGD-SA (Chapter 5). This model proved to give enhanced cell adhesion and retention at short seeding times, dynamic seeding conditions, and under harsher T/E levels (Chapter 6). This formulation appears to be the nexus at which the DL has proven its value.

Chapter 3. Validation of Mylar and Teflon-AF as suitable *in vitro* SVG surrogates for studying binding of Human Umbilical Vein Endothelial Cells (HUVECs)

3.1 Synopsis

The textured and opaque nature of Dacron™ and ePTFE has prevented the use of these fabrics in conventional cell culture techniques normally employed to optimize cell attachment and retention. This lack of optimization has led, in part, to the poor performance of endothelialization strategies for improving vascular graft patency. Here we show that thin, transparent films of Mylar™ and Teflon-AF™ are viable *in vitro* cell culture mimics of Dacron™ and ePTFE vascular graft materials, particularly for the study of protein mediated endothelial cell (EC) attachment, spreading and adhesion. Glass substrates were used as controls. Stark differences in surface texture were evident on Atomic Force Microscopy Scans. X-ray photoelectron spectroscopy (XPS) and contact angle analysis showed that Mylar™ and Teflon-AF™ have surface chemistries that closely match Dacron™ and ePTFE. ^{125}I radiolabeling and sonication were used to quantify adsorption and desorption of fibronectin (FN), and FN combined with biotinylated-BSA "dual ligand" co-adsorption onto glass, Mylar™ and Teflon-AF™ substrates. Native human umbilical vein endothelial cells (HUVEC) and streptavidin-incubated biotinylated-HUVEC (SA-b-HUVEC) spreading was measured using phase contrast microscopy. All surfaces lacking protein pretreatment, regardless of surface type, showed the lowest degree of cell spreading. Dual ligand treated Mylar™ films showed significantly greater SA-b-HUVEC spreading up to 2h, but were similar to

HUVEC on FN treated Mylar™ at longer times; whereas SA-b-HUVEC spreading on dual ligand treated Teflon-AF was never significantly different from HUVEC on FN treated Teflon-AF™ at any time point. The value of *in vitro* testing can only be realized if we are able to optimize our protein cell seeding system on synthetic materials that can better predict *in vivo* cell adhesion.

3.2 Background

The majority of approaches used to improve vascular graft endothelialization have employed integrin-dependent surface conditioning to strengthen lumenal EC adhesion and retention[10]. All of these approaches have been unsuccessful owing to the lack of rapid and firm initial cell attachment necessary to nucleate the formation of stable, adherent, and quiescent endothelium in the graft lumen. Recently, we reported a dual ligand approach to enhance endothelial cell attachment and spreading on vascular graft materials [103]. This technique combined high affinity integrin-independent ligands with low affinity integrin-dependent ligands to promote rapid EC attachment and spreading. The high affinity avidin-biotin linkages bring the cell membrane in close apposition to the pre-coated surface, thus facilitating faster integrin-fibronectin linkages that lead to downstream signaling that promotes faster cell spreading and firm attachment. The resulting formation of firm focal contacts is intended to increase EC retention on vascular grafts and lead to improved patency.

To date, we have shown that the dual ligand treatment has a profound effect on *in vitro* EC attachment to glass surfaces tested under flow. Additional *in vitro* testing showed that dual ligand treated cells exhibited enhanced expression of vasoactive agents nitric oxide (NO) and prostacyclin (PGI_2). Despite the pronounced differences demonstrated *in vitro*, *in vivo* testing of endothelialized small diameter ePTFE grafts showed that dual ligand and fibronectin treated grafts performed equivalently in short term patency testing in a rat femoral artery model[12]. Clearly, *in vitro* testing on modified

glass was a poor predictor of the *in vivo* ePTFE results. *In vitro* testing of EC adhesion to ePTFE and Dacron using standard cell culture testing methodologies has been difficult because both materials are textured and opaque fabrics.

This study describes the use of smooth, transparent films of Mylar™ and Teflon-AF™(figure 3.1) to address a persistent, albeit technical, problem that neither of the most common vascular graft materials, Dacron™ and ePTFE, are amenable to common *in vitro* cell adhesion testing protocols because of their opacity and texture. In fact, cell adhesion to Dacron™ and ePTFE fabrics can only be observed using either SEM or fluorescent imaging [109], neither of which are suitable for continuous *in situ* cell monitoring. Consequently, most EC adhesion strategies are optimized on modified glass surfaces prior to testing on vascular graft materials. As we described elsewhere[12], this is a suboptimal strategy because what works spectacularly well *in vitro* on glass may be of little consequence *in vivo* using actual vascular grafts.

This pilot study examined *in vitro* characterization of EC spreading to the following thin transparent mimics of vascular graft materials[104]: Mylar™ (DuPont, Wilmington, DE), a film version of polyethylene terephthalate (PET); spun cast Teflon-AF™ (DuPont, Wilmington, DE), a copolymer of perfluoro(2,2-dimethyl-1,3-dioxole) (PDD) and tetrafluoroethylene (TFE). Mylar™ and Teflon-AF™ have wettabilities representative of those reported for PET and PTFE in any several polymer handbooks. Mylar™ and Dacron™ possess the same surface chemical composition because both are PET; whereas the surface chemical compositions of Teflon-AF™ and ePTFE differ with respect to the oxygen content of the PDD comonomer. Mylar™ and Teflon-AF™ films

are readily amenable to transmission microscopy characterization of cell spreading, and are easily incorporated into a two-dimensional flow model for testing EC adhesion strength without the surface turbulence caused by textured materials. These studies demonstrated the utility of these materials as model substrates for *in vitro* studies of cell adhesion by comparing the spreading of HUVECs subjected to dual ligand and fibronectin surface treatments.

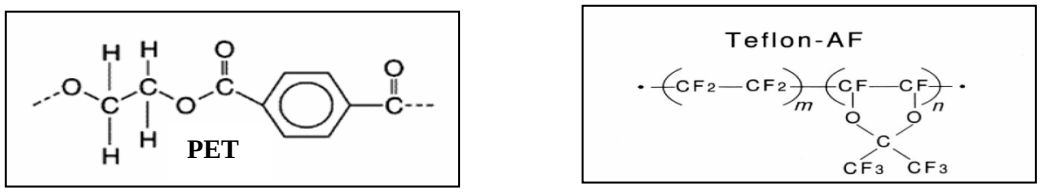

Figure 3.1. Chemical repeat structures for Mylar composed of polyethylene terephthalate (PET) and Teflon-AF. Note the structural difference in Teflon-AF compared to ePTFE structure in chapter 2.

3.3 Materials and Methods

Figure 3.2 is a flowchart of the surface characterization analyses that will be covered in this chapter.

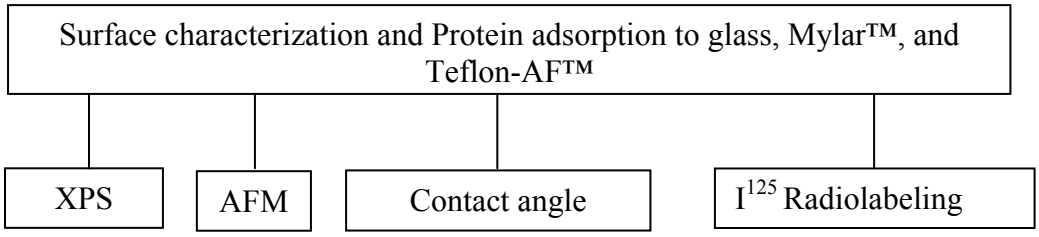

Figure 3.2. Schematic of surface characterization and protein quantification studies.

Substrates

The chemical structures of Mylar™ and Teflon-AF™ are shown in Figure 3.1. Teflon-AF™ (DuPont, Wilmington, DE) is a non-crystalline copolymer of 65 mol % 2-bistrifluoromethyl-4,5-difluoro-1,3-dioxole (PDD) and 35 mol % tetrafluoroethylene (TFE) purchased as a 6 wt % solution in Fluorinert FC-40 solution (3M, St. Paul, MN). Mylar™ (DuPont, Wilmington, DE) is a noncrystalline form of polyethylene terepthalate (PET) purchased as 37μm thick films. ePTFE cardiovascular patch (Impra, Tempe, AZ) and donated Dacron™ samples of woven PET were used as 1 cm^2 samples.

Cell adhesion studies used standard 1 x 3 inch soda lime glass slides (Gold Seal, Portsmouth, NH) with a thickness of 1 mm, 24mm x 60mm cover glass (Corning Labware and Equipment, Corning, NY), 37.7 μm thick Mylar™ films cut to shape, and Teflon-AF™ solution spun-cast onto glass microscope slides. Bare cover glass, cover glass coated with Teflon-AF™, and Mylar™ films were used for contact angle analysis,

XPS, and ^{125}I radiolabeling. Dacron™ and ePTFE cardiovascular patch samples were cut to shape (1 cm^2) and used for XPS analysis.

Three cell adhesion systems were examined in this study: "No Ligand," i.e. untreated HUVECs seeded onto untreated substrates; "FN," i.e. untreated HUVECs seeded onto substrates pre-adsorbed with FN for 1 hour; and "Dual Ligand," i.e. wild-type streptavidin (WT-SA) incubated biotinylated-HUVECs (SA-b-HUVECs) seeded onto substrates pre-adsorbed with a mixture of FN and biotinylated BSA (b-BSA). All references in association with dual ligand treatment imply the use of SA-b-HUVECs; whereas HUVECs in association with FN and untreated surfaces are native, untreated HUVEC. Seeding of untreated HUVECs to surfaces with no treatment served as controls.

Sample cleaning and preparation

Glass samples (slides and cover glass) were placed in Coplin™ jars and sonicated for 10 min in 2% PCC-54 detergent cleaning solution (Pierce, Rockford, IL), rinsed 3x with tap water and then rinsed 2x with DI water. Washed slides were placed in another Coplin™ jar and sonicated for 10 minutes in a 1:1 mixture of MeOH:HCl. The slides were allowed to sit in the Coplin™ jar for an additional 10 minutes and then sonicated for another 10 minutes. Methanol and hydrochloric acid were decanted and slides were rinsed 3x with tap water. Rinsed slides were sonicated in DI water for 10 min, rinsed 3x with DI water, and rinsed with 100% ethanol in the same Coplin™ jar. Clean slides were

dried overnight at 65 ^{o}C. Slides were stored in a square plastic Petri™ dish sealed with parafilm until used.

Mylar™ samples were cut to standard glass slide dimensions, sonicated in 70% ethanol for 10 minutes, rinsed with DI water 3x, and dried under UV overnight at room temperature**.** Samples were stored in a sealed square plastic Petri**™** dish until used.

Using the DuPont (www.dupont.com) recommended procedure, clean glass slides and cover glass were dip coated in a 2% solution of 1H, 1H, 2H, 2H-perfluorodecytriethoxy silane (Lancaster Synthesis, Windham, NH) in 95% ethanol/5% water. The slides were baked at 110 ^{o}C for 10 minutes, coated with Teflon-AF™ (1600s,DuPont, Wilmington, DE), and spin-cast on a Headway Photoresist Spinner (Garland, TX) at 1000 rpm for 90 seconds. After spinning, samples were air dried for 10 minutes, baked at 112 ^{o}C for 10 min to remove excess solvent, baked at 165 ^{o}C for 5 minutes to remove any trace of solvent, and then baked at 330 ^{o}C to anneal the film and promote adhesion to glass substrate{www.DuPont.com, 2004 18 /id}. All drying and baking was done in a high temperature oven. Surface thickness was measured using a PROF1 DekTak 3ST profilometer (Veeco, Santa Barbara, CA). The Dektak measures surface texture and film thickness by registering an electronic signal consistent with the displacement of a diamond tipped stylus position at the edge of the film. A film thickness using these spin casting condition was measured to be 61nm. Samples were stored in square plastic Petri dish slide holders sealed with parafilm until used.

X-ray Photoelectron Spectroscopy (XPS) Analysis

X-ray Photoelectron Spectroscopy (XPS) is a quantitative spectroscopic instrument that calculates empirical formula, chemical state and electronic state of elements that exist in a material. The spectra are obtained by irradiation of a material with X-ray beams while simultaneously measuring the kinetic energy (KE) and number of electrons that escape from the top 1-10nm of the material being analyzed[110]. XPS was conducted with 1 cm^2 samples. Dacron™ and ePTFE cardiovascular patch samples used for XPS analysis were cleaned by blowing with ultra pure nitrogen gas. Samples were stored in square plastic Petri™ dishes sealed with parafilm until used. Spectra were collected on a Riber LAS2000 instrument (Riber SA, Rueil Malmaison, France) equipped with a single pass, cylindrical mirror (MAC2) analyzer, and a Mg Kα X-ray source at the Analytical Instrumentation Facility (AIF) at North Carolina State University. Samples were analyzed with X-ray source at a 75^o take off angle, a spot size of 2mm, and an analysis chamber pressure of ~$3x10^{-10}$ Torr. The depth probed under these conditions was 1-5nm. Survey elemental spectra from 1200eV to 0.0eV with a step size of 1.0eV, dwell time of 0.1s, pass energy of 20eV, and 3 scans were conducted for all samples. All binding energies were calibrated to the binding energy of the C 1s peak to 285eV. High resolution spectra were obtained for F, O, and C. F 1s spectra ranged from 669-689eV with 10 scans, O 1s spectra ranged from 520-540eV with 10 scans, and C 1s spectra ranged from 270-290eV with 5 scans. All other conditions were the same as those for the survey scans. High-resolution spectra were resolved with CasaXPS version 2.2.79 (Casa

Software Ltd., Cheshire, United Kingdom). Software was used to determine percent chemical bond composition of the surface.

Atomic Force Microscopy Analysis

The atomic force microscope measures the topography of a surface with a force probe. It operates by determining the attractive and repulsive forces between the tip and the sample [110]. In this case, the tip was a TappingMode Etched Silicone Probe (TESP) shaped like a polygonal shaped pyramid with a height of 10-14μm and a tip radius less than 10nm. This was attached to a cantilever and topographic and phase images were obtained simultaneous as 512 x 512 arrays using tapping mode with a vertical deflection of 0 Volts and a scan rate of 1Hz. All samples were prepared and stored as previous mentioned. Dacron™ samples could not be analyzed because their surface texture was outside of the range of detection for the instrument and was also destructive to the probe tip.

Contact Angle

A static contact angle is defined as the angle formed by the liquid at the three phase boundary where a liquid, gas, and surface meet[110]. Sessile drop, air-water contact angles were measured on 1" x 1" samples of glass, Teflon-AF™ coated glass, and Mylar™ using a NRL Goniometer-Model 100-00 (Rame-Hart, Inc., Mountain Lakes, NJ). Six samples were analyzed in each instance.

Radiolabeling

Fibronectin (FN), biotinylated bovine serum albumin (b-BSA), and streptavidin (SA) were labeled with 1mCi Na^{125}Iodine (DuPont NEN Research, Boston, MA) for 30 minutes. Free ^{125}I was removed by passage over a PD-10 column (Pharmacia, Peapack, NJ) equilibrated with PBS. Protein bound was determined by precipitation with 10% (v/v) trichloroacetic acid (TCA). ^{125}I labeled proteins were diluted with unlabelled proteins and specific activities were determined. Protein adsorption for the dual ligand FN:b-BSA system was examined by measuring separately the adsorption of ^{125}I labeled FN with unlabeled b-BSA, and the adsorption of ^{125}I labeled b-BSA with unlabeled FN. SA binding to b-BSA was measured by titrating un-labeled FN:b-BSA surfaces with ^{125}I labeled SA. To quantify protein adsorption, 1cm^2 samples were incubated with labeled proteins for as long as the experimental incubation time. Fibronectin and b-BSA were incubated for 1 hr and SA was incubated for 40 minutes. Samples were then dipped 3x in a series of four 100ml volumes of PBS buffer solutions. Samples were placed in 12 x 75 mm tubes containing 1ml buffer. ^{125}I activity was determined by counting for 5 min in a Multi-Prias 1 gamma counter (Packard Instrument Co., Shelton, CT). On the following day, slides were rinsed, transferred to new tubes, and counted for 5 minutes. Adsorbed protein amount was determined using the second day count.

Additional studies were conducted to determine relative strength of FN binding on the different surfaces. Glass, Mylar™, and Teflon-AF™ samples were incubated with radiolabeled FN for 1hr, washed with copious amounts of PBS, put into plastic

12 x 75mm tubes, and counted in a scintillation counter for 5 minutes. FN Samples were sonicated for 5 minutes in PBS with a Bransonic Ultrasonic Cleaner (Danbury, CT), washed with PBS, put into different 12 x 75mm tubes, and counted for 5 minutes in a scintillation counter. Samples were then put into tubes with 0.1% Triton X-100, sonicated for another 5 minutes, washed with PBS, transferred to different 12 x 75mm plastic tubes, and counted for 5 minutes in a scintillation counter. In all cases the control was a tube with just PBS. Absolute and relative amounts of protein detached from surfaces were calculated in all cases.

Cell Culture and Protein Pretreatment

All cell culture reagents were obtained from Cambrex (Walkersville, MD) unless otherwise specified. Human umbilical vein endothelial cells (HUVEC), were grown to confluence in gelatin coated T25 polystyrene flasks (Corning Inc., Corning, NY) with endothelial basal media (EBM) supplemented with 0.5ml 10 g/ml hEGF (human recombinant Epidermal Growth Factor), 0.5 ml 1.0mg/ml Hydrocortisone, 0.5ml 50 mg/ml Gentamicin and 50mg/ml 50mg/ml Amphotericin-B mix, 3 mg/ml BBE (Bovine Brain Extract), and 10ml Fetal Bovine Serum (FBS). Cells were cultured in an incubator with 95% air/5% CO_2 at 37 ^{o}C. HUVECs from passage 2-4 were used for all experiments. For all experiments, confluent HUVECs were trypsinized and centrifuged at 2200rpm for 5 minutes, re-suspended in fresh serum free media warmed to 37 ^{o}C, and seeded onto glass, Mylar™ and Teflon-AF™ substrates at a concentration of 2 x 10^5

cells/ml either with or without protein pre-treatments in serum free media. Serum free media was the same as normal media just without FBS.

For "No Ligand" and "FN" cases, untreated HUVEC in serum free media were seeded onto substrates as described above, except in the FN case where the substrates had been preadsorbed with a 20μg/ml solution of FN in HEPES-buffered salt solution (HEPES-BSS) for 1 hour and washed gently with HEPES-BSS prior to seeding with untreated cells. For the Dual Ligand case [111], substrates were treated with a heterogeneous mixture of 1ml of 20μg/ml FN (Sigma Aldrich, St. Louis, MO) and 200μl of 2mg/ml b-BSA (Sigma Aldrich) in HEPES-BSS for 1 hour and washed gently with HEPES-BSS. Confluent HUVECs were trypsinized and centrifuged at 2200 rpm for 5 minutes, re-suspended in serum free EBM, and biotinylated by treatment with 1mM sulfosuccinimidyl-6-(biotinamido) hexaoate (NHS-LC-Biotin) (Pierce, Rockford, IL) in HEPES-BSS for 20 minutes. Biotinylated HUVECs were treated with 50μg/ml streptavidin (SA) for 40 minutes, yielding SA-incubated, biotinylated HUVEC (SA-b-HUVEC). SA-b-HUVECs were seeded onto dual ligand substrates at a concentration of 2×10^5 cells/ml in serum free media.

Measurement of cell spread area

Cell spread area was measured at 0.5, 1, 2, 4, 8, 12, and 24h by phase contrast microscopy (Nikon Diapot, Tokyo, Japan) with a 10x objective. Three fields were captured at each time point for each surface and 100 cells were measured for each sample at each time point. Cell images were captured by an MTI camera (Dage-MTI, Michigan City, IN) connected to the microscope and interfaced with a Macintosh computer. Images were analyzed using NIH Scion image software. The projected cell area was calculated by measuring the pixels enclosed by the cell perimeter and converting to μm^2 with the aid of a micrometer slide.

Statistical Analysis

StatView 5.0.1.0 (Cary, NC) was used to statistically compare data to determine variability. One-way ANOVA plus Fisher PLSD post hoc analysis was conducted to determine p values. All data are reported as the mean ± SE.

3.4 Results

XPS Analysis

Figure 3.3 shows superimposed survey scans of Teflon-AF™ and an ePTFE patch sample. Table 3.1 contains the gross carbon, oxygen and fluorine surface compositions of Dacron™, Mylar™, ePTFE cardiovascular patch and Teflon-AF™ as determined by survey XPS scans of the polymer substrates.

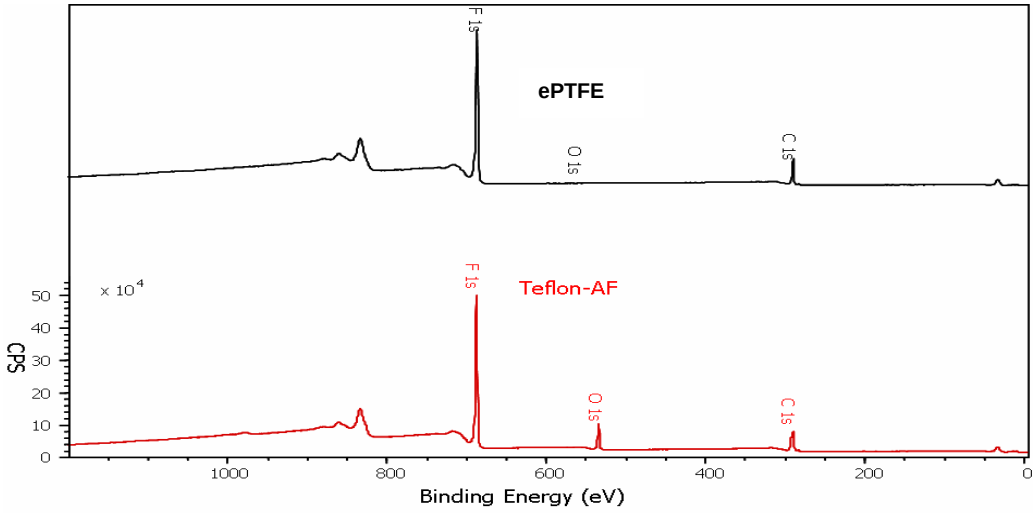

Figure 3.3. XPS survey scans of Teflon-AF and ePTFE. Note that the O 1s peak is the only difference between the chemical composition of the two polymers

The percent composition of carbon and fluorine measured for ePTFE cardiovascular patch was slightly more fluorine-rich than the XPS-determined 33.17% carbon and 66.83% fluorine content of PTFE reported elsewhere[112]. While there was no literature references for the XPS-determined composition of Teflon-AF™, the measured composition of cured Teflon-AF™ film closely matched the stoichiometrically calculated composition for Teflon–AF™ of 24.44% carbon, 9.30% oxygen and 66.27% fluorine.

High resolution XPS scans were also conducted on Teflon-AF™ to determine the different binding states for the elements in the monomeric repeats. ePTFE bonds have only one binding state due to the completely fluorocarbon structure. Spectral splittings of carbon, oxygen and fluorine peaks were resolved by numerical fitting to Gaussian functions in CasaXPS. Percent contribution due to each bond is shown in table 3.2. The C 1s peak for Teflon-AF™ resolved into four binding states: C-C (284.8eV), C-O (288.6eV), $-CF_2-CF_2-$ (289.9eV),-, and $-CF_3$ (292.2eV). The major component of the C 1s spectrum was from the polymer fluorocarbon backbone (64.0%), followed by ether (14.9%), trifluoro (11.2%), and aliphatic (9.9%) bonded carbon. Singlet peaks were observed for high resolution scans of O 1s (533.5 eV) and F 1s (687.6 eV) for Teflon-AF™.

Table 3.1. Percent elemental composition of polymers by XPS analysis.

Material	Carbon	Oxygen	Fluorine
PET	77.36	22.64	-
Mylar	75.29	24.71	-
ePTFE	29.05	-	70.95
Teflon-AF	31.36	7.90	60.74

Table 3.2. Resolved peaks of Teflon-AF™ high resolution scans.

	C 1s				O 1s	F 1s
Bond	**C-C**	**C-O**	**-CF_2-CF_2-**	**-CF_3**	**C-O**	**C-F**
Binding Energy (eV)	284.8	288.6	289.9	292.2	533.5	687.6
Area	867.6	1301.4	5592.9	979.6	10394.7	130629.3
Percent Contribution	10.0	15.0	64.0	11.0	100	100

XPS survey scans were also used to compare the elemental composition of Mylar™ and Dacron™ (figure 3.4). The percent composition of carbon and oxygen measured for Mylar™ and Dacron™ (Table 3.1) closely reflected the XPS-determined 72.03% carbon and 27.97% oxygen content of PET reported elsewhere[112].

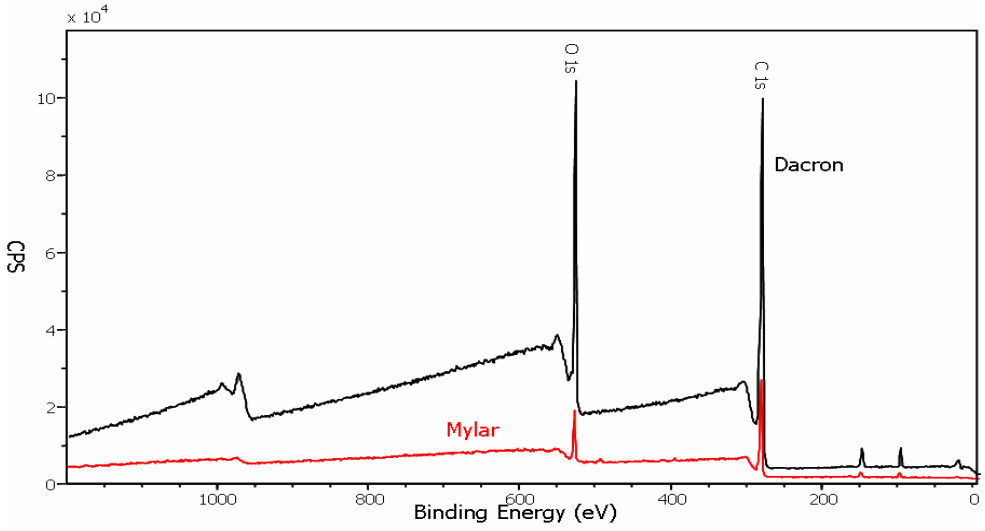

Figure 3.4. XPS survey scans of Mylar and Dacron. There is complete identity between the film and fabric.

Tables 3.3 contain the results from high resolution XPS scans of Mylar™. Spectral splittings of carbon, oxygen and fluorine peaks were resolved by numerical fitting to Gaussian functions in CasaXPS. The C 1s spectrum for Mylar™ (Table 3.3) resolved into peaks indicating the three binding states for carbon in PET: C-C (284eV), C-O (286eV), and C=O (288.6eV). The dominant features in the C 1s spectrum was aliphatic carbon (74.3%) with smaller contributions from ether (16.3%) and carbonyl (9.4%) carbons. The O 1s spectrum in Mylar™ resolved into binding states: O-C=**O** (532.0eV) and C-**O**-C=O (533.5eV). The major O 1s feature arose from carbonyl oxygen (89.27%) with a minor contribution from the ether oxygen (10.73%).

Table 3.3. Resolved peaks of Mylar™ high resolution scans.

	C 1s			**O 1s**	
Bond	**C-C**	**C-O**	**C=O**	**C=O**	**C-O-C=O**
Binding Energy (eV)	284.7	286.0	288.6	532.0	533.5
Area	10205.5	2245.7	1291.1	15025.7	1805.6
Percent Contribution	74.0	16.0	10.0	89.0	11.0

Atomic Force Microscopy (AFM) of Mylar™, Teflon-AF™ and ePTFE patch

AFM measurements were also used to illustrate and quantify topographic structure of Teflon-AF™, ePTFE patch, and Mylar™. Figure 3.5 shows representative 500 x 500nm and 30 x 30µm survey scans of bare Teflon-AF and ePTFE patch respectively.

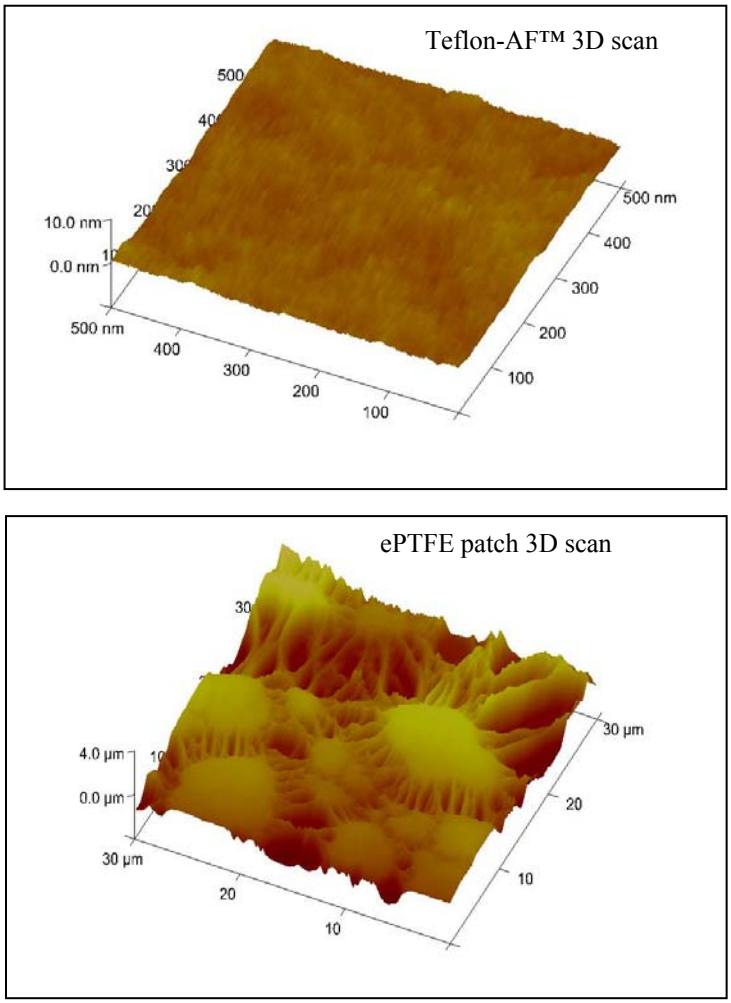

Figure 3.5 AFM 3-D projection images of typical Teflon-AF and ePTFE patch.

The AFM 3-D projection images confirm that spin-coated Teflon-AF™ was flat and contiguous. More important was that the surface texture was negligible compared to cell size. The difference in surface texture between Teflon-AF™ and ePTFE is visibly apparent and is an indication of the experimental limitation presented by such a surface.

Figure 3.6 shows a 500 x 500nm scan of Mylar™. The Mylar™ film is also flat. Heterogeneity observed on the surface is a result of handling rather than natural material surface texture.

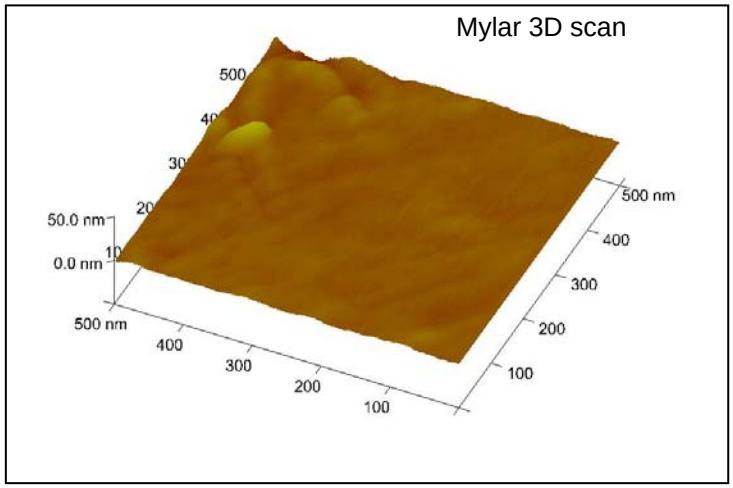

Figure 3.6. AFM 3-D projection image of Mylar™.

Table 3.4 is a summary of values for the mean roughness (Ra), the root mean squares average of height deviations (Rq), and Rmax, the maximum vertical distance between high and low points. The numbers indicate that Teflon-AF is flatter than Mylar but the biggest point to note here are the large values for ePTFE compared to all other samples in all cases.

Table 3.4. Summary of roughness measurements by AFM.

Material	**R_a (nm)**	**R_q (nm)**	**R_{max} (nm)**
Mylar	0.735±0.043	0.916±0.053	7.07±0.65
Teflon-AF	0.353±0.007	0.434±0.008	3.10±0.062
ePTFE	439±127	537±156	2792±977

Contact Angle Analysis of Glass, Mylar™, and Teflon-AF™

Sessile drop, air-water contact angle analysis was conducted on 1 x 1in samples of Mylar and Teflon-AF™. Mylar™ was determined to be moderately wetting with a contact angle of 80.2±2.30°, while Teflon-AF™ was non-wetting with a contact angle of 108±2.6°. Literature values for polar PET and nonpolar PTFE are 80^o and 105°, respectively[113]. DuPont lists a contact angle of 104° in their Teflon-AF materials specifications literature. The slightly less hydrophobic nature of Teflon-AF™ compared to PTFE is likely due to the oxygens of the PDD comonomer.

Air-water contact angles measured for Mylar™ and Teflon-AF™ were consistent with the contact angles reported elsewhere for PET and PTFE[113]. Since the attachment of proteins to the polymer surfaces in the dual ligand treatment is a physical adsorption,

rather than chemical coupling, the similarity of surface energies is the minimum requirement for establishing Mylar™ and Teflon-AF™ as tissue culture mimics of Dacron™ and ePTFE.

Protein adsorption

^{125}I radiolabeling was used to determine surface densities of adsorbed FN, b-BSA, and SA as described elsewhere{Truskey, 1990 23 /id}. Four different protein formulations were incubated with each substrate: (1) ^{125}I labeled FN, (2) ^{125}I labeled b-BSA mixed with unlabeled FN, (3) ^{125}I labeled FN mixed with unlabeled b-BSA, and (4) ^{125}I labeled WT-SA binding to a preadsorbed mixed layer of unlabeled FN and b-BSA. Table 3.6 lists the measured surface densities of protein adsorbed to glass, Mylar™, and Teflon-AF™ substrates. The general trend in adsorbed amount for all four formulations on all three substrates was glass > Mylar™ ~ Teflon-AF™. In five of eight cases the amount of protein adsorbed to glass was significantly different ($p<0.05$): FN alone relative to Teflon-AF, FN co-adsorbed with b-BSA relative to both Mylar™ and Teflon-AF™, and WT-SA bound to FN/b-BSA relative to both Mylar and Teflon-AF. There were no significant differences in the amount of protein adsorbed to either Mylar or Teflon-AF for any of the four formulations employed. Table 3.5 shows surface densities of adsorbed protein. Names in red indicate species labeled with ^{125}I.

Table 3.5. Surface densities (± SE) of adsorbed Fibronectin (FN), biotinylated BSA (b-BSA), and streptavidin (SA) on glass, Mylar™, and Teflon-AF™. Protein name in red indicates species labeled with ^{125}I.

	Glass ***(10^{10}molecules/cm^2)***	***Mylar™*** ***(10^{10}molecules/cm^2)***	***Teflon-AF™*** ***(10^{10}molecules/cm^2)***
FN	13.4±0.4[#]	12.3±0.5	9.86±0.4
*FN/**b-BSA***	63.9±1.8	56.6±3.9	54.8±3.6
***FN**/b-BSA*	9.9±0.4[*]	8.6±0.4	8.6±0.3
*FN/b-BSA/**SA***	39±1.3[*]	30±0.6	29±0.3

n=3

[#] Amount of protein adsorbed to glass significantly greater ($p<0.05$) relative to Teflon-AF

[*] Amount of protein adsorbed to glass significantly greater ($p<0.05$) relative to both Mylar and Teflon-AF

Figure 3.7 displays FN attachment on the different experimental surface after sonication in a buffer and mild surfactant. Once the samples were sonicated for 5 minutes in PBS the percent retention was greatest on Mylar, then Glass, and then Teflon-AF and total protein amount on the surface after sonication followed the same order. After sonication in a mild detergent the percent FN retention was greatest on glass, then Mylar, and then Teflon-AF but total protein amount followed the same order as sonication in PBS alone. The protein retention on Mylar was significantly greater than glass and Teflon-AF after sonication in PBS but this difference was only significantly greater than Teflon-AF after sonication in 0.1% Triton X-100.

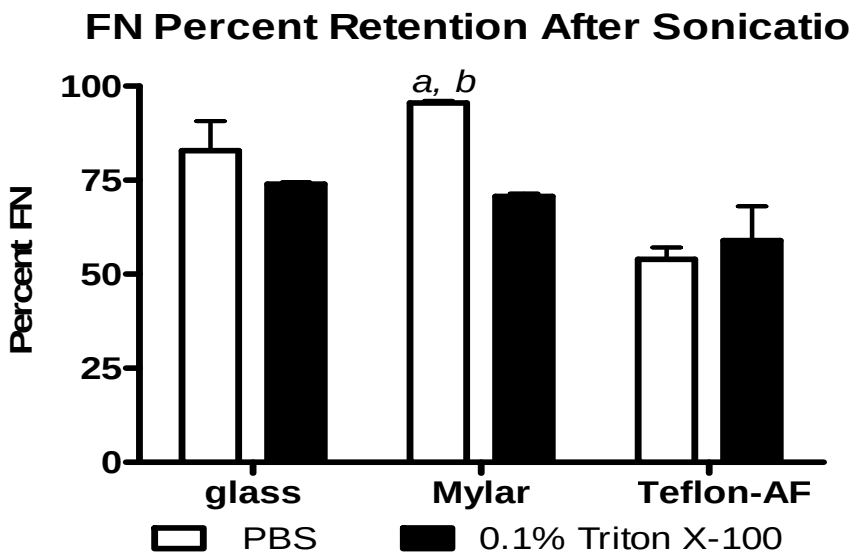

Figure 3.7. FN retention on Glass, Mylar, and Teflon-AF post sonication in PBS and 0.1% Triton X-100. Retention was highest on Mylar in PBS and highest on glass in Triton X-100. [a] represents significantly higher attachment on Mylar with PBS than Triton X-100; [b] represents significantly higher than Teflon-AF attachment on Mylar over Teflon-AF in PBS.

Cell spread area

Cell spreading was measured under static conditions as described elsewhere[114]. Figure 3.8 shows phase contrast images of SA-b-HUVEC bound to dual ligand treated Mylar™ and Teflon-AF™ films confirming their amenability to standard microscopic measurements of cell spreading.

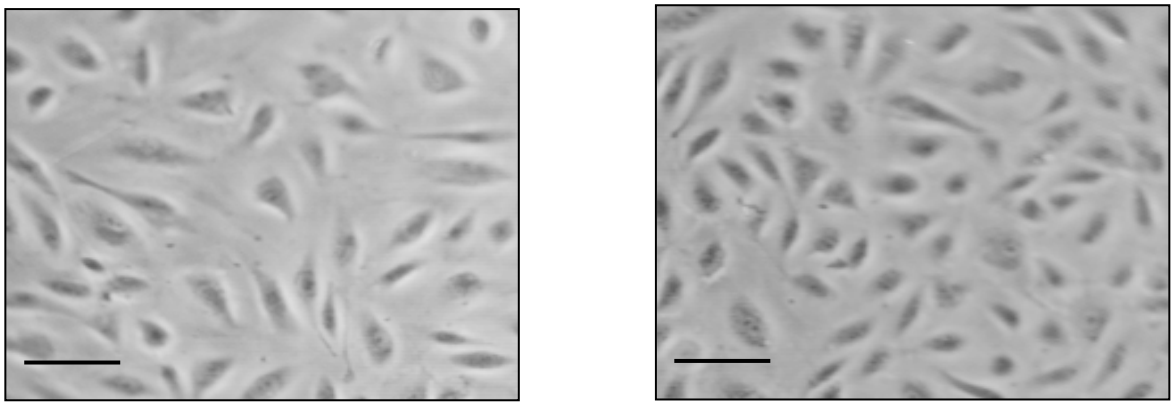

a.) SA-b-HUVEC on Mylar™ b.) SA-b-HUVEC on Teflon-AF™

Figure 3.8 . Phase contrast images of SA-b-HUVEC spread on Mylar™ (a) and Teflon-AF™ (b) treated with the dual ligand after 4 hrs of attachment (10x). Bar=100μm

Figures 3.9-3.11 are bar graphs of the average spread area of cells seeded onto the glass, Mylar™ and Teflon-AF™ substrates subjected to no ligand, FN, and dual ligand treatments. For all substrates and surface treatments, the degree of cell spreading increased monotonically with adhesion time, ranging from greater than 1600 μm^2 for dual ligand treated Teflon-AF™ at 24 hours, to less than 400μm^2 for untreated Teflon-AF™ at 30 minutes. Regardless of surface type, and for any given time point, all untreated

surfaces showed the lowest average cell spread area. With only two exceptions (glass at 24h and Mylar™ at 12h), dual ligand treated surfaces showed the highest average cell spread area for all surface types and time points. Dual ligand treated glass slides and Mylar™ films showed significantly greater cell spreading within the critical time periods (1-2 hours), but were similar to FN treated Mylar™ at longer times; whereas cell spreading on dual ligand treated Teflon-AF™ was never significantly higher than on FN treated Teflon-AF™ at any time points.

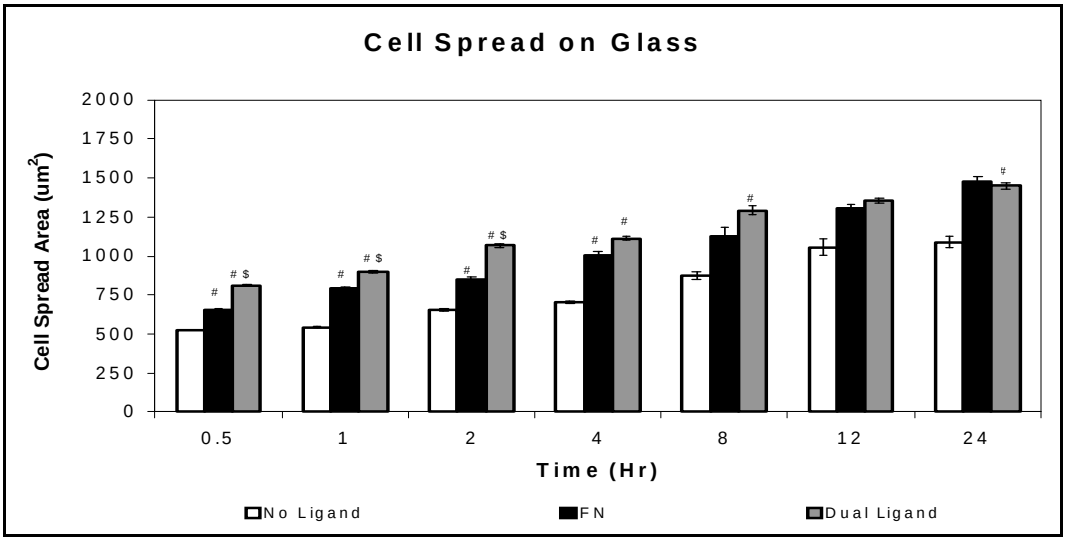

Figure 3.9. Cell spreading over a 24h period on glass (n=6). # represents significantly ($p<0.05$) greater spreading than the "No ligand" system. $ represents significantly ($p<0.05$) greater spreading than the FN system.

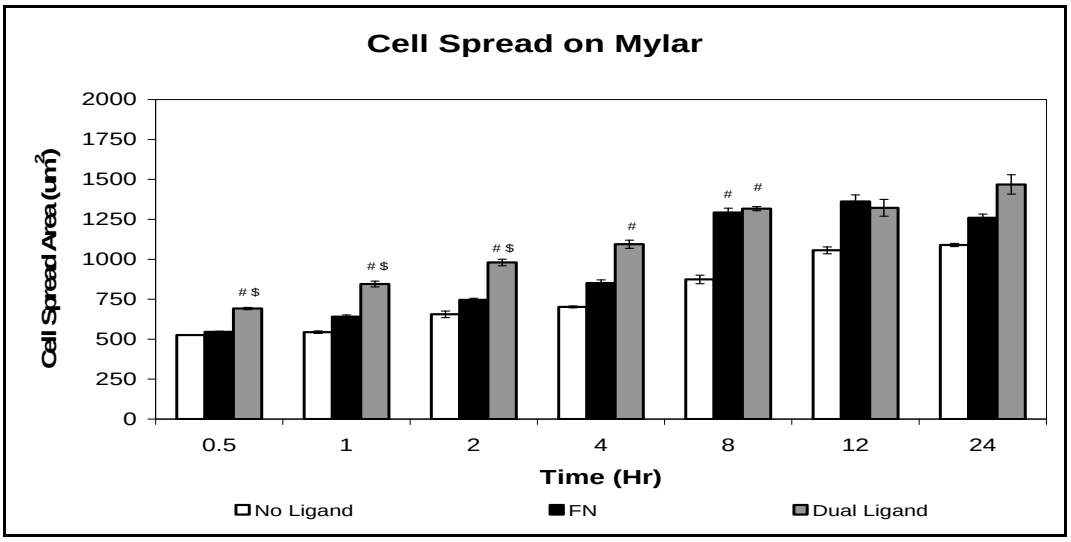

Figure 3.10. Cell spreading over a 24h period on Mylar™ (n=6). # represents significantly ($p<0.05$) greater spreading than the "No Ligand" system. $ represents significantly ($p<0.05$) greater spreading than the FN system.

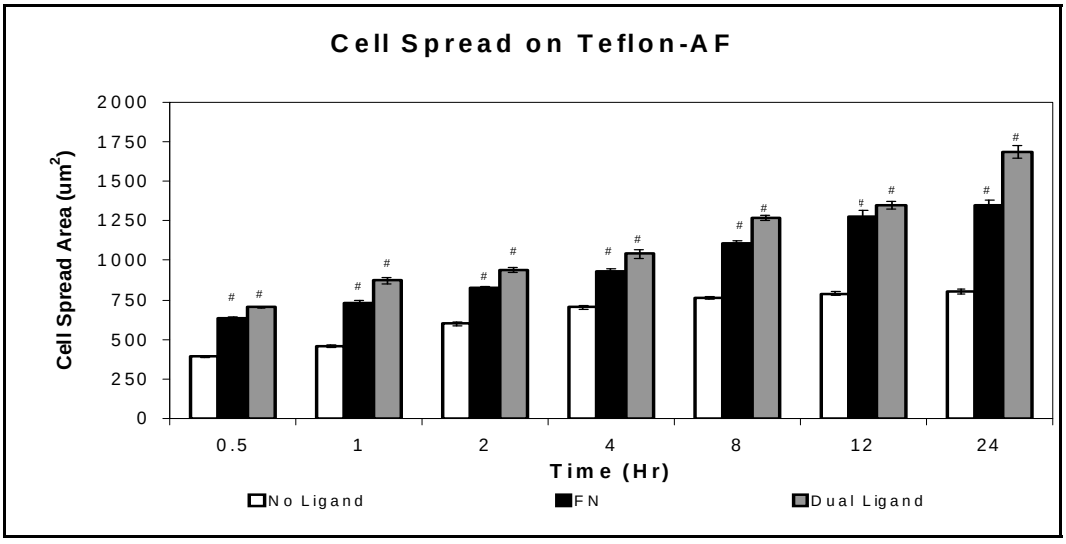

Figure 3.11. Cell spreading over a 24h period on Teflon-AF™ (n=6). # represents significantly ($p<0.05$) greater spreading than the "No Ligand" system. $ represents significantly ($p<0.05$) greater spreading than the FN system.

3.5 Discussion

This study describes the use of smooth, transparent films of Mylar™ and Teflon-AF™ to address a persistent, albeit technical, problem that neither of the most common vascular graft materials, Dacron™ and ePTFE, are amenable to common *in vitro* cell adhesion testing protocols because of their opacity and texture. In fact, cell adhesion to Dacron™ and ePTFE fabrics can only be observed using either SEM or fluorescent imaging[109] neither of which is suitable for continuous *in situ* cell monitoring. Consequently, most EC adhesion strategies are optimized on modified glass surfaces prior to testing on vascular graft materials. As we described elsewhere [12], this is a suboptimal strategy because what works spectacularly well *in vitro* on glass may be of little consequence *in vivo* using actual vascular grafts.

Survey and high resolution XPS scans of Mylar™ and Dacron™ yielded nearly identical surface chemical surface compositions; whereas the XPS of Teflon-AF™ and the ePTFE cardiovascular patch differed, as expected, by chemical shifts attributed to the oxygens of the PDD monomer. There were, however, a few observed discrepancies in the XPS measurements. The carbon composition measured for Mylar™ and Dacron™ exceeded the carbon XPS content reported elsewhere for PET by a few percent[112], and the XPS measured for ePTFE was a few percent more fluorine-rich than that reported for XPS of PTFE[112]. A likely source of excess carbon signal is contamination, possibly from residual solvents used in the cleaning procedure [115]. The origin of the difference between ePTFE and PTFE fluorine content is not apparent. The intensities of the C 1s and O 1s peak intensities also differed between Mylar™ and Dacron™. The difference in C 1s and

O 1s peak intensities between Mylar™ and Dacron™ may have arisen from differences in electron capture after x-ray excitation in thin film and textured specimens.

AFM topographic analysis confirmed the limitations with current synthetic vascular grafts to be used with *in vitro* microscopic techniques while subsequently verifying the utility of the SVG surrogates for similar studies.

Air-water contact angles measured for Mylar™ and Teflon-AF™ were consistent with the contact angles reported elsewhere for PET and PTFE[113]. Since the attachment of proteins to the polymer surfaces in the dual ligand treatment is a physical adsorption, rather than chemical coupling, the similarity of surface energies is the minimum requirement for establishing Mylar™ and Teflon-AF™ as tissue culture mimics of Dacron™ and ePTFE.

Adsorption of the dual ligand proteins to glass, Mylar™ and Teflon-AF™ were tested using ^{125}I radiolabeling. There were no significant differences in the amounts of FN, b-BSA and SA adsorbed to Mylar™ and Teflon-AF™; whereas glass bound more (11%-26%) protein in all eight comparisons to Mylar™ and Teflon-AF™, with five of these differences being statistically significant ($p<0.05$). Although glass is very hydrophilic it is well-known to adsorb significant amounts of blood plasma proteins such as BSA and FN[116]; however, it was somewhat surprising that Mylar™ and Teflon-AF™ adsorbed such similar amounts given the difference in surface polarity. Nevertheless, amount adsorbed may be secondary to the reversibility and the conformational state of the adsorbed protein[117]. Finally, while adsorbed amounts showed some variability, the ratios of surface-bound proteins were remarkably consistent between substrates: b-BSA

to FN (6.5 on glass, 6.6 on Mylar™ and 6.3 on Teflon-AF™); SA to b-BSA (1.6 on glass and 1.9 on Mylar™ and 1.9 on Teflon-AF™); and SA to FN (3.9 on glass, 3.5 on Mylar™ and 3.0 on Teflon-AF™). Percent protein retention was lowest on Teflon-AF after sonication in PBS as well as in Triton X-100. This is an indication that, though proteins might bind in sufficient quantities to fluorinated surfaces, the strength of binding is weak. This would lead to adhesive failure of endothelial cells seeded onto SVGs. Many researchers have found that protein adsorption onto hydrophilic forces involves the formation of a water-free contact layer that allows the protein to unfold without solvating its hydrophobic residues[118]. Environmental AFM has also confirmed that adsorbed FN exists in a condensed morphology compared to an elongated structure on hydrophilic surface [119]. This lack of interaction with the surface may contribute the fast desorption of FN from Teflon-AF upon agitation.

As expected, untreated surfaces showed the lowest degree of cell spreading compared to the corresponding dual ligand and FN treated surfaces. Dual ligand treated Mylar™ films showed significantly greater SA-b-HUVEC spreading up to 2 hours, but were similar to HUVEC spreading on FN treated Mylar™ at longer times; whereas SA-b-HUVEC spreading on dual ligand treated Teflon-AF™ was never significantly different than HUVEC spreading on FN treated Teflon-AF™ at any time point. This pilot study confirms the utility of these surfaces as surrogates for synthetic vascular grafts. The cell areas were consistent with what has been reported in the literature by other labs [120,121].

3.6 Conclusion

Here we demonstrated the utility of transparent films of Mylar™ and Teflon-AF™ as tissue culture mimics of Dacron™ and ePTFE vascular graft materials. This study represents the necessary first step towards developing an *in vitro* model that more accurately models endothelial cell adhesion to vascular graft materials, and that still provides for the use of conventional tissue culture methods normally used to investigate cell attachment, spreading and adhesion. These materials were characterized by contact angle, XPS, AFM, and adsorption of the dual ligand proteins FN, b-BSA and SA. Measurement of spreading of HUVEC without protein treatment, with FN treatment, and with dual ligand treatment, characterized cell adhesion. Current efforts are directed at identifying the surface chemistry necessary to optimize the impact of dual ligand treatment for Mylar™ and Teflon-AF™ films.

Chapter 4. Characterization and kinetic analysis of biotin functionalized fibronectin

4.1 Synopsis

Standard extracellular matrix (ECM) proteins used for cell adhesion are not sufficient for rapid and firm adhesion due to their low binding affinity for transmembrane integrins. This has lead us to develop a dual ligand system that uses the specific Avidin-biotin system with high binding affinity to buttress the standard ECM protein adhesion. Here, we examined the retention of high kinetic binding between biotin conjugated to fibronectin (bFN) for WT-SA and RGD-SA. Biotin conjugation was achieved with Sulfo-NHS-LC-Biotin and subsequently analyzed for retention of cell binding domain using Surface Plasmon Resonance (SPR) spectroscopy and enzyme-linked immunosorbent assay (ELISA). The affinity of conjugated biotin for WT-SA and mutant strain streptavidin (RGD-SA) was measured using SPR spectroscopy. The ELISA showed no adverse affects on the accessibility of the RGD binding site on the bFN compared to native protein. The absorbance units for bFN by ELISA were the same as those for un-modified FN. SPR analysis of $\alpha_5\beta_1$ and $\alpha_v\beta_3$ integrin binding to immobilized bFN and bFN with RGD-SA confirmed the detection of the RGD binding motif. This is promising because it means we can get the benefit of the high affinity interaction between biotin and streptavidin as well as the integrin-FN linkages with one protein. Contrary to the initial assumptions, SPR showed no increase in affinity due to increased biotins per FN. This is an indication that though biotin density is increasing, there was no cooperative effect from the proximal biotins; each event is an individual binding event.

4.2 Background

Protein adsorption has been used in the field of vascular tissue engineering to enhance cell attachment, spreading, and formation of neointima in synthetic vascular grafts. The majority of studies have adsorbed films of single proteins like fibronectin, vitronectin, or laminin to bind cells to the material surface[122,123]. Fibronectin, the most researched of the extracellular matrix proteins, is a 440kDa glycoprotein composed of a dimer joined by a pair of disulfide bonds{Alberts, 1989 724 /id}. These surface modifications, however, are often insufficient to achieve the firm cell attachment to vascular grafts due to insufficient adhesion attributed partially to the low binding affinity (K_D ~10^{-6} M) between transmembrane integrins and extracellular matrix proteins[124].

Streptavidin is a tetrametric protein isolated from *Streptomyces avidinii* that is able to bind four submits of biotin with high affinity (K_D in solution ~ 10^{-15} M). A dual ligand (DL) strategy that uses high affinity streptavidin-biotin binding to augment lower affinity FN-integrin binding shows promise as a means to improve cell adhesion. Others have used the DL system to enhance chondrocyte adhesion to tissue culture polystyrene as an indication of future tissue engineering viability[125], hepatic cell binding and spreading on biodegradable, polymer-based, flat 2-D surfaces, and in highly porous 3-D scaffolds [126], and for drug delivery using avidin to immobilize biotinylated therapeutic agents[127].

We have employed streptavidin-biotin to augment the binding of endothelial cells to vascular grafts[103]. In our initial system, surfaces were co-adsorbed with fibronectin (FN) and biotinylated bovine serum albumin (bBSA) to augment the binding of

endothelial cells decorated with biotin and subsequently incubated with streptavidin. The streptavidin-biotin binding stabilized the initial cell-substrate contact, bringing the cell membrane in close apposition to adsorbed fibronectin, and thus facilitating the formation of intrinsic integrin-mediated focal contacts[103]. Dual ligand augmented endothelial cell (EC) adhesion has been reported on Mylar and Teflon-AF that were employed as surrogates of Dacron and ePTFE vascular graft materials[104]. The system was refined by employing an RGD-streptavidin (RGD-SA) mutant, isolated from *E. coli* cells transfected with a pET plasmid, which contained integrin-independent and integrin-dependent functionality in a single protein[105]. Binding of the RGD-SA to integrin receptors on the EC membrane provided direct means of decorating the ECs with streptavidin, increasing the density of cell adhesion ligand, and also mitigating cohesive failure effects due to the non-specificity of cell substrate biotinylation[105,128].

The current study determined the utility of a second refinement that replaced co-adsorbed FN and bBSA with adsorbed biotinylated fibronectin (bFN). Like the RGD-SA, bFN has dual functionality: biotin moieties that facilitate high affinity streptavidin-biotin binding and cell binding RGD domains that promote integrin-FN binding. This enhancement makes the system more amenable to future clinical studies by eliminating xenogenic effects due to bBSA. Using SPR this study examined the affect of degree of biotinylation on the binding kinetics of biotinylated FN. Additionally, SPR and ELISA were used to confirm detection of RGD cell binding motifs on fibronectin post biotinylation by interrogating an immobilized protein laminate with $\alpha_5\beta_1$ and $\alpha_v\beta_3$ integrins.

4.3 Materials and Methods

Biotinylation of fibronectin

Fibronectin was biotinylated with Sulfo NHS-LC-Biotin (Pierce, Rockford, IL) with a spacer arm of 22 Angstroms (figure 4.1). 1mg/ml solution of FN (Chemicon, Temecula, CA) was mixed with 10mM Sulfo NHS-LC-Biotin dissolved in ultrapure water for 30 minutes at room temperature. Excess biotin was removed by dialysis in Dulbecco's phosphate buffered saline (dPBS) (Invitrogen, Carlsbad, California) for 24 hrs at 4 ^{o}C with a buffer change after 12 hours. Multiple biotin conjugation levels were achieved by stoichiometrically varying the moles of biotin reagent per FN. The amount of biotin incorporation was measured using EZ-Link-NHS-chromogenic-Biotin (Pierce) with a polyethylene glycol spacer arm of 41 Angstroms and a bis-aryl hydrazone group with a characteristic absorbance at 354nm. Absorbance values were indicative of number of biotins per fibronectin.

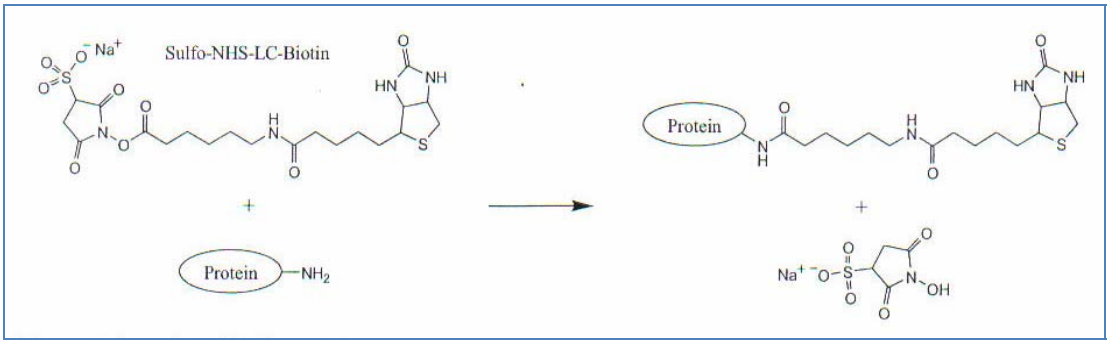

Figure 4.1. Chemical binding of biotin to terminal amines on fibronectin. Binding is primarily through lysine groups on the protein.

Surface Plasmon Resonance (SPR) Spectroscopy

Glass slides were cleaned as previously detailed[104] in chapter 3. 4nm of chromium and 20nm of gold were evaporated onto the slides under vacuum to yield transparent gold films[129] and stored under argon until used. Self assembled monolayer (SAM) formation was achieved by immersing gold coated chips in solution of 2mM 16-mercaptohexadecanoic acid (HDA) in 100% ethanol for ≥24 hours. Afterwards, chips were rinsed and dried under N_2 gas.

SPR experiments were carried out on a BIACOREX (Pharmacia Biosensor) microfluidic system as described previously[129]. After chip insertion, the surface with HDA SAM was either activated by injection of 35µl of an equal mix of 0.1M N-hydroxysuccinimide (NHS) and 0.4M 1-ethyl-3-(3-(dimethyl-amino)propyl)carbodiimide (EDC) in PBS at a flow rate of 5µl/min or left unfunctionalized for direct ligand adsorption to SAM layer. Comparisons were conducted between direct immobilization and EDC/NHS immobilization. After rinsing and baseline equilibration, 20µg/ml bFN with different molar ratios was immobilized onto the chip surface at a flow rate of 2µl/min for up to 20 minutes. After baseline equilibration, either 50µg/ml WT-SA (Pierce, Rockford, IL) or RGD-SA was flowed over the protein at 2µl/min. To determine the number of available surface biotins post bFN immobilization to EDC/NHS functionalized surfaces, 1:100 anti-biotin monoclonal antibody (Abcam, Cambridge, MA) was injected to bind to available surface biotins. The change in response units was also used to determine number of surface biotins per fibronectin.

To confirm availability of the RGD binding motif Biotinylated fibronectin was immobilized on the substrate using EDC/NHS. After washing with buffer to remove unbound protein, the surfaces were interrogated with $\alpha_5\beta_1$ and $\alpha_v\beta_3$ for availability of RGD binding motifs.

Response units (RU) were measured based on differences in refractive index. These units were eventually correlated to protein surface density based on the relationship: 1000RU=1ng/mm^2 protein. The binding kinetics and amount immobilized were calculated with BIAevalution software (Biacore AB, Uppsala, Sweden).

Enzyme-Linked ImmunoSorbent Assay (ELISA)

Ninety six well plates were coated with Teflon-AF and dried under vacuum overnight at room temperature according to the procedure of Koenig et al.[130]. bFN with 5 biotins per FN or native FN in dPBS at a concentration of 20µg/ml was adsorbed to 96 well plates for 1 hour at room temperature. Wells were blocked with 1% BSA in dPBS for 3 hours and rinsed 2x with Dulbecco's phosphate buffered saline (dPBS). The wells were incubated with 1:100 mouse anti-human FN cell binding peptide antibody (Chemicon, Temecula, CA) in dPBS for 2 hours at room temperature and rinsed 2x with dPBS. These wells were then incubated with 1:200 sheep anti-mouse horseradish peroxidase (HRP) secondary antibody in 0.5% BSA for 20 minutes and rinsed 2x with dPBS. Wells were then incubated with 100µl TMB/E developing solution in the dark for 20 minutes at room temperature. The reaction was halted with 50µl of 2N sulfuric acid

and the plate was read within 5 minutes at 450nm with a reference wavelength of 540nm to correct for background absorbance due to the plate.

Fluorescence Activated Cell Sorting (FACS)

Fluorescence activated cell sorting was used to detect RGD-SA binding specificity for $\alpha_5\beta_1$ and $\alpha_v\beta_3$ integrins. Mutant streptavidin (RGD-SA) and WT-SA were labeled with an Alexa Fluor® 488 Protein Labeling Kit (Molecular Probes, Eugene, OR) according to manufacturer's directions. Briefly, a 100µL of a 1mg/ml protein solution was mixed with 10µL of 1M sodium bicarbonate. 4.42µL of a 11.3nmol/µL Alexa Fluor® 488 TFP ester was added and incubated for 15 minutes at room temperature. After labeling, proteins are purified and isolated from unreacted dye on a resin bed in a spin filter after centrifugation at 16,000 x g in a microcentrifuge for 1 minute. HUVECs used for FACS were cultured and detached as outlined in chapter 3 of this thesis. 200,000 HUVECs in 1 mL of dPBS with Ca^{2+} and Mg^{2+} were labeled with 20µL of 50µg/ml RGD-SA based on previous saturations studies. Cells were incubated while rotating in the incubator for 40 minutes. Labeled cells were centrifuged at 2200 rpm to remove unbound protein, resuspended in 3 mL of 10% formalin, and labeled for analysis. A range of nine different cell labeling concentrations were studied to measure RGD-SA incorporation. In other studies, cells were incubated with either anti-human $\alpha_5\beta_1$ or $\alpha_v\beta_3$ integrins (Chemicon) prior to incubation with labeled RGD-SA. Figure 4.2 is an outline of labeling studies done to determine RGD-SA incorporation and specificity for two transmembrane integrins.

Fluorescence intensity per cell produced by the bound labeled RGD-SA was measured using a FACStar Plus flow cytometer (Becton Dickinson, San Jose, CA). Generally 10,000 cells were analyzed in each case. Wild type streptavidin was the control for this study and fluorescence observed for those samples were subtracted from the fluorescence intensity observed for the samples containing labeled RGD-SA.

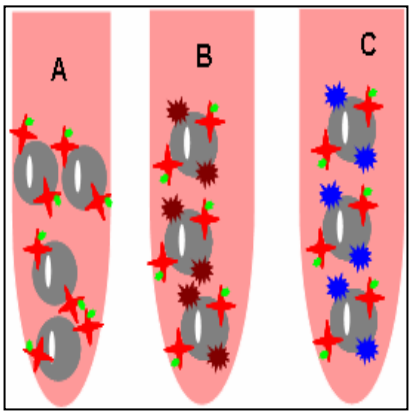

Figure 4.2. HUVEC incubated with RGD-SA labeled with Alexafluor 488® (A) and independently incubated with unlabeled $\alpha_5\beta_1$ (B) and $\alpha_v\beta_3$ antibody (C) prior to incubating with labeled RGD-SA.

Statistical Analysis

StatView 5.0 was used to statistically compare data and measure variability. One-way ANOVA plus Tukey-Kramer post hoc analyses were conducted to determine *p* values. All data reported as the mean ±SE.

4.4 Results

Fibronectin Biotinylation Characterizations

Biotinylated fibronectin (bFN) was generated by reacting 10 to 500 molar excesses of Sulfo-NHS-LC-Biotin with FN. Figure 4.3 shows the increase in the total number of biotins conjugated to FN expressed as biotins per FN molecule. Biotinylation yielded 2-21 biotins per FN across the range of molar excesses.

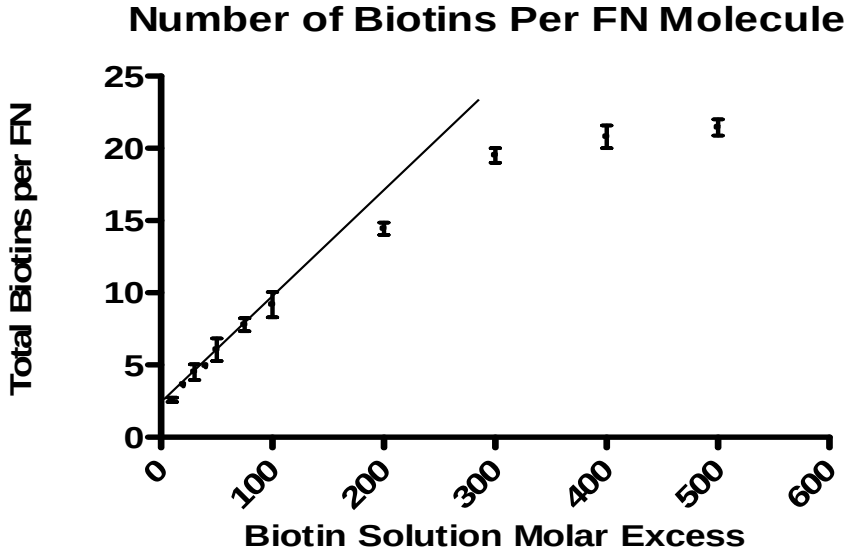

Figure 4.3. Number of biotins attached per fibronectin in solution after dialysis measured as a function of biotin solution molar excess. This number was measured by absorbance of EZ-Link-NHS-chromogenic-Biotin at 354 nm. (n=3)

The number of total biotins per fibronectin in solution was determined using the absorbance of the EZ-Link-NHS-chromogenic-Biotin. The number of biotins conjugated per FN molecule increased linearly until approximately 20 biotins at a molar excess of 300, after which the degree of biotinylation appeared to saturate. The lack of significant

differences between the values at 300, 400 and 500 were an indication that the system was saturated.

Surface Plasmon Resonance (SPR) Spectroscopy

Surface plasmon resonance (SPR) spectroscopy was used to determine the binding characteristics of WT-SA and the RGD-SA to immobilized bFN as a function of biotins per FN molecule. Figures 4.4 compares traces of passively adsorbed and EDC/NHS immobilized bFN.

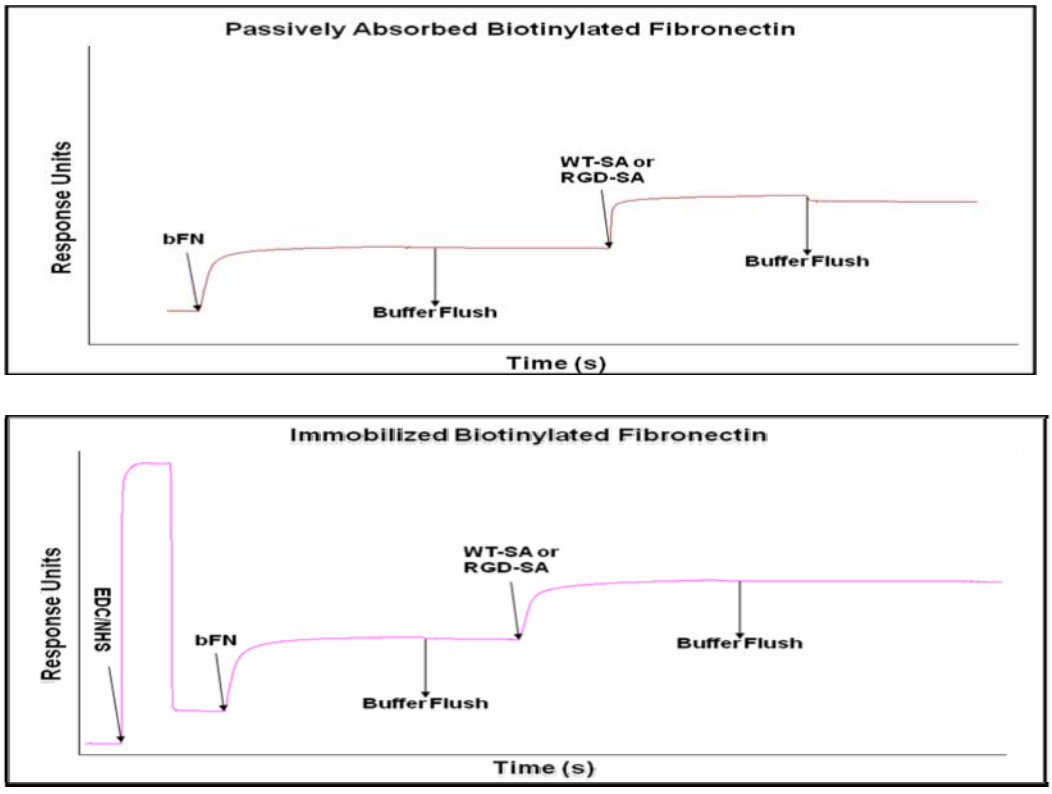

Figure 4.4. SPR traces with immobilized fibronectin compared to immobilization using EDC/NHS. Note the slight desorption of RGD-SA after buffer flush on passively adsorbed surfaces.

Desorption of RGD-SA after buffer wash ranged from 4.7±1.9% to 13.4±1.2% for all biotinylation levels on EDC/NHS functionalized surfaces but when compared to passively adsorbed bFN with 5 biotins per FN and bFN with 9 biotins per FN, desorption was 38.5±2.3% and 23.8±0.3%, respectively. These two values were chosen arbitrarily for this comparison study. Table 4.1 compares the surface densities of bFN(9) and RGD-SA before and after buffer flushing steps with passive adsorption versus EDC/NHS mediated immobilization

Table 4.1. Comparison of bFN(9) immobilized via passive adsorption versus EDC/NHS activation and subsequent binding and desorption of

Surface	bFN(9) (ng/mm^2)	Desorbed (ng/mm^2)	RGD-SA (ng/mm^2)	Desorbed (ng/mm^2)
SAM	1.76 ± 0.04	0	0.78 ±0.03	0.37±0.01
SAM + EDC/NHS	1.87 ± 0.23	0	1.54±0.17*	0.12±0.03**

Values are reported as average SEM for n=3. Column statistics was performed using ANOVA and Tukey-Kramer post hoc tests. *indicates significantly higher binding compared to passive adsorption. ** indicates significantly lower desorption when compared to EDC/NHS immobilization.

The amount of bFN immobilized by EDC/NHS was not significantly different when compared to passive adsorption, but amount of RGD-SA bound to immobilized bFN was significantly higher than with passive adsorption. RGD-SA desorption was negligible on surfaces functionalized with EDC/NHS.

Figure 4.5a shows the mass of bFN immobilized on the SPR chip and the mass of WT-SA bound to the immobilized bFN. Figure 4.5b similarly shows the mass of bFN immobilized on the SPR chip and the mass of RGD-SA bound to the immobilized bFN. Results indicate that below 10 biotins per FN the mass of bFN immobilized was

relatively constant at a value of 2ng/mm^2 (note boxed region). Above 10 biotins per FN the amount of immobilized FN decreased. The values of bound WT-SA and RGD-SA increased linearly and appeared to plateau at a value of 2ng/mm^2 after 10 biotins per FN. These data suggest well behaved binding for bFN with <10 biotins per molecule. In contrast, higher levels of biotinylation appeared to introduce steric effects which reduced binding.

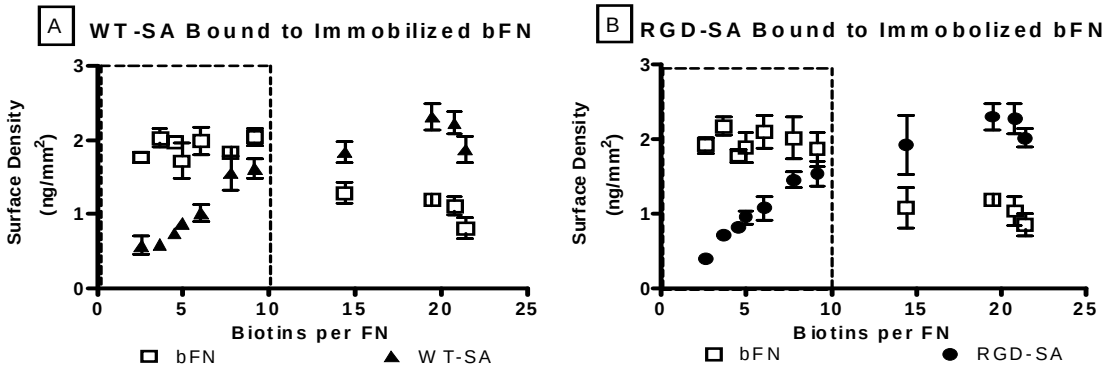

Figure 4.5. Amount of bound (a) WT-SA and (b) RGD-SA bound per immobilized bFN. All of these values were measured as a function of biotins. (n=4)

Figure 4.6 contains the molar binding ratio of WT-SA and RGD-SA per mole of immobilized bFN as a function of biotins per bFN molecule. There was remarkable similarity when these data were examined on a molar basis. The amount of bound WT-SA and RGD-SA were statistically indistinguishable ($p<0.01$) at each biotinylation level and increased linearly with slopes of 0.83±0.033 and 0.75±0.026 respectively.

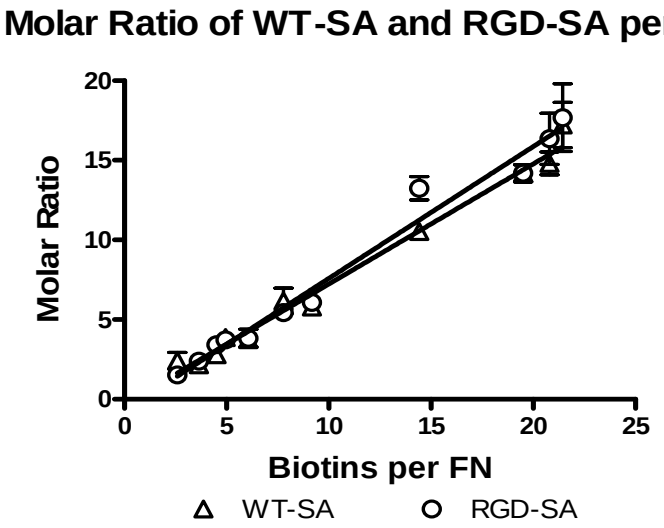

Figure 4.6 Molar ratio of WT-SA and RGD-SA per mole of bFN. Both are measured as a function of biotins per FN. Error bars represent SEM (n=3).

An antibody to biotin was used to determine number of available sites for binding on the immobilized bFN surface. Figure 4.7 displays the molar ratio of biotin antibody per immobilized mole of bFN. Note that there is a linear increase in number of surface biotins even at higher biotinylation levels when total amount of bFN immobilized begins to drop. All bound biotins, however, were not available for binding when immobilized on the 2-D substrate. A biotin monoclonal antibody was used to calculate the number of accessible surface biotins post immobilization in SPR. At all biotinylation levels, the surface biotin ratio ranged from 35% to 42% except in the cases containing molar excesses of 30, 40, and 50 where the percent surface biotin availability was 55, 64, and 72% respectively.

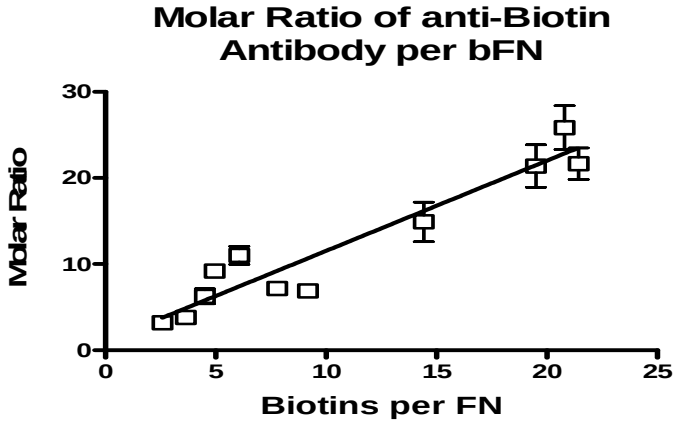

Figure 4.7. Molar ratio of biotin antibody bound to bFN determined by SPR binding

Figure 4.8a and 4.8b show the molar equilibrium dissociation constants for WT-SA and RGD-SA bound to immobilized bFN over the range of biotin molar excesses. The equilibrium dissociation constants (K_D) for all experimental groups ranged from $1.1x10^{-8}$ to $1.6x10^{-11}$ M for WT-SA and $1.1x10^{-7}$ to $5.3x10^{-11}$ M for RGD-SA bound to bFN. These dissociation constants were much higher than reported values for SA-biotin interactions in solution. However, dissociation constants of 10^{-7}-10^{-11} M are consistent with literature values observed with biotin functionalized macromolecules bound to immobilized streptavidin[136].

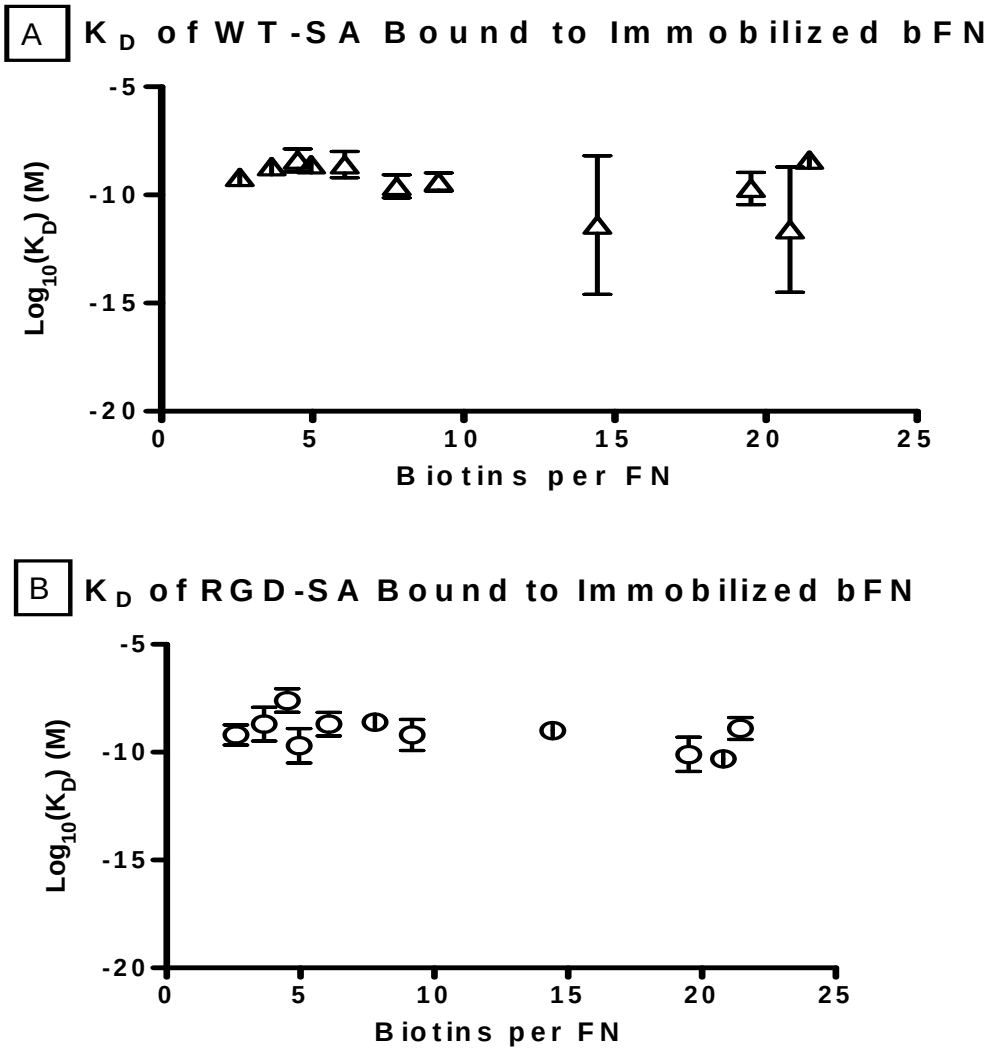

Figure 4.8. Equilibrium dissociation kinetic constants of (A)WT-SA and (B) RGD-SA.

Enzyme-Linked ImmunoSorbent Assay (ELISA)

ELISA with an antibody to the cell binding domain of FN was used to determine whether biotinylation affected accessibility of fibronectin's cell binding domain for bFN with <10 biotins per molecule. Figure 4.9 confirms that the binding of the antibody to the cell binding domain of FN and bFN was statistically indistinguishable ($p<0.05$). These results indicated that relatively mild biotinylation did not affect the accessibility of the cell binding domain when compared to the native un-modified protein.

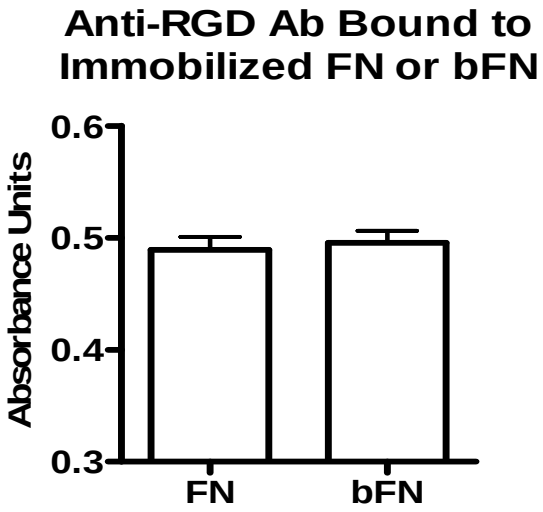

Figure 4.9. Absorbance units for native FN compared to biotin conjugate FN measured by ELISA. (n=3)

Fluorescence Activated Cell Sorting (FACS)

RGD-SA tagged with Alexa Fluor 488® was incubated with HUVECs and FACS was used to measure binding to cells and specificity of binding. Figure 4.10 HUVECs incubated with labeled RGD-SA ranging from 2µg to 60 µg.

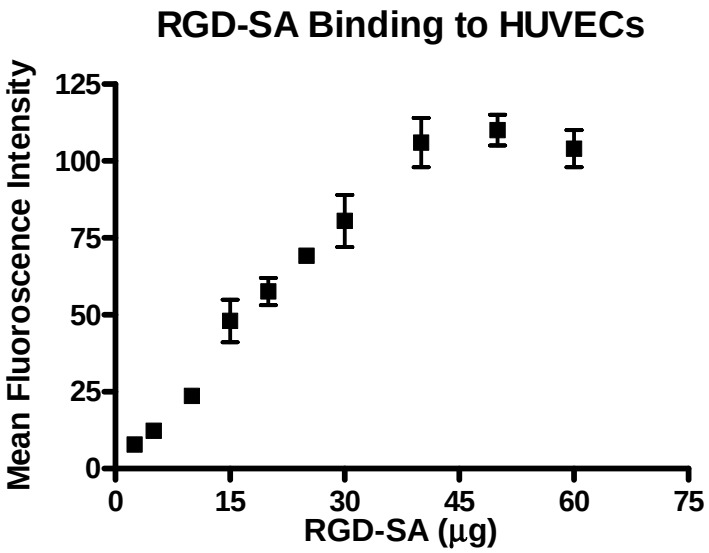

Figure 4.10. Labeled RGD-SA bound to HUVECs.
The curve appears to saturate at 50µg.

Mean fluorescence intensity increased linearly with increasing amounts of RGD-SA but appeared to saturate around 50µg. This was validation that RGD-SA bound easily to integrins on the cell membrane.

Blocking experiments using antibodies to $\alpha_5\beta_1$ and $\alpha_v\beta_3$ were done to measure the specificity of the RGD-SA attached to the cell surface. Figure 4.11 shows labeled RGD-SA binding to cells post incubation with unlabeled antibodies to $\alpha_5\beta_1$ and $\alpha_v\beta_3$. There was a statistical ($p<0.01$) difference in mean fluorescence when cells were pre-incubated

with the antibodies prior to treating with RGD-SA. This study validated that the RGD-SA is binding to the necessary surface receptors.

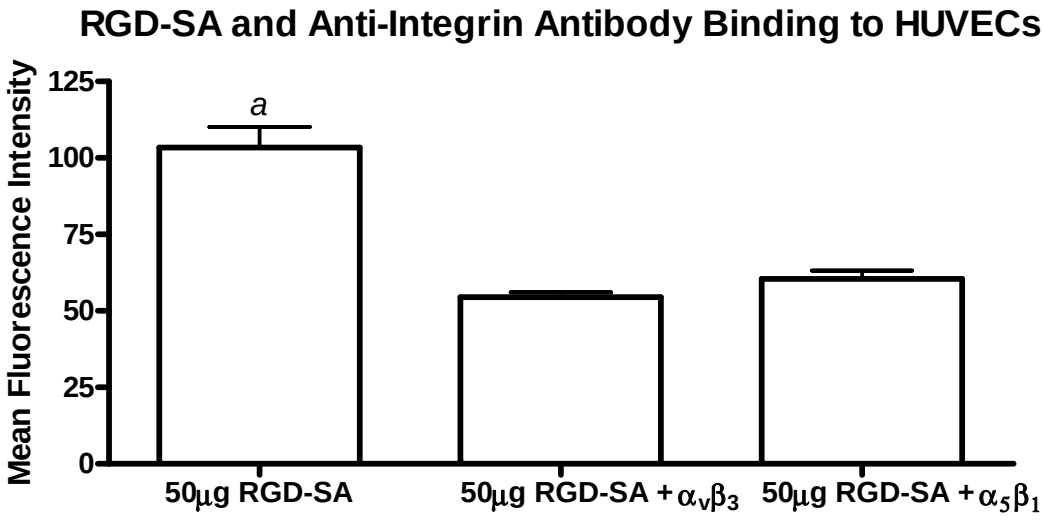

Figure 4.11. This RGD-SA binding to surface integrins was blocked by pre-incubation with antibodies to $\alpha_5\beta_1$ and $\alpha_v\beta_3$. a represents significantly greater fluorescence intensity over co-incubation groups. n=3

4.5 Discussion

Rapid cell attachment and spreading is essential in many biomedical applications. Most efforts to improve cell adhesion *in vitro* have used immobilized ECM proteins, but this approach has had limited success[66,131,132]. Any strategy to enhance cell binding and retention must bind cells in a manner that brings transmembrane integrins in close apposition to immobilized proteins, and in turn promotes the formation of mature focal contacts. Streptavidin-biotin binding is being explored as an adjuvant to the natural cell adhesion formulation because of its high binding affinity with a solution phase K_D of ~10^{-15} M.

Our group introduced a dual ligand (DL) protocol that takes advantage of the high affinity streptavidin-biotin interaction to buttress the integrin dependent cell adhesion interaction system. Biotinylated cells incubated with streptavidin were seeded onto surfaces preadsorbed with a mixture of fibronectin and biotinylated bovine serum albumin (bBSA). This system was ideal because of how quickly and efficiently cells and proteins could be biotinylated, each biotin is available to interact with 1 of 4 binding sites on the streptavidin, and the system is non-destructive to cell and protein functionality[114]. Since the initial system the protocol has been modified by introduction of a bifunctional RGD-SA mutant protein[105] as well as optimization on polymer surfaces with chemical properties more similar to vascular graft materials[104]. The current DL system employs two bifunctional protein constructs, RGD-SA and bFN, that both possess integrin-independent and integrin dependent binding properties. This construct is a shift from the

previous use of RGD-SA with bBSA as the biotin source in the system[105]. The use of human FN leaves open the potential for future clinical applications.

The essential benefit of the DL system comes from firm and stable interaction between biotin and streptavidin. In this study, the previously DL system was modified in order to increase the experimental efficiency, amenability to *in vivo* applications, and strength of adhesion by increasing number of biotins per fibronectin. The primary focus of this study was to understand the interaction between immobilized bFN with WT-SA and RGD-SA. SPR was used in this study to monitor the binding of WT-SA and RGD-SA to biotin functionalized FN. SPR binding efficiency and high kinetic binding affinity was best using EDC/NHS functionalization. The amount of bFN immobilized was relatively constant up to 10 biotins per FN at which point there was a decline in the amount bound. The decrease in bFN immobilization can be attributed to depletion of available amine groups by biotinylation, thus limiting accessibility of amine groups to EDC/NHS coupling. This drop, however, did not affect the proportionate increase in binding of WT-SA or RGD-SA to immobilized bFN. The linear increase is an indicator of increased surface biotin availability. This observation was also evident in the molar binding ratio of WT-SA or RGD-SA per bFN. The nearly 1:1 molar correlation with the number of biotins per FN indicates that only one SA binding site was occupied during each interaction.

The 1:1 correspondence was unexpected because there should be two accessible binding sites on each streptavidin. Given the calculated 2-D size of fibronectin and

streptavidin, the theoretical binding ratio under ideal conditions should approach a value of 4. This phenomenon does not appear to be occurring because the random orientation of the bound WT-SA or RGD-SA does not allow for structured binding where all SA binding sites are accessible to surface biotins. The reasons for the lack of bivalent binding may be due to surface induced conformational shifts in the binding sites, or the mass transfer limitations at the surface of the substrate[133]. More accurate control of surface biotin coverage has been shown by other groups to affect the SA binding site occupation[134]. It is clear from our results that the random orientation of the bound WT-SA or RGD-SA does not allow for structured binding where all SA binding sites are accessible to surface biotins.

SPR was used to confirm that the affinity of the SA-biotin interaction was conserved when biotin was attached to FN. Different levels of biotin incorporation were examined under the assumption that increased biotinylation would lead to increased binding affinity. This assumption was ultimately proven to be incorrect by SPR kinetic models. The binding kinetic analysis of WT-SA or RGD-SA for immobilized bFN was measured with the aid of a Langmuir model. The K_D in this system was 1.1×10^{-8} to 1.6×10^{-11} M for WT-SA and 1.1×10^{-7} to 5.3×10^{-11} M for RGD-SA. These values were a few orders of magnitude higher than that for streptavidin-biotin binding observed in solution, but were consistent with literature values for binding biotin functionalized molecules to SA[135,136]. Though Huang et al. worked with polystyrene beads with micron size diameters, there was evidence from their results to suggest that increased ligand size

increased dissociation constants[136]. This could explain the increase in dissociation kinetics on the 2-D FN surface.

Single SA-biotin valency binding appears to be dominant species across the range of biotins per FN. This indicates that though biotin density is increasing, there was no cooperative effect from the proximal biotins, i.e., binding occurs independently between one binding pocket of SA and biotin conjugated to FN. This noncooperative effect was observed previously by Jones et al. when they examined equilibrium distribution states of biotin in solutions with bound and unbound streptavidin[137].

Greater control over the biotin surface density could have led to greater cooperativity. Data from Jung et al. indicate that moderate biotin surface coverage, between 10% and 40%, facilitates doubly bound SA molecules[134]. Below this level, the binding was dominated by single bound SA. This may be the case with the current system because we have 72% coverage of the surface with biotinylated fibronectin.

Although our model ultimately showed no difference in affinity for WT-SA compared to the RGD-SA, the binding curves showed a slight desorption using the mutant strain. The overall results were promising because the affinity of biotin for SA was not diminished by coupling to fibronectin. The consistency of binding affinity and concentration levels between WT-SA and RGD-SA was further evidence that conjugation to these high molecular weight glycoproteins did not negatively affect the high affinity interaction. The most important information gained from this SPR analysis is that the binding affinity of WT-SA and RGD-SA for immobilized bFN was the same. This validates the utility of bFN for use in the DL system.

Biotin functionalization had no apparent affect on the availability of cell binding domains as seen by ELISA; evidence that the non-specificity of biotinylation does not interfere with the cell binding function of bFN. This is essential given that the effectiveness of the system would be diminished if the cell binding domain was blocked. The availability streptavidin binding sites for surface adsorbed bFN was demonstrated by FACS. Incubation of cells with increase amounts of RGD-SA showed an increase in bound protein. The amount bound at the highest level was quenched by pre-incubation with antibodies to $\alpha_5\beta_1$ and $\alpha_v\beta_3$ integrins. This demonstrated specificity means that our system is primed to take advantage of all binding relationships presented with the dual ligand model.

4.6 Conclusion

These studies validated the utility of the different parameters involved in dual ligand binding. Effective biotinylation of fibronectin was achieved without masking accessibility to the cell binding domain for integrins at <10 biotins per FN. Kinetic analysis by SPR verified that affinity of bound biotin was the same for WT-SA as well as RGD-SA. Additionally, no enhanced kinetic effect was observed with higher biotins per FN underscoring the lack of positive cooperativity in the system. FACS confirmed binding and specificity of RGD-SA to cell membrane receptors. Detailed studies need to be conducted to verify that these binding relationships confer greater cell spreading and retention when used on synthetic vascular graft surrogates.

Chapter 5. Sequentially adsorbed bFN(9) with RGD-SA gives enhanced cell functionality over cells incubated with RGD-SA prior to seeding

5.1 Synopsis

Complete endothelialization is necessary for patency and biointegration of synthetic vascular grafts. A functional neointima will mimic native vessel functionality and mitigate the thrombotic nature of the current materials available for SVG. In Chapter 3 we identified synthetic vascular graft surrogates and subsequently demonstrated the utility of biotin functionalized fibronectin to retain high affinity interaction with streptavidin without blocking accessibility to the RGD binding motif in Chapter 4. Here, modifications were made to the DL approach to address the observation that the current DL formulation failed to show an enhancement in cell spreading and percent retention when compared to using fibronectin alone[106]. The goal of these experiments was to modify properties of the DL to show an enhanced cell seeding and retention profile. The current methodology's major delineation from past procedures was the sequential co-adsorption of biotinylated fibronectin (bFN) and mutant streptavidin RGD cell binding domains (RGD-SA) onto a Teflon-AF surface prior to incubation with untreated cells in a quadriperm™ plate. This method has the advantage of not occupying transmembrane integrin binding sites. The procedural shift is highlighted in figure 5.1. Surfaces with no protein, bFN alone, and bFN with WT-SA served as controls. This model validated the amenability of bFN to improve cell adhesion and retention in the dual ligand model. We observed a significant difference in spreading when using the modified dual ligand compared to FN alone as well as a greater degree of focal adhesions formation as

observed using vinculin immunocytochemistry. It is important to note that there was no statistical difference seen in cell retention between the modified DL and FN alone underscoring the experimental observation that cell spreading is not directly analogous to cell retention.

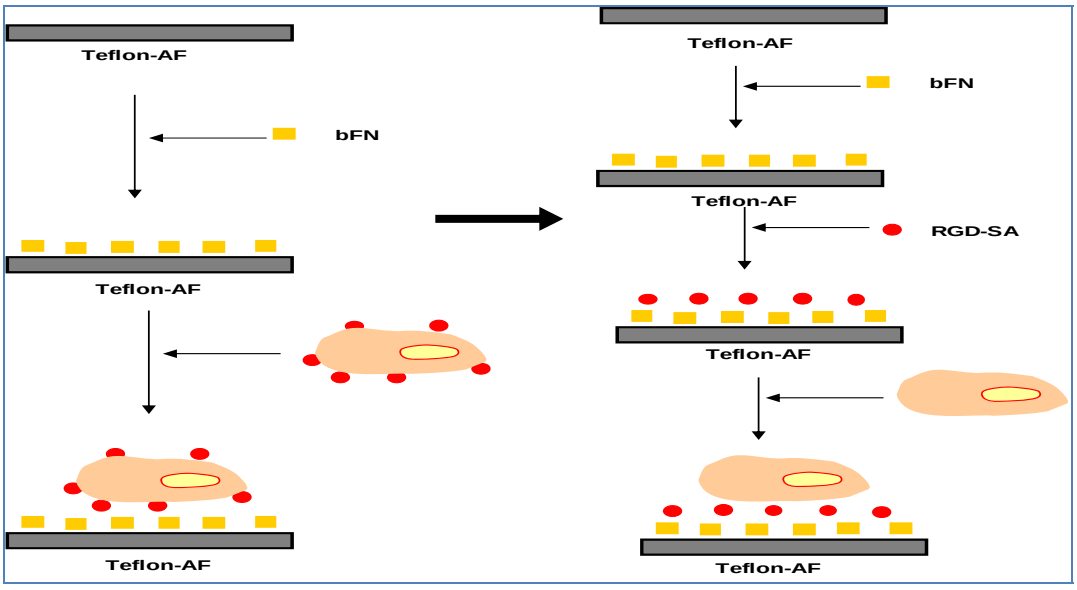

Figure 5.1. A cartoon demonstrating the shift from the old Dual Ligand procedure to the current set up where the surface is adsorbed with RGD-SA rather than incubating on the cell surface. All cell functionality experiments will be conducted on Teflon-AF because our current *in vivo* model uses Goretex™ grafts.

5.2 Background

Understanding protein biomaterial interaction is central to the field of tissue engineering. Protein adsorption has been used in the field of vascular tissue engineering to enhance cell attachment, spreading, and formation of neointima in synthetic vascular grafts. Initial studies utilized single proteins like fibronectin, vitronectin, and laminin to bind cells to the material surface[107,122]. These surface modifications were insufficient to promote firm cell attachment and formation of mature focal contacts within a physiologically relevant time period that resisted thrombosis, intimal hyperplasia, and leukocyte adhesion[9]; due partially to low binding affinity (Ka $\sim 10^6$ M^{-1}) between transmembrane integrins and ECM proteins. This problem could be remedied by using a dual ligand (DL) cell attachment system that augments standard FN-integrin binding with high affinity streptavidin-biotin (K_A in solution $\sim 10^{15}$ M^{-1}) bonding which can effectively augment the standard protein system without any negative biological effects. The binding strength of streptavidin-biotin makes it amenable to several applications. Different groups have used the system to enhance chondrocyte adhesion to tissue culture polystyrene as an indication of future tissue engineering viability[125], hepatic cell binding and spreading on biodegradable, polymer-based, flat 2-D surfaces, and in highly porous 3-D scaffolds [126], and for drug delivery using avidin to immobilize biotinylated therapeutic agents[127].

Our DL achieved desired results on glass but equivalent results were not similarly maintained on synthetic vessels in an *in vivo* model. We have taken several steps to create an *in vitro* model that better approximates behavior on synthetic vascular grafts.

First, attempts to understand this anomaly seen in *in vivo* involved identification of synthetic vascular graft surrogates with the assumption that they would better approximate protein adsorption and cell binding[104]. Secondly, we introduced biotin functionalized fibronectin into the system to replace biotinylated bovine serum albumin as the biotin source[138]. This has the advantage of not only introducing another bi-functional peptide, but also eliminates the xenogeneic protein source. SPR data suggested roughly ideal binding behavior for bFN with <10 biotins per molecule and steric hindrance above this level. For this reason, all future studies involving biotin functionalized fibronectin will be using fibronectin with 9 biotins (bFN9).

The current shift addresses another component of this procedure: direct incubation of HUVECs with RGD-SA prior to incubation on Teflon-AF surfaces adsorbed sequentially with bFN. The impetus for shifting to co-adsorption of bFN(9) and RGD-SA on the substrate surface was based on experimental observations that incubation of cells with RGD-SA did not demonstrate enhanced cell spreading or retention over using FN alone. Direct incubation may have a few major issues: 1) the incubation period is beyond the time necessary integrin internalization[108]; 2) remodeling of the cell membrane presents non-ideal conformation for efficient RGD-SA binding to the surface; [139,140]; 3) RGD-SA molecules block transmembrane integrins necessary for binding once the cells reach the surface. These effects have even greater consequences when the cells have been harvested using aggressive trypsinization conditions[106] since their integrin numbers are decreased. Does eliminating direct binding of RGD-SA to the cells give enhanced affects over using FN alone? To address this question we examined cell spreading, cell retention,

and formation of focal adhesions of untreated HUVECs seeded onto Teflon-AF slides pre-adsorbed with bFN(9) and RGD-SA. Figure 5.1 shows a cartoon of the current procedural shift.

5.3 Materials and Methods

Cell Culture

All cell culture reagents were obtained from Cambrex (Walkersville, MD) unless otherwise specified. Human umbilical vein endothelial cells (HUVEC) were grown to confluence in gelatin coated T25 polystyrene flasks (Corning Inc., Corning, NY) with endothelial basal media (EBM) supplemented with 0.5ml 10 mg/ml hEGF (human recombinant Epidermal Growth Factor), 0.5 ml 1.0 mg/ml Hydrocortisone, 0.5 ml of 50 mg/ml Gentamicin and 50 mg/ml Amphotericin-B mix, 3 mg/ml bovine brain extract (BBE), and 10 ml Fetal Bovine Serum (FBS). Cells were cultured in an incubator with 95% air/5% CO_2 at 37 ^{o}C. HUVECs from passage 3-6 were used for all experiments. For all experiments, confluent p2-5 HUVECs were trypsinized with 0.025% Trypsin/EDTA for 4 min at 37 ^{o}C, neutralized with trypsin neutralizing solution (TNS), and centrifuged at 2200 rpm for 5 minutes. These were resuspended in fresh serum free media. Figure 5.2 is a flowchart indicating the current experimental parameters.

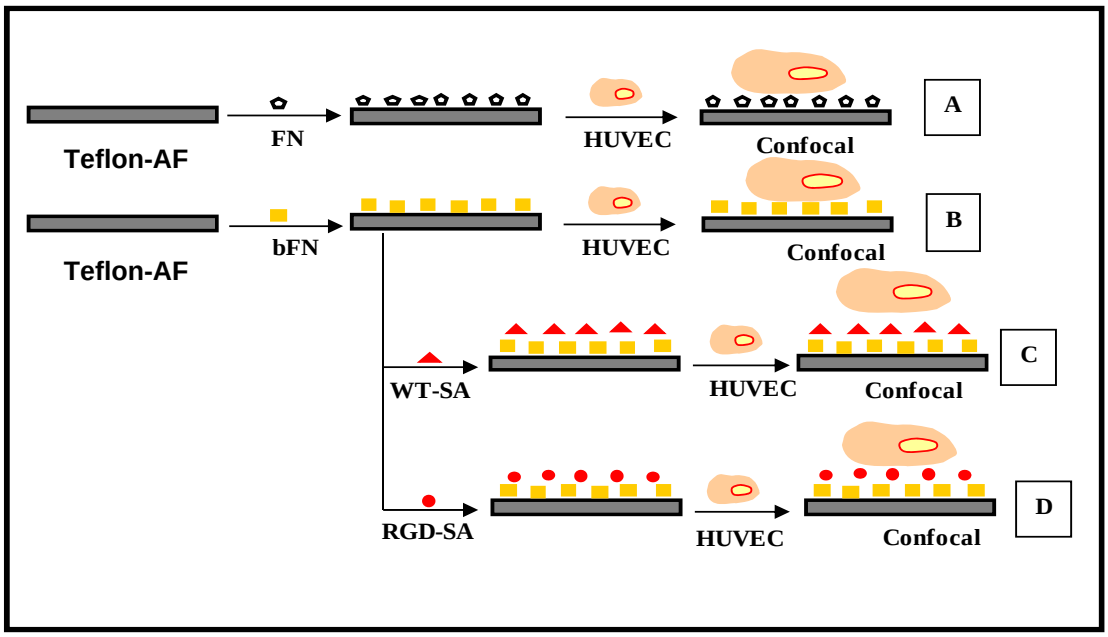

Figure 5.2. Experimental flowchart of the different formulations examined in the current study and their respective method of analysis. In addition to Confocal analysis, cell spreading measurement and strength of attachment studies were also conducted.

Cell Spreading

Cell spreading was measured as previously detailed{Anamelechi, 2005 650 /id}. Briefly, 6 well plates were blocked with BSA for 30 minutes. 0.9 inch squared Teflon-AF covered slides were placed into the wells and treated with either 20µg/ml solution of FN alone, bFN(9) alone, bFN(9) with 50 µg/ml WT-SA, or bFN(9) with 50µg/ml RGD-SA. Slides containing FN or bFN(9) alone were allowed to adsorb for 1 hour before rinsing with Dulbecco's phosphate buffered saline (dPBS) with Ca^{2+} and Mg^{2+}. Attachment of WT-SA or RGD-SA required an additional 40 minutes of incubation after which the surfaces were rinsed similarly with dPBS with Ca^{2+} and Mg^{2+}. After protein attachment, 1ml of serum free media containing 45,000 HUVECs stained with 2µM CellTracker

Orange (Invitrogen, Carlsbad, CA) for 10 minutes at 37 ^{o}C was incubated with each slide. Fluorescent images were obtained at 5 minutes, 30 minutes, 60 minutes, and 90 minutes on a Zeiss Axiovert S-100 inverted microscope connected to a digital camera interfaced with a computer. Spots were place underneath the six well plates to ensure repeated imaging at the same positions on the slide. Cell spread area was measured by hand using ImageJ software and convert to spreading rate based on differences in cell area at each time point analyzed.

Cell Retention

Cell retention analysis was performed as previously published[104] with minor modifications. $2x10^5$ HUVECs in 7 ml of serum free media were treated with Hoechst dye (Molecular Probes, Carlsbad, CA), and placed in an incubator for 15 minutes on a rotator, and then seeded onto Teflon-AF coated glass slides with the same pretreatments noted in figure 5.2. The slides with cells were incubated in the quadriperm™ plates for 1 hour prior to being assembled into a variable height flow chamber and assembled into a flow loop containing the chamber, a media reservoir, a pulse dampener, and Cole Parmer (Vernon Hills, Ill) peristaltic pump (figure 5.3). The chamber was comprised of an aluminum bottom plate and an acrylic top plate with dimensions of 17.7 x 4.4cm. The gradient on the top plate varied in the x-direction to generate a range of shear stresses according to:

$$\tau_w = \frac{6\mu Q}{wH(x)^2} \qquad (1)$$

where μ is the viscosity of the flow media, Q is the flow rate, w is the width of the flow field and H is the height. The flow media was adjusted to 4 cP, the viscosity of blood, by addition of 4.82% Dextran to 500mL PBS with Ca^{2+} and Mg^{2+}.

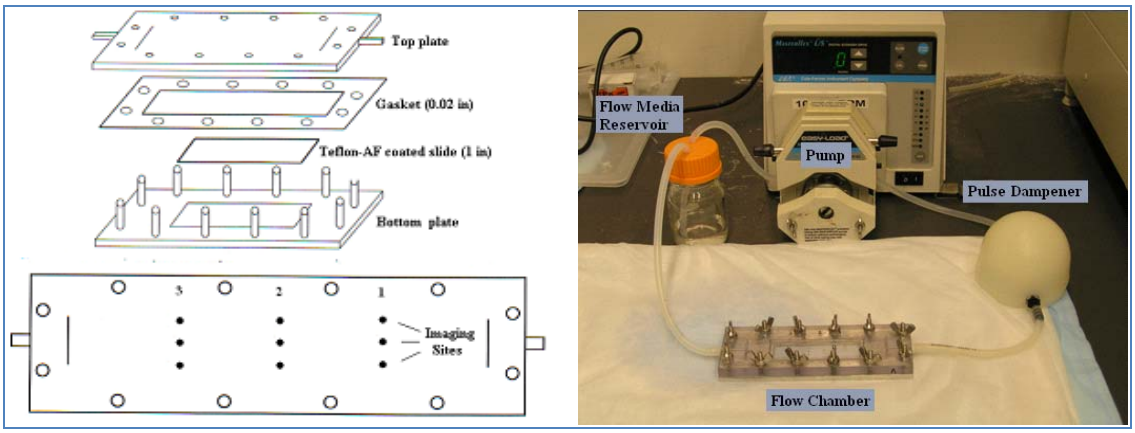

Figure 5.3. A schematic drawing showing the different components of the flow chamber. On the left is a top view of the top plate indicating positions used for imaging. The right image shows the flow loop used for conducting shear stress experiments.

Nine images were obtained pre and post flow at designated positions in the viewing region of the flow chamber using the fluorescent microscope. The imaging sites were separated by 0.25cm along the x-direction in the viewing field of the flow chamber. Cells were perturbed for 2 minutes in a variable height flow chamber with shear stresses ranging from 20-120 dynes/cm^2. Images were analyzed in ImageJ using a Matlab code that was verified to have an error rate of less than 5% when compared to hand counting

using randomly chosen images. Figure 5.4 shows the detailed procedure for conducting image analysis using this macro.

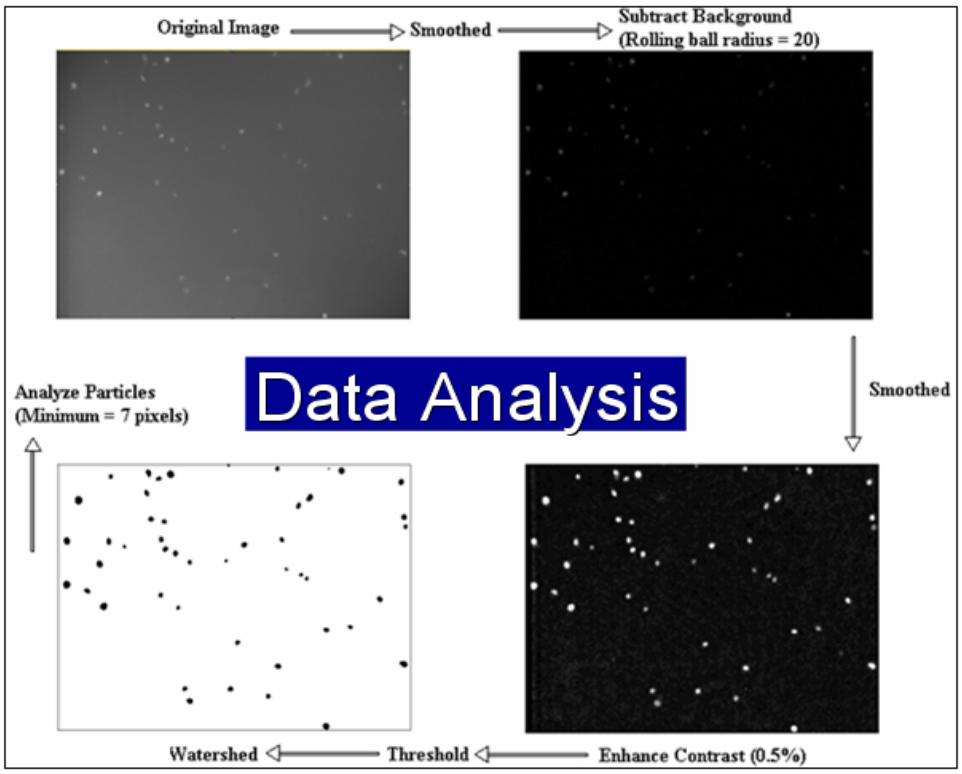

Figure 5.4. Simplified outcomes of macro used to count the cells in pre and post flow images for percent analysis. Briefly, each image analyzed as follows: smooth, subtract background (rolling background of 20), smooth, enhance contrast 0.5%, threshold, watershed, and analyze particles (minimum = 7 pixels).

Post flow images obtained at the predefined points were used to measure relative percent retention.

Immunofluorescent Stain for Focal Adhesions

Glass coverslips were cleaned as described in Chapter 2 and inserted into sterile 12 well plates. Slides were incubated with 20µg/ml of FN or (bFN) with 9 biotins for 1 hour at 37 ^{o}C, rinsed 3x with dPBS, and blocked with 2mg/ml BSA for 30 minutes at 37 ^{o}C. Coverslips were rinsed 3x with dPBS then incubated with 50µg/ml of either WT-SA RGD-SA for 40 minutes in an incubator. Coverslips were rinsed and incubated with 40,000 cells in 1ml of serum free media in an incubator. After a 1 hour attachment, cells were fixed with 3.7% fresh paraformaldehyde for 20 minutes at room temperature, permeabilized for 5 minutes with 0.2% Triton X-100 (Sigma), and washed 3x for two minute intervals on shaker with dPBS. Cells were blocked with 15% goat serum for 30 minutes in an incubator to prevent non-specific binding then incubated with 1:100 mouse anti-human vinculin antibody in 1% goat serum for 1 hour in an incubator. Cells were washed 3x for 10 minute cycles on shaker using PBS with 0.05% Tween-20 at room temperature. Cells were then incubated with 1:700 goat anti-mouse Alexa-Fluor 488 secondary antibody for 45 minutes in incubator, washed, and mounted onto glass slides using FluorSave™ (Calbiochem). Images were captured the next day using a confocal laser scanning microscope (Carl Zeiss Inc.). LSM 510 image processing tool was used to quantify size of focal contacts and number of focal adhesions was quantified using ImageJ.

Statistical Analysis

StatView 5.0 was used to statistically compare data and measure variability. One-way ANOVA plus Tukey-Kramer post hoc analyses were conducted to determine *p* values. All data reported as the mean ±SE.

5.4 Results

Cell Spreading

Cell spreading was examined over a 90 minute period on substrate treatments outlined in figure 5.2. Spreading rate was preferred over total cell spreading because calculation of initial cell seeding areas indicated a wide enough variability in cell seeding size that the total cell spread area could be misleading at such a short time point. Figure 5.5 shows cell spreading rate of untreated HUVECs attached to surfaces preadsorbed with FN alone, bFN(9) alone, bFN(9) + WT-SA, and bFN(9) + RGD-SA over a 90 minute period.

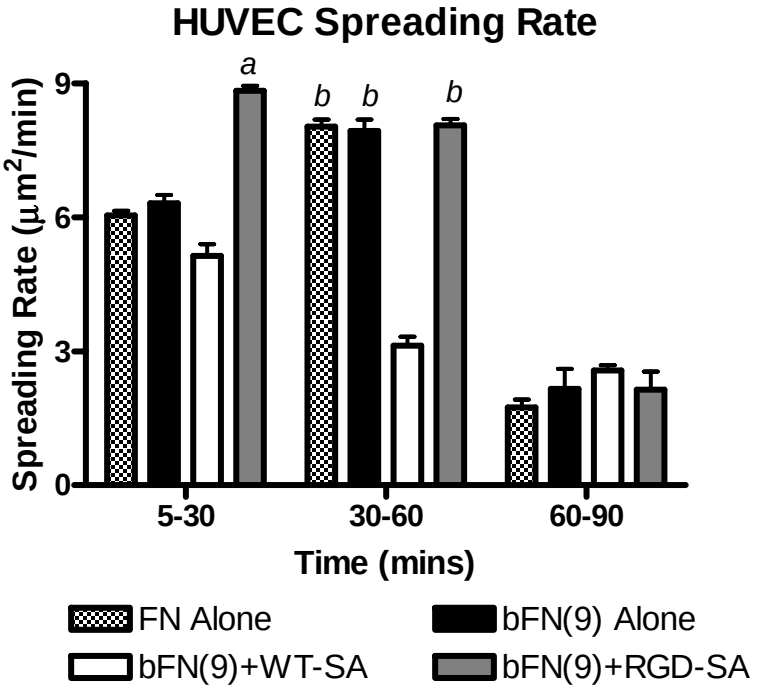

Figure 5.5. Cell spreading rate over a 90 minute period on Teflon-AF™ (n=4). [a] represents significantly ($p<0.05$) greater spreading than all other treatment groups. [b] represents significantly ($p<0.05$) greater spreading than on bFN(9)+WT-SA. Spreading is dominated early by the DL system but after 30 minutes there is no statistical difference between using the DL compared to FN or bFN(9) alone.

Figure 5.5 highlights the enhanced benefit of using the DL to promote faster spreading. After 30 minutes the spreading rate was equivalent for the DL, FN alone, and bFN(9) alone. There was no statistical difference in cell spreading rate when bFN(9) was compared to FN alone at all time points further confirming the similarities in cell binding properties between native FN and modified FN. Spreading rate using unmodified HUVECs was statistically higher than using RGD-SA-HUVECs for all surface treatments (figure 5.6).

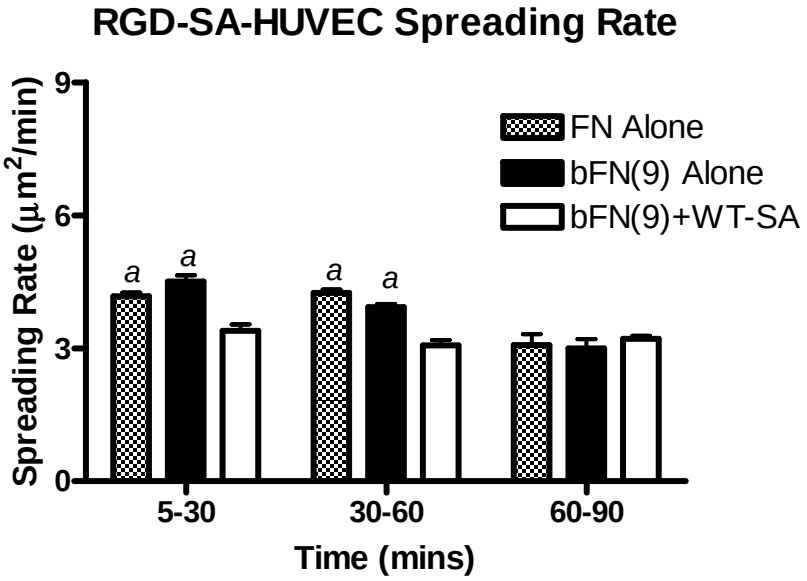

Figure 5.6. Cell spreading rate of RGD-SA-HUVECs over a 90 minute period. [a] represents significantly ($p<0.05$) greater spreading than bFN(9)+WT-SA. Spreading rate was similar on FN alone and bFN(9) surfaces. (n=3)

Cell spreading rate with RGD-SA-HUVEC across the 90 minutes measured was 22.7% lower on FN alone surface, 22.4% lower on bFN(9) alone surface, and 11% lower on bFN(9)+WT-SA surface. These decreased spreading values suggest that intrinsic integrin

properties may be blocked by incubation with RGD-SA, occupation of these integrins may be limiting accessibility of surface RGD binding motifs for transmembrane integrins, or that RGD-SA bound to the cell membrane may not be oriented optimally to attach to surface immobilized proteins. All these factors could hinder the rapid binding and spreading of cells on the protein surface.

Cell Retention

Cells seeded onto Teflon-AF surfaces with different protein formulations were examined for cell retention in a variable height flow chamber for 2 minutes at 60 dynes/cm^2. Figure 5.7 shows untreated HUVECs retention on surfaces preadsorbed with FN alone, bFN(9) alone, bFN(9)+WT-SA, and bFN(9)+RGD-SA .

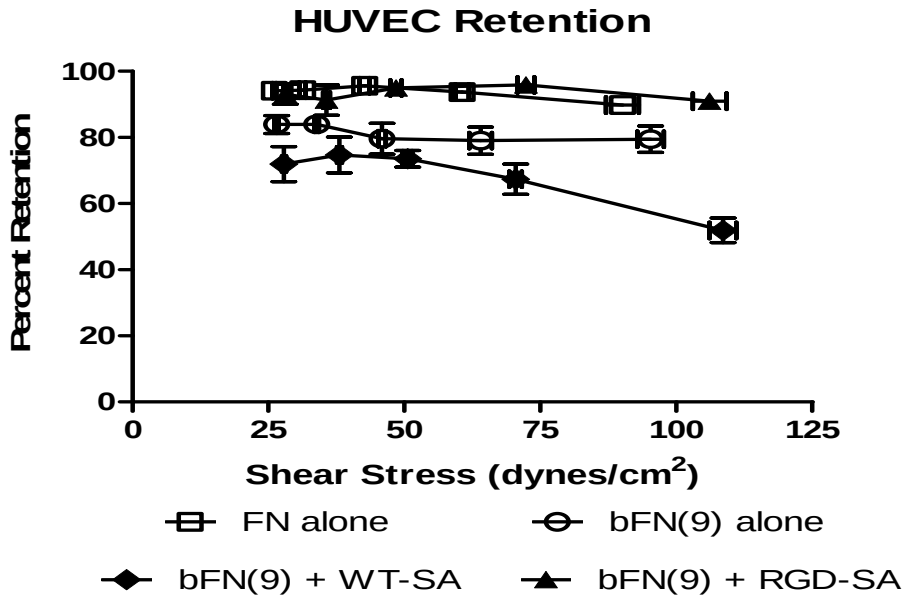

Figure 5.7. Untreated HUVEC percent retention on protein treated Teflon-AF (n=4). The bFN(9)+WT-SA treatment group showed statistical significance, but only at higher shear stresses. n=3

Though cell retention was high (~80%) in all cases examined except for bFN(9)+WT-SA, there was no increased effect on percent retention when comparing FN alone surfaces to bFN(9) + RGD-SA surfaces. This is inconsistent with the results of the cell spreading studies.

Vinculin Localization

Immuno staining for Vinculin was used to examine two phenomena: 1) the similarity in formation of focal adhesions between native and FN and bFN and 2) the ability to modulate the formation of focal adhesions using either WT-SA or RGD-SA. Figure 5.8 contains images of focal adhesions of the four conditions shown in Figure 5.2:

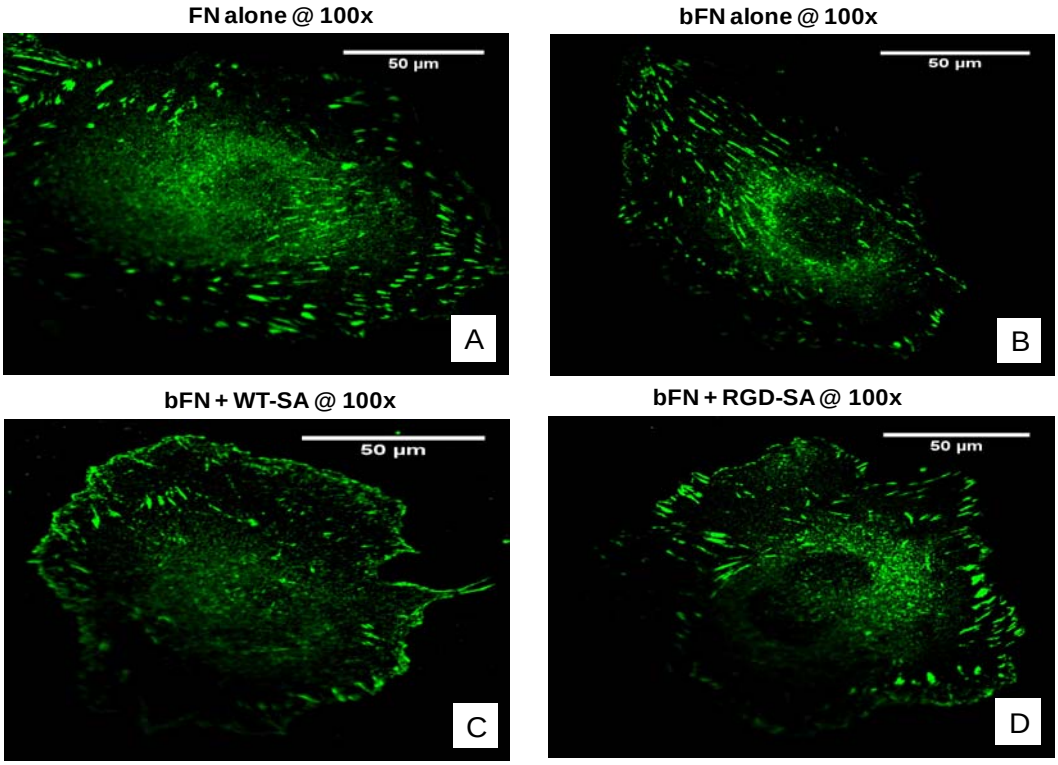

Figure 5.8. Focal adhesion formation with HUVEC bound to: FN (A); bFN (B); WT-SA-bFN (C); RGD-SA-bFN (D). (n=3)

Table 5.1 summarizes the percentage of HUVECs that exhibited focal contacts, the number of focal contacts per cell, and the average size of the focal contacts. These values were averaged over thirty confocal images of adherent cells with 10 images analyzed per experiment.

Table 5.1. Quantitative analysis of focal adhesions (FA) for HUVEC seeded onto glass cover slips for 1 hour with surfaces A-D.

Surface Treatment	Percent of Cells with FA	Average number of FA per cell	Average Size of FA (μm^2)
FN (A)	100	308.3±30.7$^{\#}$	1.73±0.19
bFN(B)	100	309.0±18.0$^{\#}$	1.57±0.10
bFN + WT-SA (C)	62.4±23.1**	203.2±12.2	1.22±0.15
bFN + RGD-SA (D)	100	430.0±19.9**,$^{\#}$	1.84±0.17

Values are reported as mean±SE for n=3. Column statistics are performed using ANOVA and Tukey-Kramer post hoc tests. **indicates significantly different compared to all other treatment groups ($p<0.01$); #indicates significantly different compared to bFN+WT-SA ($p<0.05$).

All of the cells on FN, bFN and bFN+RGD-SA exhibited focal contacts, while only 62% showed focal contacts when bFN was blocked with WT-SA. Cells on FN and bFN exhibited nearly identical focal adhesion density per cell. Cells on bFN+RGD-SA had 40% more focal adhesions per cell when compared to FN and bFN alone; whereas bFN+WT-SA had 44% fewer focal adhesions per cell compared to FN and bFN. There were no differences in the size of focal adhesions between any treatment groups at $p<0.01$.

5.5 Discussion

The endothelialization of vascular grafts has been sought vigorously by a number of groups who have taken a variety of approaches for at least 20 years[24]. Rapid cell attachment and spreading is essential in many biomedical applications. Most efforts to improve cell adhesion *in vitro* have used immobilized ECM proteins, but this approach has had limited success[66,131,132]. Even with significant advances within the last 10 years, primarily due to improvements in cell culture techniques, the promise of a patent small diameter vascular graft has yet to be realized. Technical hurdles to successful graft patency that still exist are low spontaneous re-endothelialization in humans[141] and inability of seeded cells to resist shear stress due to post operative blood flow[7].

Any strategy to enhance cell binding and retention must bind cells in a manner that brings transmembrane integrins in close apposition to immobilized proteins, and in turn promotes the formation of mature focal contacts. Our group has introduced a methodological shift from the original DL that used RGD-SA with bBSA as the biotin source in the system[105]. The current DL system employs two bifunctional protein constructs, RGD-SA and bFN, that both possess integrin-independent and integrin dependent binding properties. Previous studies confirmed the utility of this system for cell adhesion experiment[138]. The use of human FN leaves open the potential for future clinical applications. Other groups have used the avidin-biotin system to bind biotinylated chondrocytes to Avidin coated tissue culture polystyrene plates (TCPS)[125] and more recently, Kojima et al. demonstrated the effectiveness of binding biotinylated hepatic cells to poly l-lactic acid (PLLA) surfaces[126,134]. Others have examined the

binding affinity of streptavidin to surface immobilized biotin with varying densities and showed that the dissociation rate is a function of surface biotin density[134,142]. Single biotin has also been used but primarily as a separation or extraction ligand[143,144].

In this study, the previously DL system was modified in order to increase the experimental efficiency, amenability to *in vivo* applications, and adhesion complex by eliminating the direct incubation of RGD-SA with the cells prior to incubation. The primary goal of these experiments was to understand how availability of integrins on the cell surfaces effects cell spreading, cell retention, as well as formation of focal contacts.

HUVEC spreading rate up to 90 minutes with different adhesion ligands were monitored on Teflon-AF. Spreading on bFN+RGD-SA surface was significantly greater than all other surface and bFN alone and FN were statistically greater than surfaces with bFN+WT-SA. Statistical analysis confirms that the DL dominated spreading at this short time point. However, cell spread rate analysis at each imaging time point showed a rapid increase in cell spreading using the DL until 30 minutes at which point the rate of increase decreased until the 90 minute time point. This suggests that rapid attachment is occurring with the DL, but over time, the intrinsic integrin-mediated binding dominates.

Cell retention analysis was measured with HUVECs seeded onto Teflon-AF surfaces with different protein formulations in a variable height chamber with shear stresses ranging from 20-120 dynes/cm^2. There was no increase in percent cell retention with the DL compared to FN alone. While these values observed with the current setup were higher than what has been traditionally seen with this system[145], the lack of

statistical difference between the DL and system using FN alone was somewhat confounding.

Finally, biotin functionalization had no apparent effect on the availability of cell binding domains as seen by ELISA in the previous chapter. This is evidence that the non-specificity of biotinylation does not interfere with the cell binding function of bFN. This was essential given that the effectiveness of the system would be diminished if the cell binding domain was blocked. Further verification of the new modification was seen with vinculin immunofluorescent staining. Quantification of the focal adhesions confirmed that the biotinylation of fibronectin had no adverse effect on its utility in forming focal contacts after short seeding times. The prevalence, number, and size of focal adhesions were not different between native FN and bFN. Biotin functionalization did not have an adverse effect on the ability to form focal adhesion. Additionally, the DL system showed enhanced ability over FN and bFN alone in promoting statistically higher focal adhesion density as well larger focal contacts; the latter was an indication of the maturity of the focal adhesion[146,147]. This effect was enhanced in the DL because of the availability of additional RGD motifs that promoted greater formation of focal adhesions. Conversely, surfaces coated with bFN then incubated with WT-SA showed no enhanced effect and even showed decreased prevalence, number, and size of focal adhesions when compared to the other treatment groups. The large WT-SA molecule on top of the bFN layer may quench the cell adhesion effect by blocking essential domains necessary to promote formation of focal adhesions.

5.6 Conclusion

This current study examined the utility of biotinylated FN as an improvement to the DL system. Cell spreading was significantly higher on DL surfaces than on any other surface but this difference was not observed with cell retention analysis. The strong adhesion strength, however, means that this system may be used to enhance cell adhesion and presents a new strategy for promoting rapid cell attachment and spreading. Biotinylated FN also behaved similar to FN in promoting focal adhesion formation but has an enhanced effect in density of focal adhesion when used in the DL system. Further studies need to be conducted to deduce the overall affect of the DL system in short term studies.

Chapter 6. Examination of cell adhesion under dynamic seeding conditions as a function of surface adsorbed protein and Trypsin/EDTA (T/E) concentration.

6.1 Synopsis

Surface modification with exogenous extracellular matrix protein has emerged as a potential approach to promote neotimal formation, mitigate acute restenosis, and improve patency in synthetic vascular grafts. The goal of the current studies was to determine the ability of Teflon-AF surfaces sequentially adsorbed with biotinylated fibronectin (bFN) and mutant strain streptavidin (RGD-SA) to capture and retain dynamically-seeded un-modified HUVEC on the surface as a function of seeding time, different flow rates, trypsinization conditions, and shear stress. We refer to this sequentially adsorbed formulation as the dual ligand (DL). Surface plasmon resonance (SPR) spectroscopy was used to measure the amount and specificity of $\alpha_5\beta_1$ and $\alpha_v\beta_3$ integrins bound to immobilized bFN compared to the co-immobilized DL in an attempt to determine the dominant binding pathway with each protein individually and also in the co-adsorption case. In inter-experimental comparisons between 0.025% trypsin and 0.05% percent trypsin in the dynamic seeding experiments, the lower trypsin concentration showed greater cell adhesion after dynamic seeding and higher percent retention after flow. Intra-experiment statistics confirmed that the DL system was better than all other surfaces at promoting rapid cell attachment and retention. In all formulations, surfaces with no ligand treatment showed the lowest cell adhesion after dynamic seeding as well as the lowest percent retenton after flow. A mathematical model confirmed that the DL had a statistically higher rate of cell adhesion compared to other

surface treatment independent of T/E concentration. Observations with the cells isolated using 0.5% Trypsin/EDTA suggests that the DL may play a recovery role for cells isolated under harsh conditions. SPR analysis verified the ability of the DL surface treatment to bind $\alpha_5\beta_1$ and $\alpha_v\beta_3$ independently. $\alpha_5\beta_1$ binding to immobilized bFN was significantly higher than $\alpha_v\beta_3$ but this trend was reversed when integrins were bound to surface immobilized RGD-SA. The current studies demonstrate the ability of the DL system to take advantage of two independent highly efficient intrinsic cell binding pathways to promote rapid adhesion and retention at short time points. This could have benefits in neotimal formation on synthetic vascular grafts.

Nomenclature Clarification: When referring to the dual ligand in this chapter, the discussion is strictly speaking of the co-adsorption of bFN with RGD-SA incubated with unmodified endothelial cells.

6.2 Background

The binding interaction between cells and their extracellular matrix (ECM) components play in integral role on regulating cell morphology, growth, differentiation, and motility. These effects have broader implications on adhesion and attachment of cells to synthetic vascular grafts. Adhesion promoting ECM proteins like fibronectin (FN), laminin (LN), and vitronectin (VN) are multidomain molecules which interact mainly with cell surface integrin receptors[11,87,148]. Of these cell binding domains, the most widely studied of these is Arg-Gly-Asp (RGD) which is located within the cell binding region of the ECM proteins and preferentially binds to specific transmembrane integrins based its location and orientation[149,150]. Moreover, positioning and density of the RGD binding motifs on the polymer materials plays an important role on focal adhesion (FA) formation and cell migration[86,151].

Binding of cells to surface immobilized proteins is dominated by two main integrins: $\alpha_5\beta_1$ and $\alpha_v\beta_3$. Once cells bind, integrins cluster to induce complexation of proteins on the cytoplasmic side of the membrane[152] and this initiates early actin polymerization[153]. These so called "early-stage" focal contact are rich in $\alpha_v\beta_3$ integrins. In the presence of fibronectin (FN), $\alpha_5\beta_1$ integrin modulate the formation of fibrillar adhesions while $\alpha_v\beta_3$ remain to develop into mature focal contacts[154,155]. This specific interaction of FN with $\alpha_5\beta_1$ is due to the synergy PHSRN but $\alpha_v\beta_3$ mediated interactions are not affected by the synergy site. These two integrins have been shown to activate independently activate RhoA-GTP binding[156]. RhoA is implicated in actin polymerization and maturation of matrix adhesions to mature focal contacts.

It has been widely acknowledged that cell to surface behavior is determined by sensing of the chemical and physical environment of the substrate. These interactions are influenced greatly by the density and organization of specific ECM proteins. Understanding how adhesion mediated interactions are regulated by spatial arrangement of the ECM has been elucidated through micro- and nanopatterning technologies[149,151]. These researchers quantified the effects of adsorption and density of cell adhesion molecules on cell adhesion and functionality.

In this study, we exploit the increased density of RGD binding motifs introduced by co-adsorption of RGD-SA with bFN to facilitate enhanced cell adhesion and retention on dynamically seeded HUVECs. The main questions asked in this study were: i) Was co-adsorption of RGD-SA with bFN more effective at promote cell adhesion and retention over FN alone? ii) What impact does Trypsin/EDTA concentration have on the impact of the DL? Figure 6.1 is a flowchart indicating the current experimental parameters. For all studies in this aim, the term DL refers to the substrate sequentially adsorbed with bFN and RGD-SA prior to incubating with un-modified HUVEC.

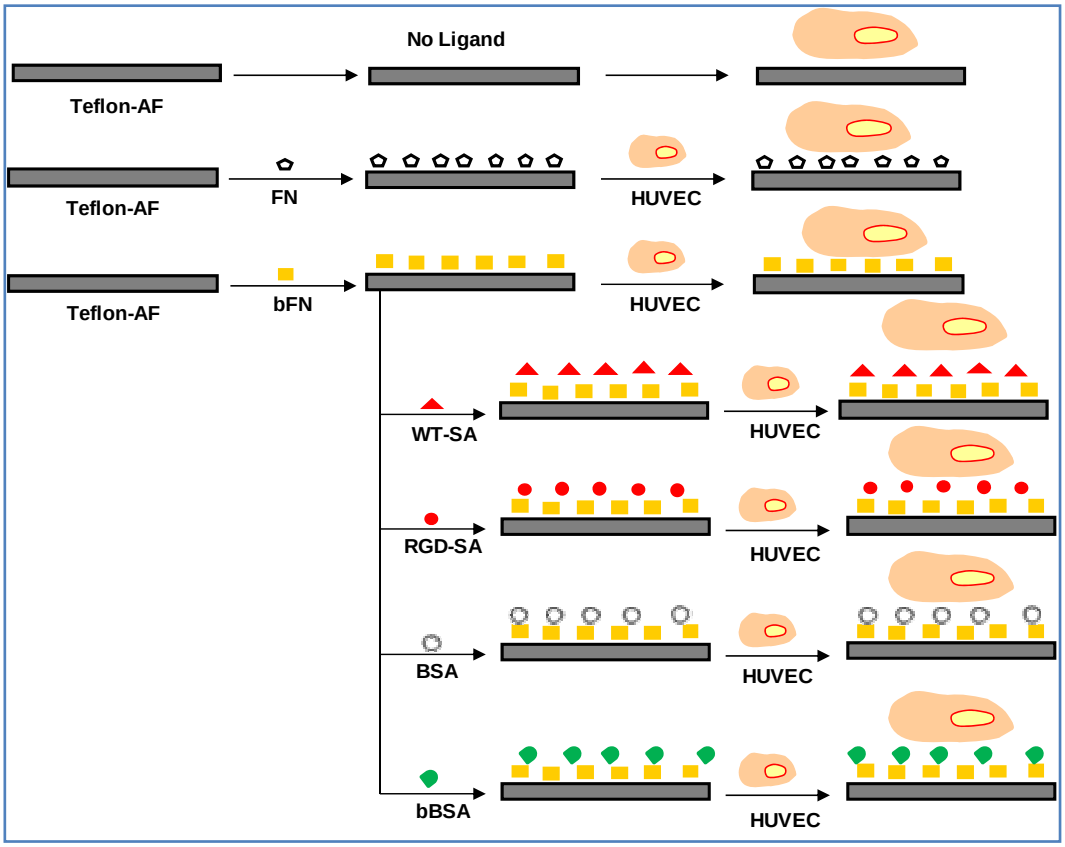

Figure 6.1 Flow chart with all formulations examined in this aim.

6.3 Materials and Methods

Cell Culture

All cell culture reagents were obtained from Cambrex (Walkersville, MD) unless otherwise specified. Human umbilical vein endothelial cells (HUVEC) were grown to confluence in gelatin coated T25 polystyrene flasks (Corning Inc., Corning, NY) with endothelial basal media (EBM) supplemented with 0.5ml 10 mg/ml hEGF (human recombinant Epidermal Growth Factor), 0.5 ml 1.0 mg/ml Hydrocortisone, 0.5 ml of 50 mg/ml Gentamicin and 50 mg/ml Amphotericin-B mix, 3 mg/ml bovine brain extract (BBE), and 10 ml Fetal Bovine Serum (FBS). Cells were cultured in an incubator with 95% air/5% CO_2 at 37 ^{o}C. Two confluent T-25 HUVECs from passage 3-6 were rinsed with dPBS without Ca^{2+} and $Mg^{2+,}$ incubated with 2ml each of either 0.025% or 0.05% Trypsin/EDTA for 4 min at 37 ^{o}C, neutralized with trypsin neutralizing solution (TNS), and centrifuged at 2200 rpm for 5 minutes. For all experiments, $1x10^{6}$ cells were diluted into 8mL of fresh serum free media, treated with 64µl Hoechst Dye (Molecular Probes, Carlsbad, CA) and rotated in incubator for 15 minutes then transferred to a 10mL syringe prior to use in the cell infusion assembly.

Dynamic Cell Seeding Experiments

Teflon-AF coated slides were incubated with Dulbecco's phosphate buffered saline (bPBS) with Ca^{2+} and Mg^{2+} for 1 hour in a quadriperm plate™ for the "no ligand" surface and treated with 20µg/ml of FN solution for 1 hour in the "FN only" case then rinsed with dPBS with Ca^{2+} and Mg^{2+} prior to assembling into the flow chamber. For all

other experimental formulation, Teflon-AF slides were incubated with 20µg/ml bFN(9) for 1 hour in the quadriperm plate, rinsed with dPBS with Ca^{2+} and Mg^{2+}, then incubated with 7ml of 50µg/ml of RGD-SA for 40 minutes at room temperature. After the incubation period, slides were rinse, assembled into laminar flow chamber (figure 6.2), and used in flow infusion loop.

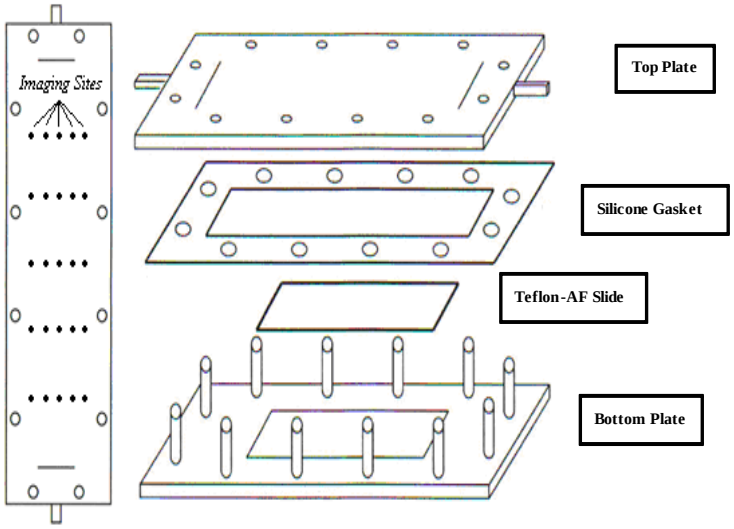

Figure 6.2 Schematic of laminar flow chamber showing imaging sites from the top plate. The chamber dimensions are 14.7 x 4.4 cm

Figure 6.3 is a picture of the infusion set up with the chamber on top of a microscope stage and infusion with a syringe pump (Harvard Apparatus, Holliston, MA). During infusion, 30 second movies were captured on the different treatments to quantify number of cells bound in real time. After infusion at 1ml/min, slides were rinsed at 2.5ml/min for 1 minute to remove any unattached cells still in the chamber.

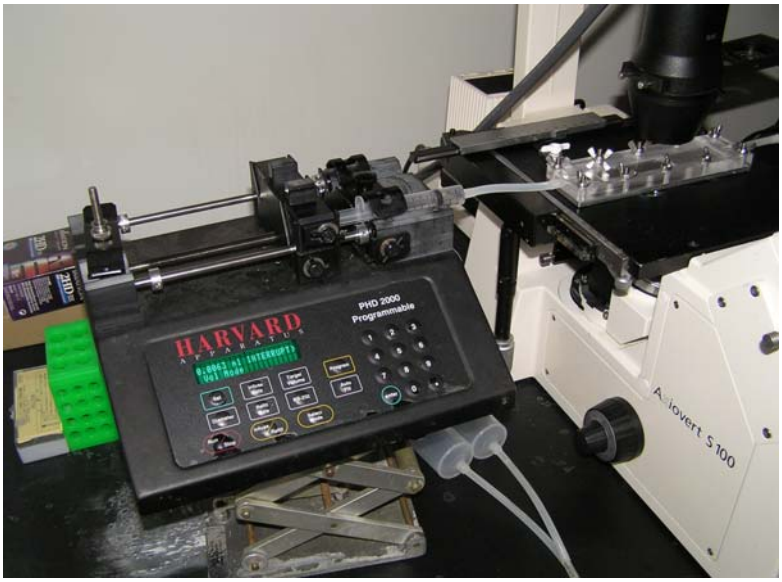

Figure 6.3. Picture of cell injection into flow chamber with a 10 ml syringe hooked up to a pump at 1 ml/min. The viewing field of the microscope is directly over the objective and is positioned at 5.2 cm from the injection point.

After rinse, pre flow images were taken at the 25 imaging sites. The cells were then detached at a shear stress of 60 dynes/cm^2 for 2 minutes. After shear stress perturbation, post flow images were obtained at the same sites. Images were analyzed in Image J using a macro written in Matlab.

Computational model of dynamic cell seeding

A computational model for the description of cell concentration around the bottom surface of a rectangular flow chamber was adapted from Munn, et al[157]. In their analysis of cell flux through a parallel plate flow chamber, Munn et al. described how cell concentrations changed at a fixed layer above the bottom surface of the chamber. This layer, with height 13 μm, was defined by the depth of field of the microscope objective used in their experimental observations. Cells were posited to accumulate within this layer for two different reasons. First, cells may not achieve stable adhesion to the bottom substrate of the chamber, causing an increased cellular flux near the surface until adhesion is achieved. Secondly, there is a sharp decrease in sedimentation velocity as cells approach a surface, thereby leading to a cellular concentration in the layer that is greater than that found in the bulk solution.

Munn described the flux of cells near the surface according to the following partial differential equation, where Ψ is the concentration within the layer, C is the bulk concentration of cells, v is the sedimentation velocity, h_l is the height of the layer (13 μm) and R is the rate of binding to the surface, and u is the average cell velocity within the layer h_l in the x direction:

$$\frac{\partial \Psi}{\partial t} = \frac{Cv - R}{h_l} - u\frac{\partial \Psi}{\partial x} \qquad (1)$$

A steady state solution of the above may be obtained by setting the temporal derivative equal to zero and noting that the rate of entry into the layer is greater than the rate of binding ($C\,v >> R$) to give the following differential equation (2) and its solution (3):

$$\frac{d\Psi_{ss}}{dx} = \frac{Cv}{uh_l} \qquad \Psi_{ss}(x=0) = C \tag{2}$$

$$\Psi_{ss} = C\left(1 + \frac{vx}{uh_l}\right) \tag{3}$$

In order to obtain Ψ_{ss}, both the sedimentation velocity v and the average cell velocity u must be calculated. Assuming a low Reynolds number flow near the surface, the sedimentation velocity v is given by the following, where μ is the fluid viscosity, R_{HUVEC} is the radius of a human umbilical vein endothelial cell, g is the acceleration due to gravity, ρ_{HUVEC} is the density of a human umbilical vein endothelial cell, and ρ is the density of the fluid in the flow chamber:

$$v = -\frac{2R_{HUVEC}{}^2 g}{9\mu}\left(\rho_{HUVEC} - \rho\right) \tag{4}$$

For a rectangular flow chamber, the velocity profile in the x direction as a function of the height of the chamber is given by the following, where Q is the volumetric flow rate, which is known for this model, w is the width of the flow chamber and h_c is the height of the chamber:

$$v_x(y) = \frac{6Q}{wh^3}\left(h_c y - y^2\right) \tag{5}$$

The average cell velocity u within the layer h_l is then determined by integrating the profile through the layer and dividing by the layer thickness.

$$u = \frac{1}{h_l}\int_0^{h_l} v_x(y)dy = \frac{1}{h_l}\int_0^{h_l} \frac{6Q}{wh^3}\left(h_c y - y^2\right)dy \tag{6}$$

Using the *trapz* command in MATLAB (The MathWorks, Natick, MA), the average cell velocity was tabulated for a range of flow rates (1, 4, 8, 40, 80 mL/min). With these values, Ψ_{ss} could now be calculated as a function of the length of the flow chamber, x, for the above range of flow rates.

In an effort to quantify the effects of the dual ligand system relative to other substrate approaches, a rate constant of binding k was calculated for each substrate at different trypsinization values (0.025% and 0.05%). Our approach for the calculation of the rate constants was based upon the assumption that N_{sub}, the amount of adherent cells for a substrate in cells/unit area, can be represented as a function of time by the following equation:

$$N_{sub} = k\Psi_{ss}t \tag{7}$$

Using data for N_{sub} obtained as a function of distance along the flow chamber at a specific time point, k could be calculated for each substrate at different trypsinization values. It should be noted that in the formulation of this relationship, it was assumed that once cells adhered to a substrate that they did not dissociate, meaning that k is only an association rate constant and not a net binding/unbinding constant. This assertion is based upon experimental findings that once the endothelial cells become bound to a substrate that they remain bound during the duration of the flow experiment.

Surface Plasmon Resonance (SPR) Studies

SPR surface and functionalization were the same as those noted in chapter 4. The experimental formulations examined were surface immobilized with either Biotinylated fibronectin, a co-immobilization of bFN and RGD-SA, or RGD-SA alone. After washing with buffer to remove unbound protein, the surfaces were interrogated with soluble $\alpha_5\beta_1$ and $\alpha_v\beta_3$ integrins (Chemicon) purified from human smooth muscle cells and verified for binding in an RGD dependent manner on surfaces coated with fibronectin.

Response units (RU) were measured based on differences in refractive index. These units were eventually correlated to protein surface density based on the relationship: 1000RU=1ng/mm^2 protein. The binding kinetics and amount immobilized were calculated with BIAevalution software (Biacore AB, Uppsala, Sweden).

6.4 Results

Dynamic Cell Seeding Experiments

In these experiments we expand on knowledge built from results in the past aim to exploit this modification to the DL which includes co-adsorption of bFN and RGD-SA in order to get greater strength of adhesion compared to single ligand protein surfaces. We injected $1x10^6$ cells diluted in 8mL of serum free media, quantified adhered cells to the protein treated surfaces, and calculated percent cell adhesion after shearing at 60 dynes/cm^2 for 2 minutes. Figure 6.4 shows HUVEC adhered after injection and retained after flow. These cells were detached using 0.025% Trypsin/EDTA.

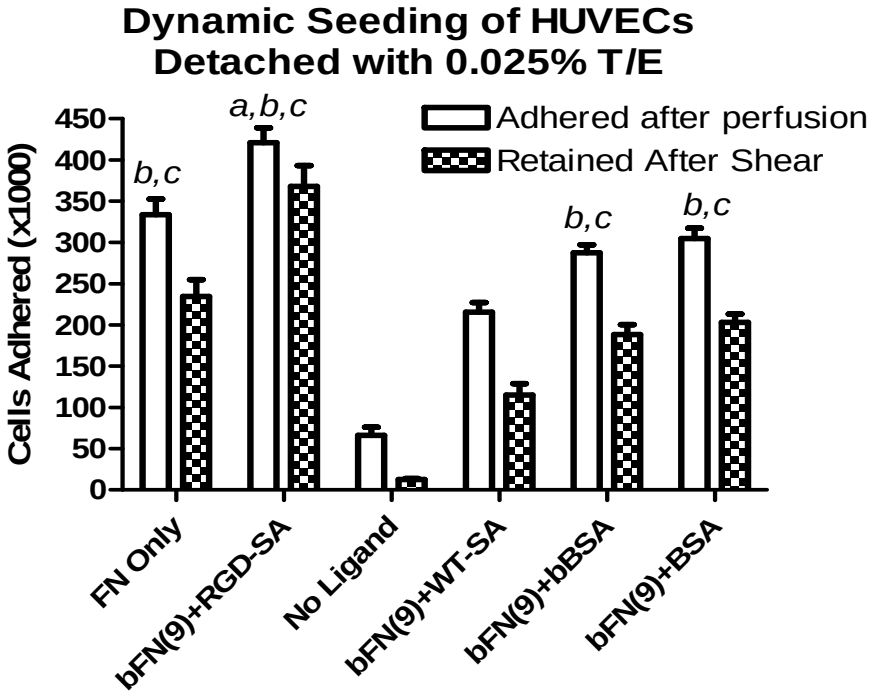

Figure 6.4. Error bars represent standard error of the mean (n=4). *a* adhesion on bFN+RGD-SA surfaces was greater than all other treatment groups. *b* adhesion was greater than bFN+WT-SA. *c* adhesion was greater than No Ligand treatment. $P<0.05$ for all statistical differences.

After perfusion at 1 ml/min, cells adhered across all treatment groups ranged from 66,000 cells on the slide with no protein treatment to 420,000 cells on the slides with bFN+RGD-SA. The DL had an enhanced affect over using single ligand proteins alone. This difference was more pronounced when compared to surface co-adsorbed with WT-SA or bBSA. These differences were apparent as well in the percent retention data. This was calculated by examining the relative percentage differences observed in figure 6.4 between cells retained after flow and cells adhered after perfusion. Figure 6.5 shows percent retention of HUVEC shown in figure 6.4 after flow at 60 dynes/cm^2.

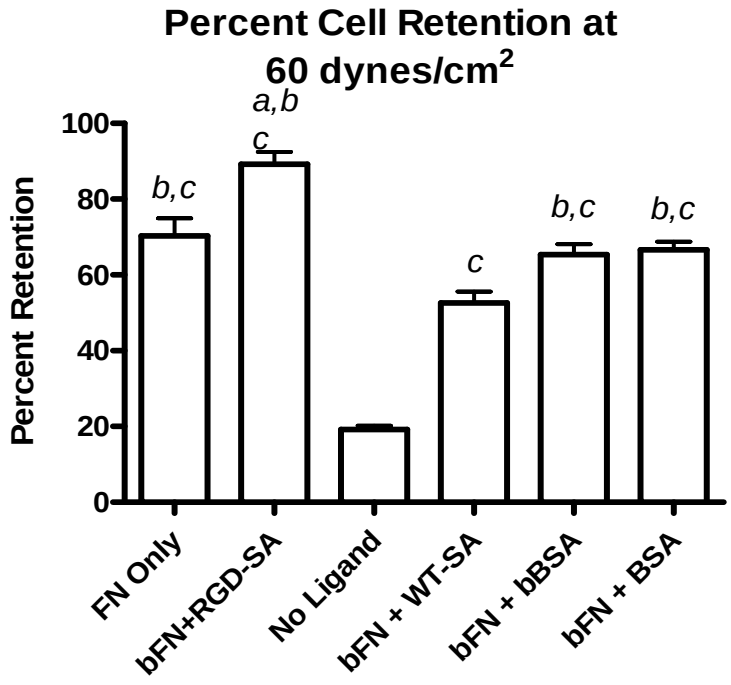

Figure 6.5. Error bars represent standard error of the mean (n=4). *a* adhesion on bFN+RGD-SA surfaces was greater than all other treatment groups. *b* adhesion was greater than "bFN+WT-SA". *c* adhesion was greater than "No Ligand" treatment. $P<0.05$ for all statistical differences.

The DL had a clear advantage in percent retention compared to all other groups. For all sample surfaces the order was bFN+RGD-A > FNonly > bFN+BSA > bFN+BSA > bFN+WT-SA > No ligand.

HUVEC were detached using higher Trypsin/EDTA concentration to determine the effect of a harsher detachment system on cell adhesion and retention. Figure 6.6 shows overall decrease in the number of cells adhered.

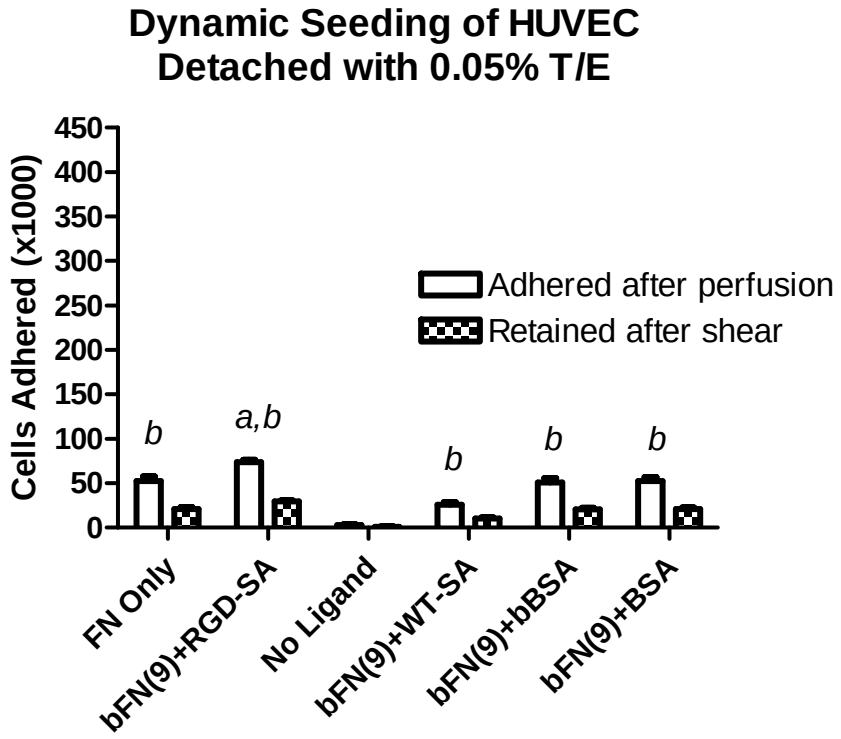

Figure 6.6. Error bars represent standard error of the mean (n=4). *a* adhesion on bFN+RGD-SA surfaces was greater than all other treatment groups. *b* adhesion was greater than "No Ligand". $P<0.05$ for all statistical differences.

Cell adhesion, even with the harsher isolation method was statistically different with the DL versus all other surface. Adhered cell numbers ranged from 2700 cells on "No Ligand" to 73,000 on the DL surface. When compared to isolation using 0.025% Trypsin/EDTA, the number of cells adhered after injection was statistically lower when using 0.05% Trypsin/EDTA at all surface protein formulations used. Cell retention after flow followed the same trend. Figure 6.7 shows the percent retention of HUVEC detached using 0.05% Trypsin/EDTA after flow at 60 dynes/cm^2 for two minutes. These values were calculated in the same way as values in figure 6.5.

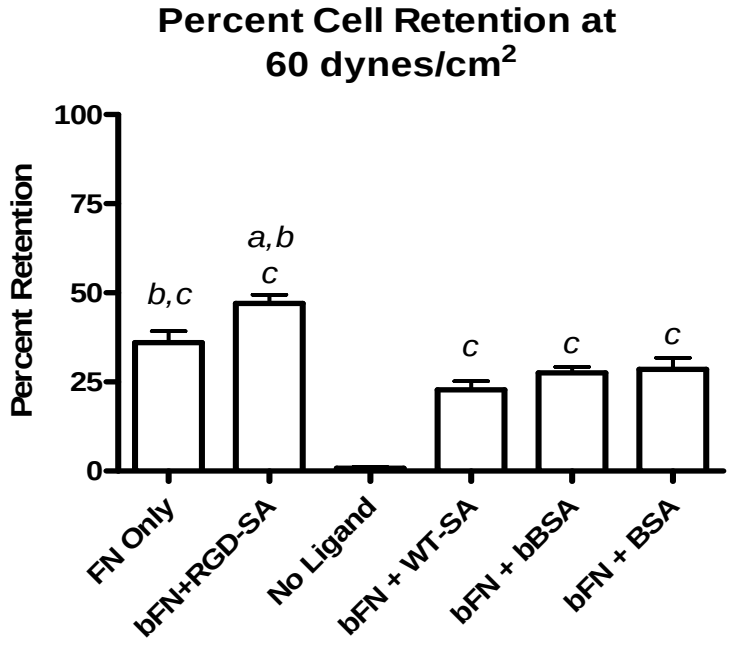

Figure 6.7. Error bars represent standard error of the mean (n=4). *a* adhesion on bFN+RGD-SA surfaces was greater than all other treatment groups. *b* adhesion was greater than "bFN+WT-SA", "bFN+bBSA," and 'bFN+BSA." *c* adhesion was greater than "No Ligand" treatment. P<0.05 for all statistical differences.

Though total cells number were lower with the harsher trypsinization method; surfaces modified with the DL retained 47% of their cells whereas those surfaces with no ligand retained less than 1% of their cells. In all, no surface retained greater than 50% of attached cells after shearing at 60 dynes/cm^2.

Computational Model of Experimental Parameters during Dynamic Seeding

To further understand the factors affecting the rate of binding of these cells to the surface, a computational model was developed based on a Munn et al. paper[157]. Using both equation 7 and values calculated for concentration of cells within the membrane as a function of the bulk concentration, a rate constant of association for different adhesion substrates and trypsinization values could be obtained. Since Ψ_{ss} varies with position, the number of adherent cells is a function of both position along the chamber as well as time. The number of adherent cells for each different substrate and trypsinization value was experimentally found at five imaging positions along the flow chamber at 480 seconds and with a flow rate of 1 mL/min. Figure 6.8 shows the rate constants calculated for each of the different substrate types and trypsinization values knowing N_{sub}, Ψ_{ss}, and t.

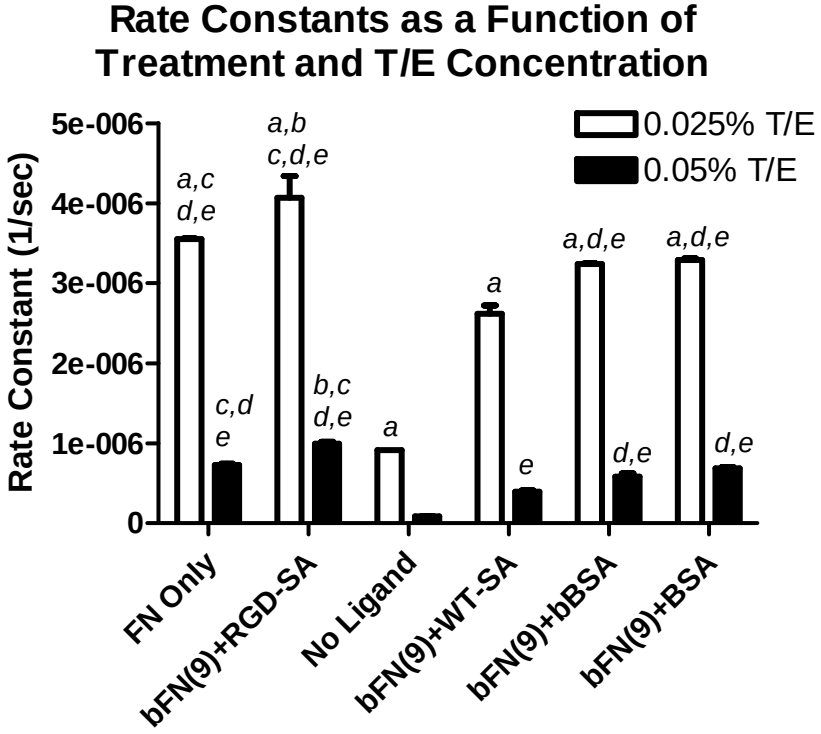

Figure 6.8. Rate constants for different substrate treatment types and trypsinization values. [a]Rate of binding was statistically higher with cells detached with 0.025% T/E. [b]Rate of binding was higher with the dual ligand compared to using "FN alone." [c]Rate of binding was higher compared to using "bFN(9)+BSA" or "bFN(9)+bBSA." [d]Rate of binding was higher compared to using "bFN(9)+WT-SA." [e]Rate of binding was higher compared to using "No Ligand" treatment.

Cells detached with 0.025% T/E have statistically ($p<0.05$) higher binding rates than cells with 0.05% T/E across all surface treatments examines. This was consistent with experimental data. Binding rate results indicate that the increase in binding rate as a function of T/E concentration was lowest on "FN only" surfaces with a value of 4.7 and highest on "No Ligand" surfaces with a value of 16. The increase in binding rates as a

function of protein treatment was 5.3 orders of magnitude higher with 0.025% T/E and 17.8 with 0.05% T/E.

Surface Plasmon Resonance (SPR) Studies

SPR analysis for the availability of RGD motifs on singular protein surfaces and DL surfaces was done to validate the results observed with cell binding data. Surfaces analyzed were bFN(9) alone, bFN(9)+RGD-SA, or RGD-SA alone immobilized using EDC/NHS. Figure 6.9 shows integrins bound to surface immobilized bFN(9) alone.

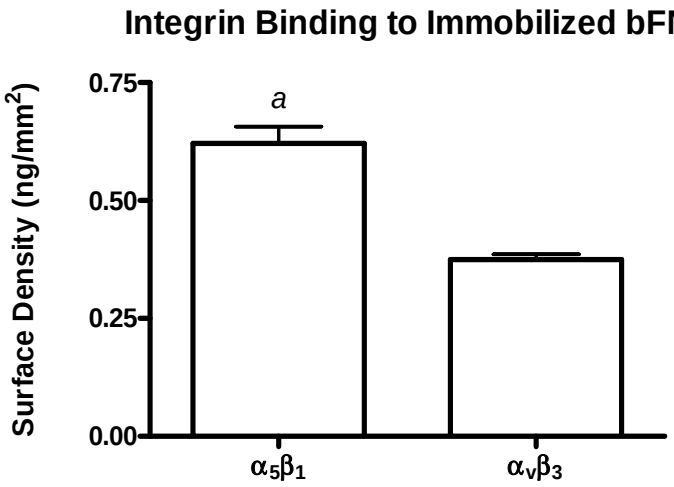

Figure 6.9. Error bars represent standard error of the mean. $\alpha_5\beta_1$ integrin binding was statistically higher than binding of $\alpha_v\beta_3$ integrin. P>0.05

Surfaces immobilized with bFN alone showed that $\alpha_5\beta_1$ integrins bind more preferentially over $\alpha_v\beta_3$ integrins. The combined binding was 0.99ng/mm2 but $\alpha_5\beta_1$ was responsible for 63 percent of those RGD binding sites bound. Figure 6.10 shows integrins bound to co-immobilized bFN(9)+RGD-SA.

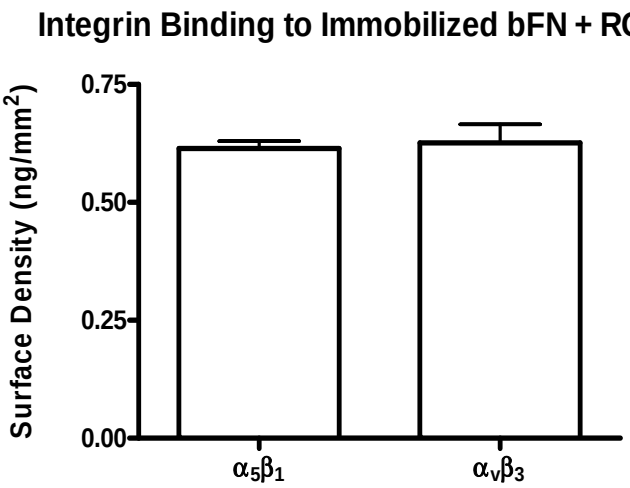

Figure 6.10. Error bars represent standard error of the mean. $\alpha_5\beta_1$ integrin binding equivalent to binding of $\alpha_v\beta_3$ integrin. $P>0.05$

What was observed was statistically indistinguishable binding between the two integrins to the immobilized proteins. The total amount of surface RGD bound was 1.24ng/mm^2. $\alpha_5\beta_1$ binding accounted for 49.5 percent of this value while $\alpha_v\beta_3$ accounted for 50.5 percent of this value. Figure 6.11 shows integrins bound to immobilized RGD-SA.

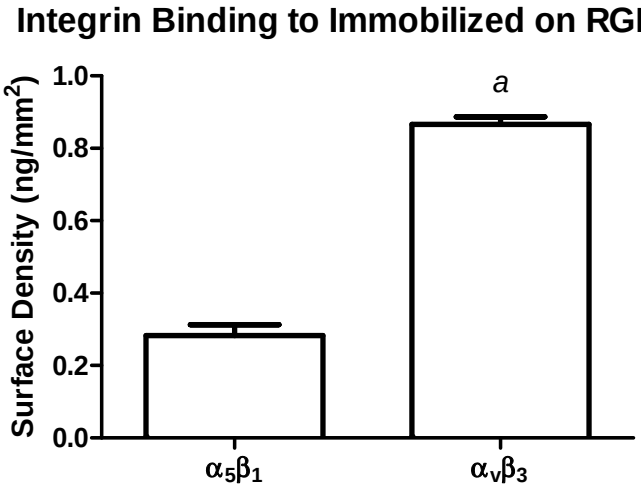

Figure 6.11. Error bars represent standard error of the mean. $\alpha_v\beta_3$ integrin binding was statistically higher than binding of integrin $\alpha_5\beta_1$. P>0.05

Binding on immobilized RGD-SA is a reversal of what was observed on surfaces immobilized with bFN. RGD-SA surfaces show more preferential binding for $\alpha_v\beta_3$ over $\alpha_5\beta_1$. Combined binding totaled 1.07ng/mm^2; $\alpha_v\beta_3$ accounted for 73.8 percent of this binding while $\alpha_5\beta_1$ accounted for 26.2 of the binding

6.5 Discussion

Experiments with dynamically seeded HUVEC were conducted to both determine effect due to T/E concentration and protein surface modifications. SPR was used to gain insight into mechanisms governing cell binding with this system. This is the first study investigating HUVEC attachment on synthetic vascular graft surrogates by using high affinity ligands that show binding preference for different transmembrane integrins. The initial motivation stemmed from observations in chapter 5 from focal adhesion data which demonstrated the benefit of using a modified ligand system that involved sequential adsorption of bFN and RGD-SA onto Teflon-AF™ substrates prior to incubation of unmodified HUVEC.

The effect of the modified DL was apparent in figure 6.4 where the difference in cells adhered after injection and also post flow analysis were higher than on other tested surface treatments. The DL had close to 90,000 more cells than its closest surface, the "FN only" surface. This represents 26 percent higher cell attachment with the DL at this T/E concentration. This effect was conserved after flow analysis as shown in figure 6.5. The percent difference between DL and FN decreased to 21 percent but the DL showed statistically higher retention over other protein formulation tested.

Unmodified HUVECs detached with 0.05 percent T/E showed a marked decrease in cell adhesion and cell retention after flow (figure 6.6). This can be attributed to a lack of transmembrane integrins for surface interactions due to harsh digestion of the cell membrane proteins at the higher T/E level[106]. Of note in figure 6.7 is that cells that attached remained attached at a higher percentage with the DL than any of the other

proteins but this difference is not as large as what was observed at the lower T/E level. When comparing the binding rates of the two systems, the range of rates observed suggest that T/E concentration and surface modification contribute almost equally to the impact on cells bound over time. This was observed when comparing "No Ligand" and "bFN+RGD-SA" surface at 0.025 percent T/E and comparing the same surfaces at the higher T/E level.

SPR validations of the two unique cell binding pathways is shown in figures 6.9-6.11. Others have reported on these phenomenological differences between cells spreading and retention mediated through distinct integrin pathways[86,158]. Other researchers have observed the phenomenon where $\alpha_5\beta_1$ and $\alpha_v\beta_3$ independently activate RhoA loading to focal contacts[156]. While $\alpha_5\beta_1$ appears to dominate on surfaces with either whole fibronectin or $FNIII_{10}$ with $FNIII_9$, there is a decrease in activation of focal adhesion kinase (FAK) necessary for mature focal contacts on these surfaces when using $\alpha_v\beta_3$ integrins[149,158]. These observations highlight the preferential binding for specific integrins by RGD cell binding motif with and without the synergy site. The higher binding of $\alpha_5\beta_1$ on surfaces with bFN alone (figure 6.9) is indicative of the need for the synergy site to facilitate this rapid interaction. Conversely, surfaces with RGD-SA alone bound $\alpha_v\beta_3$ more abundantly and preferentially over $\alpha_5\beta_1$ integrins (figure 6.11). These results indicate that these integrins bind more preferentially to RGDs without any synergy site needed and this dominates over $\alpha_5\beta_1$[159].

The resultant increase in RGD density with the sequential adsorption of bFN and RGD-SA led to enhanced cell attachment and retention with this current system over

previous DL formulations. Binding of $\alpha_5\beta_1$ and $\alpha_v\beta_3$ integrins to surface immobilized bFN and RGD-SA are mirror images of each other. When immobilized together, there is a subtle difference in amount of each integrin bound but this difference was not statistically significant. Our system presents a surface with RGD motifs in proximity to the fibronectin synergy site PHSRN while also providing RGD motifs on the RGD-SA that are more efficiently bound by $\alpha_v\beta_3$ integrins.

The ability to promote morphological changes[160,161], gene expression profile[162] and enhanced cell retention on SVG through shear [22] has also been well researched. Dynamic cell seeding of cells into SVG prior to static culture for a period of time has shown enhanced properties in promoting confluent neointmas in 4m polyurethane grafts[163]. Our system could be adapted to such a system by promoting rapid cell binding and subsequently promoting preferential remodeling of the cell-protein surface through the two binding systems to produce a graft with firmly attached ECs prior to implantation. The current issues with this system are that individuals are only able to get 10 percent of injected cells attached to their surface when $3x10^6$ cells were injected into synthetic vascular grafts[164]. Our system shows greater than 50 percent attachment of injected cells and retained greater than 35% of cells after shear at 60 dynes/cm^2.

In an *in vivo* system with low cell numbers, this treatment can be used to attach more cells and create and optimal environmental for seeding autologous cells onto SVG prior to implantation. While static culture has better control properties, the ability to bind flowing EC could better mimic the *in vivo* environment. This study has developed a protein system that can readily bind perfusing cells. Hsu et al., Soletti et al., and Nasseri

et al. have all developed rotational seeding systems that are able seed cells onto SVG while rotating and take advantage of integrin activation low flow perturbations to produce endothelialized vessels *in vitro*[163,165,166]. The main challenge with their systems is the time required for desired cell attachment and coverage ranged from 7-10 days. Our system demonstrated actin polymerization 1 hour after attaching the cells in the dynamic system which may help shorten the time needed in the dynamic perfusion models to get desired cell coverage.

6.6 Conclusions

The DL system was used to increase RGD density on the surface leading to enhanced cell adhesion in a dynamic cell seeding system as well as greater percent retention over all other surface treatments after shear. There was a reduction in cell adhesion and retention using higher T/E concentration but the DL still outperformed all other surfaces tested. SPR analysis confirmed that specificity of RGD motifs on the surface were preferential to either $\alpha_5\beta_1$ or $\alpha_v\beta_3$ integrin. The current DL formulation primes two distinct cell binding pathways to modulate phenotypic changes in cells adhered on the surface after dynamic seeding. These results could have broader impact when combined with dynamic cell seeding techniques for SVG to promote endothelialization at shorter time points.

Chapter 7. Overview and future studies

7.1 Overview

The focus of these experiments was to optimize the dual ligand (DL) system to show enhanced cell adhesion, spreading, and retention on synthetic vascular graft (SVG) surrogates. The ultimate goal was to create a vasoprotective neointima with native functionality. This project has demonstrated the ability to promote firm adhesions and formation of mature focal contact in a protein dependent manner but additional studies need to be conducted to determine that the attached cells possess native endothelium biofunctionality as evidenced by secretion of bioactive molecules. These measurements, coupled with the retention data presented in this thesis, would be indication that this system is fit for an *in vivo* model.

Initially, two SVG surrogates were identified through characterization by X-ray photoelectron spectroscopy (XPS), atomic force microscopy (AFM), and ^{125}I radiolabeling as shown in Chapter 3. Chapter 4 presented the analysis of the first modification to the DL system which involved direct biotinylation of fibronectin (bFN) as a replacement co-adsorption of FN with biotinylated bovine serum albumin (bBSA). Langmuir models using surface plasmon resonance (SPR) spectroscopy verified the binding affinity of bFN, Enzyme-Linked ImmunoSorbent Assay (ELISA) was used to detect the availability of the RGD binding motif post biotinylation, and fluorescence activated cell sorting (FACS) confirmed the specificity of RGD-SA for transmembrane integrins.

The second major change in this project examined cell binding and formation of focal adhesion after shifting from direct incubation of HUVECs with RGD-SA to co-adsorbing RGD-SA and bFN(9) prior to introducing unmodified HUVECs (Chapter 5). These experiments were still conducted under static seeding conditions for 1 hour. Chapter 6 examined dynamic cell seeding onto sequentially adsorbed protein surfaces as a function of surface immobilized protein and T/E concentration. These experiments verified an increase in surface density of RGD binding motifs which lead to greater cell retention and spreading of the DL over FN alone.

7.2 Future Studies

The work presented in this thesis highlight a time course of experiments that identified optimal parameters for promoting rapid cell attachment and retention on SVG surrogate. The identified protocol is a powerful tool for rapidly attaching cells and with additional characterization studies, would be an ideal model for future *in vivo* studies. RGD peptides have been proven to attach to transmembrane integrin and attach cells in a peptide dependent manner[83,86]. RGD density is related to cell spreading, cell survival, focal contact formation, and proliferation. This project adds to that body of work through development of ideal formulation for capture and spreading of perfused endothelial cells. This system, with its ability to rapidly bind and retain cells under flow after short time adhesion, is an advancement over previous methods. However, there are modifications that can be made to improve its efficiency and potentially create a surface to promote complete endothelialization at short time points.

The current data was observed by using biotin functionalized fibronectin to introduce RGD groups onto the surface through tethering of RGD-SA. A simplification of this system would replace RGD-SA with GRGDY peptides that have been proven to attach more preferentially to $\alpha_v\beta_3$ integrins[83,86]. In this manner we are able to retain the advantage conferred by our formulations to prime preferential binding to $\alpha_v\beta_3$ and $\alpha_5\beta_1$ integrins.

Surface Characterization

With current experimental data, there is some question about the nature of cell binding on the examined surfaces. In order to accurately determine whether cells bind in an instantaneous manner or roll prior to arresting on the surface, longer timed movies will be captured. Cells will be analyzed in the viewing field to determine their method of attachment and graphed as percent of rolling cells as a function of protein surface treatment. Arrest will be defined as settling for ½ second prior to rolling. The primary limitation with this analysis lies in the inability to track the cell across the length of the glass slide, but these studies will give needed insight into the mode of attachment as a function of proteins adsorbed or trypsinization method.

Cell attachment to polymer surfaces has been shown to improve in an RGD-dependent manner. With this finding, the necessary next step in this experiment after removing avidin-biotin binding is characterization of the RGD surface density with different GRGDY:FN ratios to determine optimal densities needed for ideal cell capture and retention. Initial studies will modulate ratios of GRGDY:FN. The analysis will determine the best ratio necessary to attach the highest percentage of HUVECs in serum free media perfused at a physiological flow rate in a laminar flow chamber onto Teflon-AF surfaces preadsorbed with GRGDY:FN mix. Microdistribution of RGD binding motifs on the sample surface can be verified with environmental atomic force microscopy (AFM) using integrin or RGD antibody coated tips. Finally, Western Blots will be conducted after cell attachment to better understanding the dominant protein species upregulated when cells bind to this surface. The Western analysis will include sampling

after specific times to develop a protein profile over the duration of cell attachment at short and longer time points.

Validation of Biofunctionality HUVECs on SVG Surrogates

In addition to rapid and firm cell adhesion, enhanced bioactivity of immobilized endothelial cells is required for viability of the current system. To this end, experiments will be conducted to confirm that attached cells exhibit a quiescent phenotype that can secrete mediators to ward off platelet aggregation and adhesion such as nitric oxide, prostacyclin, and experiments will be conducted to determine the biofunctionality of the cell layer. Post endothelial cell attachment, platelet rich plasma will be flowed over the cell layer and platelet adhesion will be measured with the aid of an epifluorescent microscope with murine antibody to platelet GP IIb/IIa. Secondly, nitric oxide and prostacylin production can be in as a function of shear stress. Lastly, Western Blot measurement of eNOS would be an early indicator for production of the vasoprotective chemical nitric oxide. These experiments will provide the data to support the biofunctionality of this system.

Rotation Seeding of HUVECs on PU and ePTFE Grafts

Current grafts used in our *in vivo* experiments, beyond being inherently thrombogenic, a problem being mitigated by *in vitro* endothelialization, are also non-compliant and this often leads to hyperplasia initiated at the anastomotic site. Myolink, a compliant polyurethane-based synthetic vascular graft currently in clinical trials, would

be an ideal choice due to comparable compliance to native arteries[2]. Additionally, the potential for greater protein adsorption, and naturally more RGD moieties to promote enhanced cell adhesion, could be achieved on Myolink because of its higher surface energy. Using a rotational seeding system, cell attachment onto Myolink can be compared to values observed on ePTFE small diameter vessels[166]. We would assess the biofunctionality of the cells on the graft surfaces by flowing platelet rich plasma after cell attachment. These data would give a complete idea of cell behavior on graft surfaces and would necessarily be the platform for developing *in vivo* experimental protocols. This formulation can be used in an animal model after a short culture and examined for patency at 2, 7, 14, and 28 days.

APPENDICES

Appendix 1. Matlab scripts for cell adhesion analysis

Developed in collaboration with Miao Wang

Cell spreading Analysis

This script creates a macro in ImageJ to analyze cell spreading

```
% Reset all
clear all; clc;
 % Input file directory
temp.input = input('Enter directory location:\n#','s');
 temp.location = [ temp.input '\images'];
 mkdir(temp.input,'rawdata');
 % Generate file path with 4 blackslashes (for macro)
count2 = 1;
for count = 1:length(temp.location)
    temp.macrolocation(count2) = temp.location(count);
    if strcmp(temp.location(count),'\')
        temp.macrolocation(count2+1) = '\';
        temp.macrolocation(count2+2) = '\';
        temp.macrolocation(count2+3) = '\';
        count2 = count2 + 3;
    end
    count2 = count2 + 1;
```

```
end
 count2 = 1;
for count = 1:length(temp.input)
    temp.outlocation(count2) = temp.input(count);
    if strcmp(temp.input(count),'\')
        temp.outlocation(count2+1) = '\';
        temp.outlocation(count2+2) = '\';
        temp.outlocation(count2+3) = '\';
        count2 = count2 + 3;
    end
    count2 = count2 + 1;
end
 % List files
temp.list = dir(temp.location);
 % Copy valid file names
count2 = 1;
for count = 1:length(temp.list)
    if strfind(temp.list(count).name,'.tif') >= 1
        if strfind(temp.list(count).name,'(glass)') >= 1
            list(count).images = temp.list(count).name;
            count2 = count2 + 1;
        elseif strfind(temp.list(count).name, '(teflon)') >= 1
```

```
            list(count).images = temp.list(count).name;
            count2 = count2 + 1;
        end
% Error check if no files found
if (length(list) < 1); error('No valid files found.'); end
 % Generate sample list
for count = 1:length(list)
    for count2 = 1:strfind(list(count).images,'.tif')-1
        list(count).samples(count2) = list(count).images(count2);
    end
% Generate data list
for count = 1:length(list)
    list(count).data = [ list(count).samples '.txt'];
end
 % Write to files
filename = [ temp.location '\macro_ImageJ.txt'];
fid = fopen(filename,'w');
 % Macro code for each image
 for count = 1:length(list)
    fprintf(fid,[ 'open("' temp.macrolocation '\\\\' list(count).images '");\n' ]);
    fprintf(fid,[ 'run("Subtract Background...", "rolling=10 white");\n' ]);
    fprintf(fid,[ 'run("Smooth"); run("Smooth"); run("Threshold"); run("Watershed");\n' ]);
```

```
    fprintf(fid,[ 'run("Set Scale...", "distance=0.476 known=1 pixel=1 unit=micrometer
global");\n' ]);
    if strfind(list(count).images,'none') >= 1
fprintf(fid,[ 'run("Analyze Particles...", "minimum=100 maximum=2000 bins=8
show=Nothing display exclude clear");\n' ]);
    elseif strfind(list(count).images,'(bbsa)') >= 1
        fprintf(fid,[ 'run("Analyze Particles...", "minimum=110 maximum=2000 bins=8
show=Nothing display exclude clear");\n' ]);
    else
        fprintf(fid,[ 'run("Analyze Particles...", "minimum=120 maximum=2000 bins=8
show=Nothing display exclude clear");\n' ]);
    end
    fprintf(fid,[ 'run("Text...", "save=[' temp.outlocation '\\\\rawdata\\\\' list(count).data
']");\n' ]);
    fprintf(fid,[ 'run("Close"); close(); \n\n' ]);
end
 fclose(fid);
```

Cell adhesion analysis

This script processes and analyzes cell retention data then outputs the data into Excel sheets.

```
% processdata.m
% does all the data processing for an ImageJ macro generated file.
% clear all variables
clear all; clc;
% set experiment variables
type.cells = {'untreated','biotin-SA','RGD-SA'};
type.slides = {'teflon','glass'};
type.treatments = {'bbsa','bfn20','bfn40','bfn60',...
                   'bfn80','fn','none'};
 % get directory location and treatments
location.dir = input('Enter directory location: ','s');
num.celltype = menu('Enter cell treatment: ',type.cells);
 location.rawdata = fullfile(location.dir,type.cells{num.celltype},'rawdata');
location.newdata = fullfile(location.dir,type.cells{num.celltype},'newdata');
 % Begin script processing
disp('Begin running script...');
 % create new data folder
[z.SUCCESS,z.MESSAGE,z.MESSAGEID] =
mkdir(fullfile(location.dir,type.cells{num.celltype}),'newdata'); clear z;
```

```
 % get list of files
disp('Getting file list...');
 temp.filelist = dir(location.rawdata);


% copy valid filenames
count2 = 1;
for count = 1:length(temp.filelist)
    if strfind(temp.filelist(count).name,'.txt') >= 1
        if strfind(temp.filelist(count).name,'glass') >= 1
            vars.filelist{count2} = temp.filelist(count).name;
            count2 = count2 + 1;
        elseif strfind(temp.filelist(count).name, 'teflon') >= 1
            vars.filelist{count2} = temp.filelist(count).name;
            count2 = count2 + 1;
        end
% error check if no files found
if (length(vars.filelist) < 1); error('No valid files found.'); end
 % read data from files
disp('Reading data from files...');
 for count=1:length(vars.filelist)
    sourcefile = [ location.rawdata '\' vars.filelist{count} ];
    temp = importdata(sourcefile);
```

```
    vars.datapoints{count} = temp.data(:,2);
end
 % combine data from the 3 images per hour per treatment
disp('Combining image data...');
for slidecount = 1:length(type.slides)
    for treatcount = 1:length(type.treatments)
        for expcount = 1:3
            for timecount = 1:4


                fo count = 1:length(vars.filelist)


                    if strfind(vars.filelist{count},['(' type.slides{slidecount} ')']) >= 1
                        if strfind(vars.filelist{count},['(' type.treatments{treatcount} ')']) >= 1
                            if strfind(vars.filelist{count},['(' num2str(expcount) ')']) >= 1
                                if strfnd(vars.filelist{count},['(' num2str(timecount) '-'] ) >= 1


                                    if strfind(vars.filelist{count},'-1') >= 1
                                        temp.slide1 = vars.datapoints{count};
                                    elseif strfind(vars.filelist{count},'-2') >= 1
                                        temp.slide2 = vars.datapoints{count};
                                    elseif strfind(vars.filelist{count},'-3') >= 1
                                    end
```

```
            %store data in memory
            data{slidecount}{treatcount}{expcount}{timecount} =
[temp.slide1;temp.slide2;temp.slide3];
              %write data to new files
            filename = fullfile(location.newdata,['(' type.slides{slidecount}  ')('
type.cells{num.celltype} ')(' type.treatments{treatcount} ')(' num2str(expcount) ')('
num2str(timecount) ').txt'  ]);
            fid = fopen(filename,'w');
            fprintf(fid,'%g\n',temp.slide1);
            fprintf(fid,'%g\n',temp.slide2);
            fprintf(fid,'%g\n',temp.slide3);
            fclose(fid);

            end
        % write data to excel file
disp('Writing data to excel file...');
 excelfile = fullfile(location.dir,[ type.cells{num.celltype} '.xls']);
finalfile = fullfile(location.dir,'analysis.xls');
 expposition = {'A1','E1','I1'};
titleposition = {'A3','B3','C3','D3';'E3','F3','G3','H3';'I3','J3','K3','L3'};
dataposition = {'A5','B5','C5','D5';'E5','F5','G5','H5';'I5','J5','K5','L5'};
 warning off MATLAB:xlswrite:AddSheet;
```

```
 for slidecount = 1:length(type.slides)
    for treatcount = 1:length(type.treatments)
        for expcount = 1:3
            for timecount = 1:4
                xlswrite(excelfile,timecount,[type.slides{slidecount} '-'
type.treatments{treatcount}],titleposition{expcount,timecount});

xlswrite(excelfile,data{slidecount}{treatcount}{expcount}{timecount},[type.slides{slide
count} '-' type.treatments{treatcount}],dataposition{expcount,timecount});
            end
            xlswrite(excelfile,expcount,[type.slides{slidecount} '-'
type.treatments{treatcount}],expposition{expcount});
        end
        disp(['Processing: ' type.slides{slidecount} ' ' type.treatments{treatcount}]);
    end
% calculate averages and write to file
disp('Analyzing data...');

positions = {2 6 10 14 18 22 26 30 34 38 42 46 50 54};
 for slidecount = 1:length(type.slides)
    for treatcount = 1:length(type.treatments)
        for timecount = 1:4
```

```
        for expcount = 1:3
            averages{slidecount}{treatcount}{expcount}{timecount} =
mean(data{slidecount}{treatcount}{expcount}{timecount});
            m(expcount) = averages{slidecount}{treatcount}{expcount}{timecount};
        end
         totalavg{slidecount}{treatcount}{timecount} = mean(m);
         mod(1) = totalavg{slidecount}{treatcount}{timecount}/m(1);
        mod(2) = totalavg{slidecount}{treatcount}{timecount}/m(2);
        mod(3) = totalavg{slidecount}{treatcount}{timecount}/m(3);
         normdata{1} = data{slidecount}{treatcount}{1}{timecount}.*mod(1);
        normdata{2} = data{slidecount}{treatcount}{2}{timecount}.*mod(2);
        normdata{3} = data{slidecount}{treatcount}{3}{timecount}.*mod(3);
         totaldata = [normdata{1}; normdata{2}; normdata{3}];
        totalmean = mean(totaldata);
        totalerror = std(totaldata)/sqrt(length(totaldata));
        sampleerror = std(m)/sqrt(3);
          writedata = {type.treatments{treatcount}, timecount, totalmean, sampleerror,
totalerror, m(1), m(2), m(3)};
        xlswrite(excelfile, writedata, 'analysis', ['A' num2str(positions{treatcount} +
timecount)]);
        xlswrite(finalfile, writedata, type.cells{num.celltype}, ['A'
num2str(positions{treatcount} + timecount)]);
```

```
        end
writetitle{1} = type.cells{num.celltype};
writeheaders = {'hour' 'mean' 'SE' 'SE(all)' 'mean1' 'mean2' 'mean3'};
xlswrite(excelfile, writetitle, 'analysis', 'A1');
xlswrite(excelfile, writeheaders, 'analysis', 'B2');
xlswrite(finalfile, writetitle, type.cells{num.celltype}, 'A1');
xlswrite(finalfile, writeheaders, type.cells{num.celltype}, 'B2');
 disp('Finished.');
```

Appendix 2. Computational model for DL attachment

Developed in collaboration with Matthew T. Novak

Cell sedimentation along the chamber

A computational model for the description of cell concentration around the bottom surface of a rectangular flow chamber was adapted from Munn, et al. In their analysis of cell flux through a parallel plate flow chamber, Munn et al. sought to understand how cell concentrations changed at a fixed layer above the bottom surface of the chamber. This layer, with height 13 μm, was defined by the depth of field of the microscope objective used in their experimental observations. Cells were posited to accumulate within this layer for two different reasons. First, cells may not achieve stable adhesion to the bottom substrate of the chamber, causing an increased cellular flux near the surface until adhesion is achieved. Secondly, there is a sharp decrease in sedimentation velocity as cells approach a surface, thereby leading to a cellular concentration in the layer that is greater than that found in the bulk solution.

Munn described the flux of cells near the surface according to the following partial differential equation, where Ψ is the concentration within the layer, C is the bulk concentration of cells, v is the sedimentation velocity, h_l is the height of the layer (13 μm) and R is the rate of binding to the surface:

$$\frac{\partial \Psi}{\partial t} = \frac{Cv - R}{h_l} \frac{\partial \Psi}{\partial x} \qquad (1)$$

A steady state solution of the above may be obtained by setting the temporal derivative equal to zero and noting that the rate of entry into the layer is greater than the rate of binding ($C\ v >> R$) to give the following, where u is the average cell velocity within the layer h_l in the x direction:

$$\Psi_{ss} = C\left(1+\frac{vx}{uh_l}\right) \qquad (2)$$

In order to obtain Ψ_{ss}, both the sedimentation velocity v and the average cell velocity u must be calculated. Assuming a low Reynolds number flow near the surface, the sedimentation velocity v is given by the following, where μ is the fluid viscosity, R_{HUVEC} is the radius of a human umbilical vein endothelial cell, g is the acceleration due to gravity, ρ_{HUVEC} is the density of a human umbilical vein endothelial cell, and ρ is the density of the fluid in the flow chamber:

$$v = -\frac{2R_{HUVEC}{}^2 g}{9\mu}\left(\rho_{HUVEC} - \rho\right) \qquad (3)$$

For a rectangular flow chamber, the velocity profile in the x direction as a function of the height of the chamber is given by the following, where Q is the volumetric flow rate, which is known for this model, w is the width of the flow chamber and h_c is the height of the chamber:

$$v_x(y) = \frac{6Q}{wh^3}\left(h_c y - y^2\right) \qquad (4)$$

The average cell velocity u within the layer h_l is then determined by integrating the profile through the layer and dividing by the layer thickness.

$$u = \frac{1}{h_l}\int_0^{h_l} v_x(y)dy = \frac{1}{h_l}\int_0^{h_l} \frac{6Q}{wh^3}\left(h_c y - y^2\right)dy \qquad (5)$$

Using the *trapz* command in MATLAB (The MathWorks, Natick, MA), the average cell velocity was tabulated for a range of flow rates (1, 4, 8, 40, 80 mL/min). With these values, Ψ_{ss} could now be calculated as a function of the length of the flow chamber, x, for the above range of flow rates.

In an effort to quantify the effects of the dual ligand system relative to other substrate approaches, a rate constant of binding k was calculated for each substrate at different trypsinization values (0.025% and 0.05%). Our approach for the calculation of the rate constants was based upon the assumption that N_{sub}, the amount of adherent cells for a substrate in cells/unit area, can be represented as a function of time by the following equation:

$$N_{sub} = k\Psi_{ss}t \qquad (6)$$

Using data for N_{sub} obtained as a function of distance along the flow chamber at a specific time point, k could be calculated for each substrate at different trypsinization values. It should be noted that in the formulation of this relationship, it was assumed that once cells adhered to a substrate that they did not dissociate, meaning that k is only an association rate constant and not a net binding/unbinding constant. This assertion is based upon experimental findings that once the endothelial cells become bound to a substrate that they remain bound during the duration of the flow experiment.

In addition to modeling cell concentration near the bottom surface of the chamber, cell trajectories for different flow rates and entrance points along the chamber were

modeled by noting that the terminal sedimentation velocity described in Eq. 3 is equal to $\frac{dy}{dt}$ and that the translational fluid velocity described in Eq. 4 is equal to $\frac{dx}{dt}$. Using *ode45* in MATLAB, these two equations were solved numerically for $x(t)$ and $y(t)$ and the solutions were plotted against one another. This model could then be used as a guide for predicting cellular trajectory and settling for dynamic seeding at different flow rates.

Results of Computational Model

Figure A1 shows the plots of the concentration Ψ_{ss} within the layer h_l normalized by the bulk concentration C_o as a function of distance within the chamber for varying flow rates. This normalized concentration was calculated at five different points along the length of the chamber. From the point of entry into the chamber, these distances were measured as: 2.848 cm, 3.982 cm, 5.214 cm, 6.686 cm, and 7.744 cm. As expected from Eq. 2, these normalized concentrations increase linearly with time. Moreover, these normalized concentrations increased in magnitude as the flow rate is decreased. This finding should be expected, as cells will have a better opportunity to settle on the surface when they are traveling at lower flow rates.

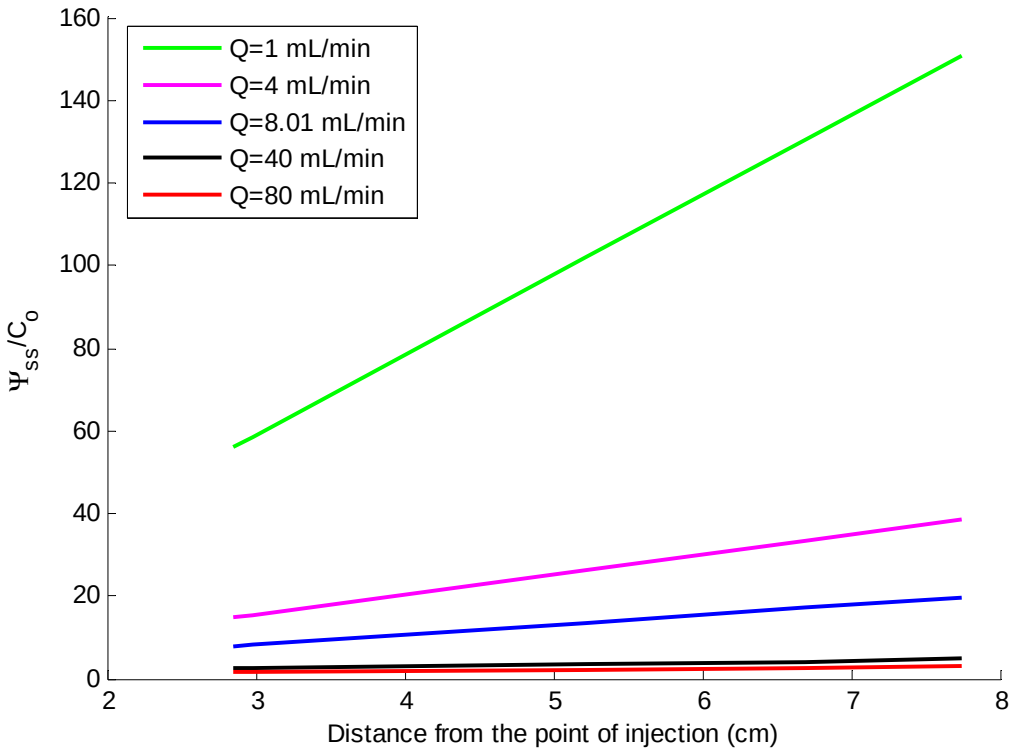

Figure A1: Normalized concentration $\frac{\Psi_{ss}}{C_o}$ as a function of distance from the site of injection for varying flow rates.

Figures A2 and A3 support the finding in Figure 1 that sedimentation will decrease with increasing flow rate. Figure A2 shows the trajectory of the cells as a function of distance from the site of injection at varying flow rates. For this simulation, it was assumed both that the cells were a well-mixed solution before entrance into the chamber and that mean point of entrance would most likely be at the midpoint of the chamber (0.0329 cm). At a flow rate of just 1mL/min, the model predicted settling to occur about 24 cm from entrance into the chamber. However, the seeding region of the chamber is only 7.5 cm in length, meaning that this simulation would predict no settling

along the length of the chamber. The assumption of cells entering directly at the midpoint of the chamber height was therefore not consistent with the experimental constraints. The data in Figure A3 were modeled to find at what entrance heights that cells would be able to seed along the length of the chamber. The chamber height h_c was divided into 10 strata of equal height, which are delineated by the horizontal dotted lines in Figure A3. The settling simulation was then run for each stratum with initial positions for each simulation being at the midpoint of each respective stratum. These simulations were executed using a volumetric flow rate of 1 mL/min, as that flow rate was the closest to having seeding along the length of the chamber. From the graph, a reasonable cutoff entrance height for seeding in the chamber would be about 0.015 cm, which is about the bottom quarter of the chamber.

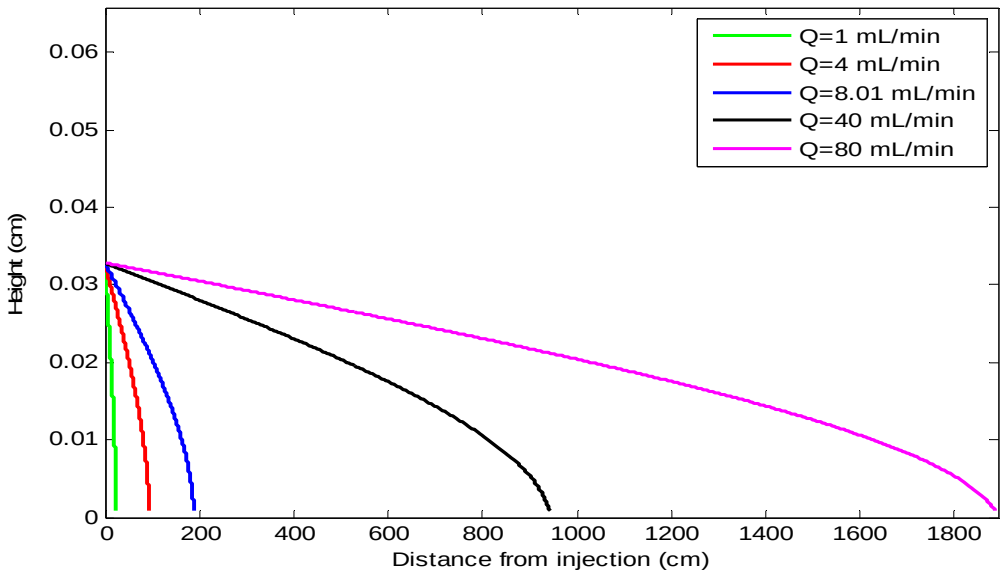

Figure A2: Trajectory of HUVECs as a function of distance from the site of injection for varying flow rates.

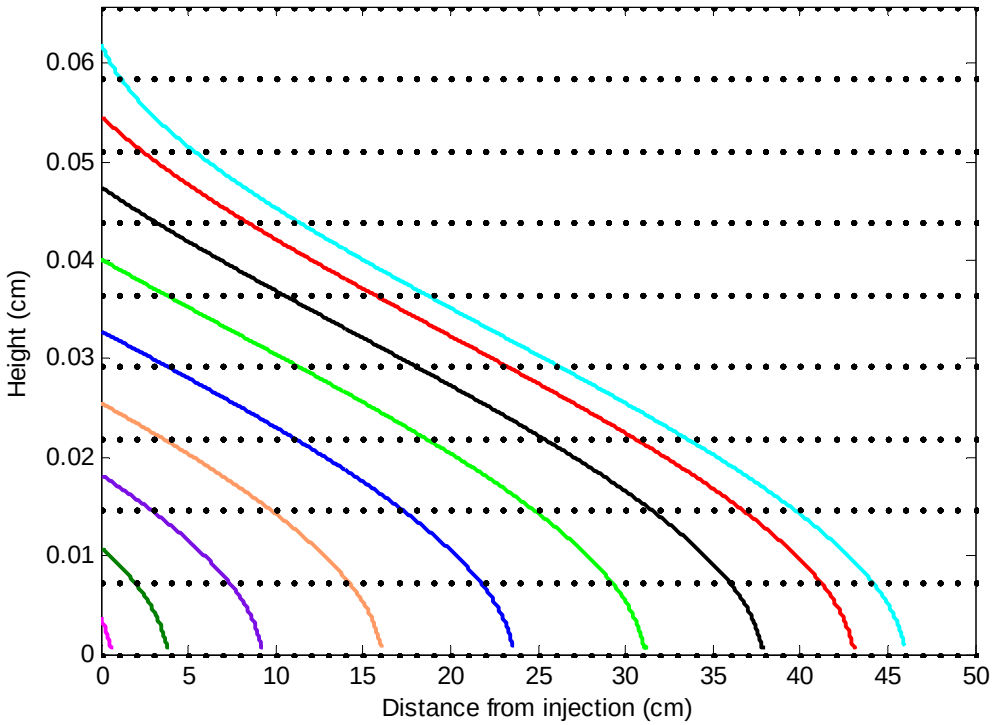

Figure A3: Trajectory of HUVECs as a function of distance from the site of injection for a flow rate of 1 mL/min at different points of entry along the chamber.

Matlab script for model cell sedimentation

```
%rateconstant.m
clear all
%Calculation of average velocity in layer of thickness 13 um
Q=[1,4,8.01,40,80]; %Flow rate in mL/min
w=1.85; %width of flow chamber in cm
h=0.0658; %height of flow chamber in cm
y=0:0.00005:0.0013; %measurement of height of bottom layer in cm
R=6.8e-4; %radius of huvec cell
rho_huvec=1.09; %g/cm^3 density of huvec cell
rho=1.01; %g/cm^3 density of fluid
g=-980; %cm/sec^2 acceleration due to gravity
mu=0.04; %g/sec/cm fluid viscosity
C=125000; %concentration of cells in cells/mL
vol=8; %volume of fluid flown through chamber in mL
t=480; %time of flow chamber experiment
for k=1:length(y)
   v(:,k)=((6.*Q./(w.*(h).^3)).*(h.*y(k)-y(k).^2)); %calculation of fully developed
velocity in rectangular chamber as a function of y
end
for n=1:length(Q)
```

```
  u(n,:)=(1./max(y).*trapz(y,v(n,:))./60); %calculation of the average fluid velocity in the
bottom layer of height h=13um in cm/sec
  p(n,:)=u(n,:)./max(v(n,:)); %check that calculation is correct
  hold on
  plot(v(1,:),y)
end
%Calculation of settling velocity of cell
vs=-2.*R.^2.*g./(9.*mu).*(rho_huvec-rho)
%Determination of psi
x=[28.48 29.82 52.14 66.86 77.44]./10;
for m=1:length(u)
  psi(m,:)=C.*(1+(vs.*x)./(u(m).*max(y)))
end
figure(2)
hold on
plot(x,(psi(1,:)./C),'g','LineWidth',1.5)
plot(x,(psi(2,:)./C),'m','LineWidth',1.5)
plot(x,(psi(3,:)./C),'b','LineWidth',1.5)
plot(x,(psi(4,:)./C),'k','LineWidth',1.5)
plot(x,(psi(5,:)./C),'r','LineWidth',1.5)
legend('Q=1 mL/min','Q=4 mL/min','Q=8.01 mL/min','Q=40 mL/min','Q=80 mL/min')
title('\Psi_{ss}/C_o as a function of the distance from the site of injection')
```

```
ylabel('\Psi_{ss}/C_o')
xlabel('Distance from the point of injection (cm)')
%
% Determination of rate constant
% Number of cells adhered in cells/area
Nfn_50=[14000,11000,15000]./4;
Nfn_501=[15200,12000,13400,11000]./4;
Nfn_25=[70000,68800,79600,66600,80000]./4;
Nfn_251=[72300,65800,81200,68000,82000]./4;
Nbfn_rgd_50=[18000,16000,18400]./4;
Nbfn_rgd_501=[20000,17300,17000,16300]./4;
Nbfn_rgd_25=[100000,84400,85600,88600]./4;
Nbfn_rgd_251=[10200,86200,83000,92000,88600]./4;
Ncon_50=[2000,1200,2400]./4;
Ncon_501=[1000,2000,1600,2700,2000]./4;
Ncon_25=[20000,16000,13200,22000]./4;
Ncon_251=[22000,18100,14400,13200,23000]./4;
Nbfn_wtsa_50=[9000,6400,5800,7800]./4;
Nbfn_wtsa_501=[7000,8300,6200,8100]./4;
Nbfn_wtsa_25=[44000,56000,50000,58000]./4;
Nbfn_wtsa_251=[48000,52000,49370,55000,56200]./4;
Nbbsa_50=[11800,13200,11000,14400]./4;
```

```
Nbbsa_501=[13000,12600,15000,10000,12000]./4;
Nbbsa_25=[68800,68000,62000,65000,58000]./4;
Nbbsa_251=[70300,63530,66000,68000,59000]./4;
Nbsa_50=[10000,15400,12400,11800]./4;
Nbsa_501=[9000,17200,13000,14200]./4;
Nbsa_25=[64000,60800,69600,72600,76000]./4;
Nbsa_251=[65000,62800,71000,78000,67000]./4;
%Number of cells adhered for dual ligand design for different flow rates
Nbfn_rgd_1=[100000 84400 85600 88600]./4;
Nbfn_rgd_4=[38000 36000 41000 32000]./4;
Nbfn_rgd_8=[4200 6800 5000 4600]./4;
Nbfn_rgd_40=[0 600 400 1000 2000]./4;
Nbfn_rgd_80=[200 0 0 400 0]./4;
%determination of point rate constants from equation N=k*psi*t
rfn_501=Nfn_50(1)./(psi(1,1).*t);
rfn_502=Nfn_50(2)./(psi(1,2).*t);
rfn_503=Nfn_50(3)./(psi(1,5).*t);
rfn_5011=Nfn_501(1)./(psi(1,1).*t);
rfn_5012=Nfn_501(2)./(psi(1,2).*t);
rfn_5013=Nfn_501(3)./(psi(1,3).*t);
rfn_5014=Nfn_501(4)./(psi(1,5).*t);
rfn_251=Nfn_25(1)./(psi(1,1).*t);
```

```
rfn_252=Nfn_25(2)./(psi(1,2).*t);
rfn_253=Nfn_25(3)./(psi(1,3).*t);
rfn_254=Nfn_25(4)./(psi(1,4).*t);
rfn_255=Nfn_25(5)./(psi(1,5).*t);
rfn_2511=Nfn_251(1)./(psi(1,1).*t);
rfn_2512=Nfn_251(2)./(psi(1,2).*t);
rfn_2513=Nfn_251(3)./(psi(1,3).*t);
rfn_2514=Nfn_251(4)./(psi(1,4).*t);
rfn_2515=Nfn_251(5)./(psi(1,5).*t);
rbfn_rgd_501=Nbfn_rgd_50(1)./(psi(1,1).*t);
rbfn_rgd_502=Nbfn_rgd_50(2)./(psi(1,2).*t);
rbfn_rgd_503=Nbfn_rgd_50(3)./(psi(1,4).*t);
rbfn_rgd_5011=Nbfn_rgd_501(1)./(psi(1,1).*t);
rbfn_rgd_5012=Nbfn_rgd_501(2)./(psi(1,2).*t);
rbfn_rgd_5013=Nbfn_rgd_501(3)./(psi(1,3).*t);
rbfn_rgd_5014=Nbfn_rgd_501(4)./(psi(1,5).*t);
rbfn_rgd_251=Nbfn_rgd_25(1)./(psi(1,1).*t);
rbfn_rgd_252=Nbfn_rgd_25(2)./(psi(1,2).*t);
rbfn_rgd_253=Nbfn_rgd_25(3)./(psi(1,3).*t);
rbfn_rgd_254=Nbfn_rgd_25(4)./(psi(1,5).*t);
rbfn_rgd_2511=Nbfn_rgd_251(1)./(psi(1,1).*t);
rbfn_rgd_2512=Nbfn_rgd_251(2)./(psi(1,2).*t);
```

```
rbfn_rgd_2513=Nbfn_rgd_251(3)./(psi(1,3).*t);
rbfn_rgd_2514=Nbfn_rgd_251(4)./(psi(1,4).*t);
rbfn_rgd_2515=Nbfn_rgd_251(5)./(psi(1,5).*t);
rcon_501=Ncon_50(1)./(psi(1,1).*t);
rcon_502=Ncon_50(2)./(psi(1,3).*t);
rcon_503=Ncon_50(3)./(psi(1,5).*t);
rcon_5011=Ncon_501(1)./(psi(1,1).*t);
rcon_5012=Ncon_501(2)./(psi(1,2).*t);
rcon_5013=Ncon_501(3)./(psi(1,3).*t);
rcon_5014=Ncon_501(4)./(psi(1,4).*t);
rcon_5015=Ncon_501(5)./(psi(1,5).*t);
rcon_251=Ncon_25(1)./(psi(1,1).*t);
rcon_252=Ncon_25(2)./(psi(1,2).*t);
rcon_253=Ncon_25(3)./(psi(1,4).*t);
rcon_254=Ncon_25(4)./(psi(1,5).*t);
rcon_2511=Ncon_251(1)./(psi(1,1).*t);
rcon_2512=Ncon_251(2)./(psi(1,2).*t);
rcon_2513=Ncon_251(3)./(psi(1,3).*t);
rcon_2514=Ncon_251(4)./(psi(1,4).*t);
rcon_2515=Ncon_251(5)./(psi(1,5).*t);
rbfn_wtsa_501=Nbfn_wtsa_50(1)./(psi(1,1).*t);
rbfn_wtsa_502=Nbfn_wtsa_50(2)./(psi(1,2).*t);
```

```
rbfn_wtsa_503=Nbfn_wtsa_50(3)./(psi(1,3).*t);
rbfn_wtsa_504=Nbfn_wtsa_50(4)./(psi(1,5).*t);
rbfn_wtsa_5011=Nbfn_wtsa_501(1)./(psi(1,1).*t);
rbfn_wtsa_5012=Nbfn_wtsa_501(2)./(psi(1,2).*t);
rbfn_wtsa_5013=Nbfn_wtsa_501(3)./(psi(1,3).*t);
rbfn_wtsa_5014=Nbfn_wtsa_501(4)./(psi(1,5).*t);
rbfn_wtsa_251=Nbfn_wtsa_25(1)./(psi(1,1).*t);
rbfn_wtsa_252=Nbfn_wtsa_25(2)./(psi(1,2).*t);
rbfn_wtsa_253=Nbfn_wtsa_25(3)./(psi(1,3).*t);
rbfn_wtsa_254=Nbfn_wtsa_25(4)./(psi(1,5).*t);
rbfn_wtsa_2511=Nbfn_wtsa_251(1)./(psi(1,1).*t);
rbfn_wtsa_2512=Nbfn_wtsa_251(2)./(psi(1,2).*t);
rbfn_wtsa_2513=Nbfn_wtsa_251(3)./(psi(1,3).*t);
rbfn_wtsa_2514=Nbfn_wtsa_251(4)./(psi(1,4).*t);
rbfn_wtsa_2515=Nbfn_wtsa_251(5)./(psi(1,5).*t);
rbbsa_501=Nbbsa_50(1)./(psi(1,1).*t);
rbbsa_502=Nbbsa_50(2)./(psi(1,3).*t);
rbbsa_503=Nbbsa_50(3)./(psi(1,4).*t);
rbbsa_504=Nbbsa_50(4)./(psi(1,5).*t);
rbbsa_5011=Nbbsa_501(1)./(psi(1,1).*t);
rbbsa_5012=Nbbsa_501(2)./(psi(1,2).*t);
rbbsa_5013=Nbbsa_501(3)./(psi(1,3).*t);
```

```
rbbsa_5014=Nbbsa_501(4)./(psi(1,4).*t);

rbbsa_5015=Nbbsa_501(5)./(psi(1,5).*t);

rbbsa_251=Nbbsa_25(1)./(psi(1,1).*t);

rbbsa_252=Nbbsa_25(2)./(psi(1,2).*t);

rbbsa_253=Nbbsa_25(3)./(psi(1,3).*t);

rbbsa_254=Nbbsa_25(4)./(psi(1,4).*t);

rbbsa_255=Nbbsa_25(5)./(psi(1,5).*t);

rbbsa_2511=Nbbsa_251(1)./(psi(1,1).*t);

rbbsa_2512=Nbbsa_251(2)./(psi(1,2).*t);

rbbsa_2513=Nbbsa_251(3)./(psi(1,3).*t);

rbbsa_2514=Nbbsa_251(4)./(psi(1,4).*t);

rbbsa_2515=Nbbsa_251(5)./(psi(1,5).*t);

rbsa_501=Nbsa_50(1)./(psi(1,1).*t);

rbsa_502=Nbsa_50(2)./(psi(1,2).*t);

rbsa_503=Nbsa_50(3)./(psi(1,3).*t);

rbsa_504=Nbsa_50(4)./(psi(1,5).*t);

rbsa_5011=Nbsa_501(1)./(psi(1,1).*t);

rbsa_5012=Nbsa_501(2)./(psi(1,2).*t);

rbsa_5013=Nbsa_501(3)./(psi(1,3).*t);

rbsa_5014=Nbsa_501(4)./(psi(1,5).*t);

rbsa_251=Nbsa_25(1)./(psi(1,1).*t);

rbsa_252=Nbsa_25(2)./(psi(1,2).*t);
```

```
rbsa_253=Nbsa_25(3)./(psi(1,3).*t);

rbsa_254=Nbsa_25(4)./(psi(1,4).*t);

rbsa_255=Nbsa_25(5)./(psi(1,5).*t);

rbsa_2511=Nbsa_251(1)./(psi(1,1).*t);

rbsa_2512=Nbsa_251(2)./(psi(1,2).*t);

rbsa_2513=Nbsa_251(3)./(psi(1,3).*t);

rbsa_2514=Nbsa_251(4)./(psi(1,4).*t);

rbsa_2515=Nbsa_251(5)./(psi(1,5).*t);

%determination of point rate constants for dual ligand at varying flow

%rates

rbfn_rgd_11=Nbfn_rgd_1(1)./(psi(1,1).*t);

rbfn_rgd_12=Nbfn_rgd_1(2)./(psi(1,2).*t);

rbfn_rgd_13=Nbfn_rgd_1(3)./(psi(1,3).*t);

rbfn_rgd_14=Nbfn_rgd_1(4)./(psi(1,5).*t);

rbfn_rgd_41=Nbfn_rgd_4(1)./(psi(2,1).*t);

rbfn_rgd_42=Nbfn_rgd_4(2)./(psi(2,2).*t);

rbfn_rgd_43=Nbfn_rgd_4(3)./(psi(2,3).*t);

rbfn_rgd_44=Nbfn_rgd_4(4)./(psi(2,4).*t);

rbfn_rgd_81=Nbfn_rgd_8(1)./(psi(3,1).*t);

rbfn_rgd_82=Nbfn_rgd_8(2)./(psi(3,3).*t);

rbfn_rgd_83=Nbfn_rgd_8(3)./(psi(3,4).*t);

rbfn_rgd_84=Nbfn_rgd_8(4)./(psi(3,5).*t);
```

```
rbfn_rgd_401=Nbfn_rgd_40(1)./(psi(4,1).*t);
rbfn_rgd_402=Nbfn_rgd_40(2)./(psi(4,2).*t);
rbfn_rgd_403=Nbfn_rgd_40(3)./(psi(4,3).*t);
rbfn_rgd_404=Nbfn_rgd_40(4)./(psi(4,4).*t);
rbfn_rgd_405=Nbfn_rgd_40(5)./(psi(4,5).*t);
rbfn_rgd_801=Nbfn_rgd_80(1)./(psi(5,1).*t);
rbfn_rgd_802=Nbfn_rgd_80(2)./(psi(5,2).*t);
rbfn_rgd_803=Nbfn_rgd_80(3)./(psi(5,3).*t);
rbfn_rgd_804=Nbfn_rgd_80(4)./(psi(5,4).*t);
rbfn_rgd_805=Nbfn_rgd_80(5)./(psi(5,5).*t);
%average all point values of rate constants
rfn_50=mean([rfn_501 rfn_502 rfn_503]);
rfn_502=mean([rfn_5011 rfn_5012 rfn_5013 rfn_5014]);
rfn_25=mean([rfn_251 rfn_252 rfn_253 rfn_254 rfn_255]);
rfn_252=mean([rfn_2511 rfn_2512 rfn_2513 rfn_2514 rfn_2515]);
rbfn_rgd_50=mean([rbfn_rgd_501 rbfn_rgd_502 rbfn_rgd_503]);
rbfn_rgd_502=mean([rbfn_rgd_5011 rbfn_rgd_5012 rbfn_rgd_5013 rbfn_rgd_5014]);
rbfn_rgd_25=mean([rbfn_rgd_251 rbfn_rgd_252 rbfn_rgd_253 rbfn_rgd_254]);
rbfn_rgd_252=mean([rbfn_rgd_2511 rbfn_rgd_2512 rbfn_rgd_2513 rbfn_rgd_2514]);
rcon_50=mean([rcon_501 rcon_502 rcon_503]);
rcon_502=mean([rcon_5011 rcon_5012 rcon_5013 rcon_5014 rcon_5015]);
rcon_25=mean([rcon_251 rcon_252 rcon_253 rcon_254]);
```

```
rcon_252=mean([rcon_2511 rcon_2512 rcon_2513 rcon_2514 rcon_2515]);
rbfn_wtsa_50=mean([rbfn_wtsa_501 rbfn_wtsa_502 rbfn_wtsa_503 rbfn_wtsa_504]);
rbfn_wtsa_502=mean([rbfn_wtsa_5011 rbfn_wtsa_5012 rbfn_wtsa_5013
rbfn_wtsa_5014]);
rbfn_wtsa_25=mean([rbfn_wtsa_251 rbfn_wtsa_252 rbfn_wtsa_253 rbfn_wtsa_254]);
rbfn_wtsa_252=mean([rbfn_wtsa_2511 rbfn_wtsa_2512 rbfn_wtsa_2513
rbfn_wtsa_2514 rbfn_wtsa_2515]);
rbbsa_50=mean([rbbsa_501 rbbsa_502 rbbsa_503 rbbsa_504]);
rbbsa_502=mean([rbbsa_5011 rbbsa_5012 rbbsa_5013 rbbsa_5014 rbbsa_5015]);
rbbsa_25=mean([rbbsa_251 rbbsa_252 rbbsa_253 rbbsa_254 rbbsa_255]);
rbbsa_252=mean([rbbsa_2511 rbbsa_2512 rbbsa_2513 rbbsa_2514 rbbsa_2515]);
rbsa_50=mean([rbsa_501 rbsa_502 rbsa_503 rbsa_504]);
rbsa_502=mean([rbsa_5011 rbsa_5012 rbsa_5013 rbsa_5014]);
rbsa_25=mean([rbsa_251 rbsa_252 rbsa_253 rbsa_254 rbsa_255]);
rbsa_252=mean([rbsa_2511 rbsa_2512 rbsa_2513 rbsa_2514 rbsa_2515]);
%average all point values of rate constants for differing flow rates
rbfn_rgd_1=mean([rbfn_rgd_11 rbfn_rgd_12 rbfn_rgd_13 rbfn_rgd_14]);
rbfn_rgd_4=mean([rbfn_rgd_41 rbfn_rgd_42 rbfn_rgd_43 rbfn_rgd_44]);
rbfn_rgd_8=mean([rbfn_rgd_81 rbfn_rgd_82 rbfn_rgd_83 rbfn_rgd_84]);
rbfn_rgd_40=mean([rbfn_rgd_401 rbfn_rgd_402 rbfn_rgd_403 rbfn_rgd_404
rbfn_rgd_405]);
```

```
rbfn_rgd_80=mean([rbfn_rgd_801 rbfn_rgd_802 rbfn_rgd_803 rbfn_rgd_804
rbfn_rgd_805]);
%plot solutions for different substrates
r_ht=([mean([rfn_50 rfn_502]) mean([rbfn_rgd_50 rbfn_rgd_502]) mean([rcon_50
rcon_502]) mean([rbfn_wtsa_50 rbfn_wtsa_502]) mean([rbbsa_50 rbbsa_502])
mean([rbsa_50 rbsa_502])]')
r_lt=([mean([rfn_25 rfn_252]) mean([rbfn_rgd_25 rbfn_rgd_252]) mean([rcon_25
rcon_252]) mean([rbfn_wtsa_25 rbfn_wtsa_252]) mean([rbbsa_25 rbbsa_252])
mean([rbsa_25 rbsa_252])]')
e_ht=([std([rfn_50 rfn_502]) std([rbfn_rgd_50 rbfn_rgd_502]) std([rcon_50 rcon_502])
std([rbfn_wtsa_50 rbfn_wtsa_502]) std([rbbsa_50 rbbsa_502]) std([rbsa_50
rbsa_502])]')./sqrt(2)
e_lt=([std([rfn_25 rfn_252]) std([rbfn_rgd_25 rbfn_rgd_252]) std([rcon_25 rcon_252])
std([rbfn_wtsa_25 rbfn_wtsa_252]) std([rbbsa_25 rbbsa_252]) std([rbsa_25
rbsa_252])]')./sqrt(2)
figure(3)
bar([r_lt r_ht],'group')
hold on
e=[e_lt(1) e_ht(1) e_lt(2) e_ht(2) e_lt(3) e_ht(3) e_lt(4) e_ht(4) e_lt(5) e_ht(5) e_lt(6)
e_ht(6)];
legend('0.025% TE','0.05% TE')
xlabel('Treatment Type')
```

```
ylabel('Rate Constant (cm/sec^{-1})')
title('Rate Constants for Different Substrate Treatment Types')
set(gca,'XTickLabel',{'FN';'bFN+RGD-SA';'No Ligand';'bFN-WT-
SA';'bBSA';'BSA'},'Fontsize',8)
%plot solutions for differing flow rates
figure(4)
bar([rbfn_rgd_1 rbfn_rgd_4 rbfn_rgd_8 rbfn_rgd_40 rbfn_rgd_80])
xlabel('Flow rate (mL/min)')
ylabel('Rate Constant (cm/sec^{-1})')
title('Rate Constants for Flow Rates for BFn-RGD System with 0.025%
Trypsin','FontSize',8)
set(gca,'XTickLabel',{'1 mL/min';'4 mL/min';'8 mL/min';'40 mL/min';'80
mL/min'},'Fontsize',8)
function huvecdragsettling
clear all
%constants
g=-980; %cm/s^2, gravity
mu=0.04; %g/cm/s, fluid viscosity
h=0.0658; %height of chamber in cm
R=6.8e-4; %radius of huvec in cm
w=1.85; %width of chamber in cm
L=10; %length of chamber in cm
```

```
rho_huvec=1.09; %density of leukocyte in g/cm^3
rho=1.01; %density of fluid in g/cm^3
tau_wall=1; %shear stress at wall in dyne/cm^2
%calculation of settling velocity
vs=((2/9).*(rho_huvec-rho)*g*R.^2)./mu; %cm/sec
Q=[1 4 8.01 40 80]; %Flow rate in mL/min
%calculation of average velocity in x-direction
vav=(Q./(w.*h))./60 %cm^3/sec
%set up initial conditions
sol_init=[0,0.0621];
%set up time interval
t_interval=0:0.05:325;
%solve using ode45
[tnum,sol]=ode45(@ode_system,t_interval,sol_init);
%extract individual solutions
plot(real(sol(:,1)),real(sol(:,2)),'c','LineWidth',2)
axis([0 50 0 h])
title('HUVEC Trajectory at Q=1 mL/min for Varying Entry Points')
xlabel('Distance from injection (cm)')
ylabel('Height (cm)')
hold on
x=linspace(0,0.0658,10);
```

```
xplot=0:1:50;
for k=1:length(x)
  plot(xplot,x(k),'k--')
end
function dydt=ode_system(t,y)
x=y(1);
y=y(2);
alpha=log(y/0.00068+sqrt((y/0.00068).^2-1));
z=log(log10(y/0.00068));
f1=exp((-4.92E-7*z.^6-3.0674E-5*z.^5-7.43194E-4*z.^4-8.646551E-3*z.^3-
0.044100646*z.^2+0.057316483*z-0.013336984));
for yindex = 1:length(alpha);
  for i = 1:20;
     elements(i) = ((i*(i+1))/((2*i-1)*(2*i+3)))*...
        (((2*sinh((2*i+1)*alpha(yindex)))+((2*i+1)*sinh(2*alpha(yindex))))/...
        ((4*(sinh((i+0.5)*alpha(yindex)))^2)-(((2*i+1)^2)*(sinh(alpha(yindex)))^2))-1);
  end
  summation = sum(elements);
  f2(yindex) = (4/3)*sinh(alpha(yindex)).*summation;
end
dydt=[(6.*0.1369.*(0.0658.^-1.*y-0.0658.^-2.*y.*y).*f1)
  (-0.00020140./f2)   ];
```

Appendix 3 Detailed Experimental Protocols

Surface plasmon resonance (SPR) spectroscopy protocol

Objective: Determine amount of wild type SA and mutant RGD-SA binding to biotinylated fibronectin (bFN) and the kinetics of the binding

Materials:

-Gold coated 1 cm^2 chips

-2mM 16-mercaptohexadecanoic acid in EtOH(Sigma, 448303)

-0.4M EDC (Sigma, E1769) in dPBS ; 0.1M NHS in dPBS (Sigma, H7377)

-Degassed dPBS

-Well calibrated P100

-200 ul pipette tips

Procedure:

A: Prior to using instrument

1. Make 100 ul each of EDC and NHS and freeze ahead of time
2. Make gold coated chips (courtesy of Jason Smith)
3. Generate Self assembled monolayer on gold chips by incubating for 24 hours in ~ 4.5 ml of 2 mM 16-mercaptohexadecanoic acid
4. Rinse chips with ethanol and dry with compressed Nitrogen gas
5. Cut chips to 1cm^2 size using template and diamond-tipped glass cutter

6. Assemble chip holder using double stick tape; keep gold coated side exposed to flow path

B: Once at instrument

1. Switch buffer to degassed dPBS
2. There is usually buffer running so stop sensorgram from “command” menu
3. Undock chip from “command” menu
4. Insert new, unused chip and proceed with docking
5. From “command” menu, run sensorgram
    a. Multi-channel; check both channel 1 and 2
6. Set flow rate to 20ul/min or something higher to flush any debris or junk on gold chip
7. Allow the slope of the baseline of the curve to get to <= 0.01
    a. Check the slope by adding report point from the reference line
    b. Check the slope over a range between 80-100 seconds
    c. Change flow rate to 5ul/min from command menu
8. Inject 35 ul of EDC/NHS mix (already thawed out and degassed for ~ 5 min) from the command menu
    a. Pull out 60 ul of the mix; add 10 ul of air; pull out another 5 ul of the mix; add 5 ul of air
9. Inject and let run for ~7 min
10. After injection is finished, change flow rate to 2ul/min

11. After injection allow the slope of the baseline to drop below ~0.01 prior to injecting ligand of interest
    a. Inject from command menu; in the window change the injection volume to 55ul
    b. Pull out 75 ul of ligand; add 10ul of air; pull out another 5 ul; Inject
12. Allow to run for ~29 min
13. Check baseline to make sure the slope is ~0.01 prior to injection of analyte
14. Inject analyte with the same injection pattern as the ligand
15. Allow to run for ~29 min or longer depending on your needs

BIBLIOGRAPHY

1. www.americanheart.com. 2006.

2. Salacinski,H.J., Punshon,G., Krijgsman,B., Hamilton,G., & Seifalian,A.M. A hybrid compliant vascular graft seeded with microvascular endothelial cells extracted from human omentum. *Artificial Organs.* **25**, 974-82 (2001).

3. Eisenberg,M.J., Filion,K.B., Azoulay,A., Brox,A.C., Haider,S., & Pilote,L. Outcomes and cost of coronary artery bypass graft surgery in the United States and Canada. *Archives of Internal Medicine. 165(13):1506-13,* (2005).

4. Tiwari,A., Salacinski,H., Seifalian,A.M., & Hamilton,G. New prostheses for use in bypass grafts with special emphasis on polyurethanes. *Cardiovascular Surgery. 10(3):191-7,* (2002).

5. Zilla,P., Deutsch,M., & Meinhart,J. Endothelial cell transplantation. *Seminars in Vascular Surgery.* **12**, 52-63 (1999).

6. Walluscheck,K.P., Steinhoff,G., Kelm,S., & Haverich,A. Improved endothelial cell attachment on ePTFE vascular grafts pretreated with synthetic RGD-containing peptides. *European Journal of Vascular & Endovascular Surgery.* **12**, 321-30 (1996).

7. Poole-Warren,L.A., Schindhelm,K., Graham,A.R., Slowiaczek,P.R., & Noble,K.R. Performance of small diameter synthetic vascular prostheses with confluent autologous endothelial cell linings. *Journal of Biomedical Materials Research. 30(2):221-29,* (1996).

8. Gumpenberger,T., Heitz,J., Bauerle,D., Kahr,H., Graz,I., Romanin,C., Svorcik,V., & Leisch,F. Adhesion and proliferation of human endothelial cells on photochemically modified polytetrafluoroethylene. *Biomaterials. 24(28):5139-44,* (2003).

9. Hagerty,R.D., Salzmann,D.L., Kleinert,L.B., & Williams,S.K. Cellular proliferation and macrophage populations associated with implanted expanded polytetrafluoroethylene and polyethyleneterephthalate. *Journal of Biomedical Materials Research. 49(4):489-97,* (2000).

10. James,N.L., Schindhelm,K., Slowiaczek,P., Milthorpe,B.K., Dudman,N.P., Johnson,G., & Steele,J.G. Endothelial cell seeding of small diameter vascular grafts. *Artificial Organs.* **14**, 355-60 (1990).

11. Honduvilla,N.G., Bujan,J., Lizarbe,M.A., Bellon,J.M., Olmo,N., & Hernando,A. Adhesion and stability of fibronectin on PTFE before and after seeding with normal and synchronized endothelial cells: in vitro study. *Artificial Organs.* 144-153 (1919).

12. Chan,B.P., Liu,W., Klitzman,B., Reichert,W.M., & Truskey,G.A. In vivo performance of dual ligand augmented endothelialized expanded polytetrafluoroethylene vascular grafts. *Journal of Biomedical Materials Research. Part B, Applied Biomaterials. 72(1):52-63,* (2005).

13. Hirose,H., Amano,A., Takanashi,S., & Takahashi,A. Coronary artery bypass grafting using the gastroepiploic artery in 1,000 patients. *Annals of Thoracic Surgery. 73(5):1371-9,* (2002).

14. Motwani,J.G. & Topol,E.J. Aortocoronary saphenous vein graft disease: pathogenesis, predisposition, and prevention. *Circulation. 97(9):916-31,* (1998).

15. Weintraub,W.S., Jones,E.L., Craver,J.M., & Guyton,R.A. Frequency of repeat coronary bypass or coronary angioplasty after coronary artery bypass surgery using saphenous venous grafts. *American Journal of Cardiology. 73(2):103-12,* (1994).

16. Sayers,R.D., Raptis,S., Berce,M., & Miller,J.H. Long-term results of femorotibial bypass with vein or polytetrafluoroethylene.. *British Journal of Surgery. 85(7):934-8,* (1998).

17. Deutsch,M., Meinhart,J., Fischlein,T., Preiss,P., & Zilla,P. Clinical autologous in vitro endothelialization of infrainguinal ePTFE grafts in 100 patients: a 9-year experience. *Surgery.* **126**, 847-55 (1999).

18. Bos,G.W., Poot,A.A., Beugeling,T., van Aken,W.G., & Feijen,J. Small-diameter vascular graft prostheses: Current status. *Archives of Physiology and Biochemistry* **106**, 100-115 (1998).

19. Ballermann,B.J., Dardik,A., Eng,E., & Liu,A. Shear stress and the endothelium. [Review] [91 refs]. *Kidney International - Supplement. 67:S100-8,* (1998).

20. Zilla,P. Endothelialization of vascular grafts. *Current Opinion in Cardiology.* **6**, 877-86 (1991).

21. Nerem,R.M. & Seliktar,D. Vascular tissue engineering. *Annual Review of Biomedical Engineering. 3:225-43,* (2001).

22. Dardik,A., Liu,A., & Ballermann,B.J. Chronic in vitro shear stress stimulates endothelial cell retention on prosthetic vascular grafts and reduces subsequent in vivo neointimal thickness. *Journal of Vascular Surgery.* **29**, 157-67 (1999).

23. L'Heureux,N., Paquet,S., Labbe,R., Germain,L., & Auger,F.A. A completely biological tissue-engineered human blood vessel. *FASEB Journal. 12(1):47-56,* (1998).

24. Seifalian,A.M., Tiwari,A., Hamilton,G., & Salacinski,H.J. Improving the clinical patency of prosthetic vascular and coronary bypass grafts: the role of seeding and tissue engineering. *Artificial Organs. 26(4):307-20,* (2002).

25. Kannan,R.Y., Salacinski,H.J., Butler,P.E., Hamilton,G., & Seifalian,A.M. Current status of prosthetic bypass grafts: a review. *Journal of Biomedical Materials Research. Part B, Applied Biomaterials. 74(1):570-81,* (2005).

26. Niklason,L.E., Gao,J., Abbott,W.M., Hirschi,K.K., Houser,S., Marini,R., & Langer,R. Functional arteries grown in vitro. *Science. 284(5413):489-93,* (1999).

27. Weinberg,C.B. & Bell,E. A blood vessel model constructed from collagen and cultured vascular cells. *Science. 231(4736):397-400,* (1986).

28. Xue,L. & Greisler,H.P. Biomaterials in the development and future of vascular grafts. *Journal of Vascular Surgery. 37(2):472-80,* (2003).

29. Quarmby,J.W., Burnand,K.G., Lockhart,S.J., Donald,A.E., Sommerville,K.M., Jamieson,C.W., & Browse,N.L. Prospective randomized trial of woven versus collagen-impregnated knitted prosthetic Dacron grafts in aortoiliac surgery. *British Journal of Surgery. 85(6):775-7,* (1998).

30. Fournier,N. & Doillon,C.J. Biological molecule-impregnated polyester: an in vivo angiogenesis study. *Biomaterials. 17(17):1659-65,* (1996).

31. Eberhart,A., Zhang,Z., Guidoin,R., Laroche,G., Guay,L., De La Faye,D., Batt,M., & King,M.W. A new generation of polyurethane vascular prostheses: rara avis or ignis fatuus? *Journal of Biomedical Materials Research.* **48**, 546-58 (1999).

32. Tai,N.R., Salacinski,H.J., Edwards,A., Hamilton,G., & Seifalian,A.M. Compliance properties of conduits used in vascular reconstruction. *British Journal of Surgery. 87(11):1516-24,* (2000).

33. Edwards,A., Carson,R.J., Szycher,M., & Bowald,S. In vitro and in vivo biodurability of a compliant microporous vascular graft. *Journal of Biomaterials Applications. 13(1):23-45,* (1998).

34. Walden,R., L'Italien,G.J., Megerman,J., & Abbott,W.M. Matched elastic properties and successful arterial grafting. *Archives of Surgery. 115(10):1166-9,* (1980).

35. Abbott,W.M., Megerman,J., Hasson,J.E., L'Italien,G., & Warnock,D.F. Effect of compliance mismatch on vascular graft patency. *Journal of Vascular Surgery. 5(2):376-82,* (1987).

36. Herring,M., Gardner,A., & Glover,J. A single-staged technique for seeding vascular grafts with autogenous endothelium. *Surgery. 84(4):498-504,* (1978).

37. Phaneuf,M.D., Dempsey,D.J., Bide,M.J., Quist,W.C., & LoGerfo,F.W. Coating of Dacron vascular grafts with an ionic polyurethane: a novel sealant with protein binding properties. *Biomaterials.* **22**, 463-9 (2001).

38. Xiao,L. & Shi,D. Role of precoating in artificial vessel endothelialization. [Review] [29 refs]. *Chinese Journal of Traumatology. 7(5):312-6,* (2004).

39. Bensen,C.V., Vann,R.D., Koger,K.E., & Klitzman,B. Quantification of gas denucleation and thrombogenicity of vascular grafts. *Journal of Biomedical Materials Research. 25(3):373-86,* (1991).

40. Trudell,L.A., Boudreau,L., Van de Water,J.M., Jauregui,H., Richardson,P.D., & Galletti,P.M. Alcohol-treated PTFE vascular grafts. *Transactions - American Society for Artificial Internal Organs. 24:320-3,* (1978).

41. Ritter,E.F., Vann,R.D., Wyble,C., Barwick,W.J., & Klitzman,B. Hydrostatic pressure reduces thrombogenicity of polytetrafluoroethylene vascular grafts. *American Journal of Physiology.* **257**, t-81 (1989).

42. Rashid,S.N., Clark,H.G., Vann,R.D., Gerth,W.A., Palmos,L.A., & Mikat,E.M. The effect of interstitial air on the in vitro thrombogenicity of ePTFE vascular grafts. *Journal of Bioactive & Compatible Polymers. 7(1):54-64,* (1992).

43. Chen,M., Zamora,P.O., Som,P., Pena,L.A., & Osaki,S. Cell attachment and biocompatibility of polytetrafluoroethylene (PTFE) treated with glow-discharge plasma of mixed ammonia and oxygen. *Journal of Biomaterials Science, Polymer Edition. 14(9):917-35,* (2003).

44. Chandy,T., Das,G.S., Wilson,R.F., & Rao,G.H. Use of plasma glow for surface-engineering biomolecules to enhance bloodcompatibility of Dacron and PTFE vascular prosthesis. *Biomaterials.* **21**, 699-712 (2000).

45. Pu,F.R., Williams,R.L., Markkula,T.K., & Hunt,J.A. Effects of plasma treated PET and PTFE on expression of adhesion molecules by human endothelial cells in vitro. *Biomaterials.* **23**, 2411-28 (2002).

46. Dekker,A., Reitsma,K., Beugeling,T., Bantjes,A., Feijen,J., & van Aken,W.G. Adhesion of endothelial cells and adsorption of serum proteins on gas plasma-treated polytetrafluoroethylene. *Biomaterials. 12(2):130-8,* (1991).

47. Ramires,P.A., Mirenghi,L., Romano,A.R., Palumbo,F., & Nicolardi,G. Plasma-treated PET surfaces improve the biocompatibility of human endothelial cells. *Journal of Biomedical Materials Research.* **51**, 535-9 (2000).

48. Sipehia,R., Martucci,G., Barbarosie,M., & Wu,C. Enhanced attachment and growth of human endothelial cells derived from umbilical veins on ammonia plasma modified surfaces of PTFE and ePTFE synthetic vascular graft biomaterials. *Biomaterials, Artificial Cells, & Immobilization Biotechnology. 21(4):455-68,* (1993).

49. Cenni,E., Granchi,D., Arciola,C.R., Ciapetti,G., Savarino,L., Stea,S., Cavedagna,D., Di Leo,A., & Pizzoferrato,A. Adhesive protein expression on endothelial cells after contact in vitro with polyethylene terephthalate coated with pyrolytic carbon. *Biomaterials.* **16**, 1223-7 (1995).

50. Hsu,S.H. & Chen,W.C. Improved cell adhesion by plasma-induced grafting of L-lactide onto polyurethane surface. *Biomaterials.* **21**, 359-67 (2000).

51. Chinn,J.A., Sauter,J.A., Phillips,R.E., Jr., Kao,W.J., Anderson,J.M., Hanson,S.R., & Ashton,T.R. Blood and tissue compatibility of modified polyester: thrombosis, inflammation, and healing. *Journal of Biomedical Materials Research.* **39**, 130-40 (1998).

52. Jensen,N., Lindblad,B., & Bergqvist,D. In vitro attachment of endothelial cells to different graft materials. *European Surgical Research.* **28**, 49-54 (1996).

53. Stone,D., Phaneuf,M., Sivamurthy,N., LoGerfo,F.W., & Quist,W.C. A biologically active VEGF construct in vitro: implications for bioengineering-improved prosthetic vascular grafts. *Journal of Biomedical Materials Research.* **59**, 160-5 (2002).

54. Bos,G.W., Scharenborg,N.M., Poot,A.A., Engbers,G.H., Beugeling,T., van Aken,W.G., & Feijen,J. Endothelialization of crosslinked albumin-heparin gels. *Thrombosis & Haemostasis. 82(6):1757-63,* (1999).

55. Grosskreutz,C.L., Anand-Apte,B., Duplaa,C., Quinn,T.P., Terman,B.I., Zetter,B., & D'Amore,P.A. Vascular endothelial growth factor-induced migration of vascular smooth muscle cells in vitro. *Microvascular Research. 58(2):128-36,* (1999).

56. Burgess,W.H. & Maciag,T. The heparin-binding (fibroblast) growth factor family of proteins. *Annual Review of Biochemistry. 58:575-606,* (1989).

57. Bos,G.W., Scharenborg,N.M., Poot,A.A., Engbers,G.H., Beugeling,T., van Aken,W.G., & Feijen,J. Proliferation of endothelial cells on surface-immobilized albumin-heparin conjugate loaded with basic fibroblast growth factor. *Journal of Biomedical Materials Research.* **44**, 330-40 (1999).

58. Bos,G.W., Scharenborg,N.M., Poot,A.A., Engbers,G.H., Terlingen,J.G., Beugeling,T., van Aken,W.G., & Feijen,J. Adherence and proliferation of endothelial cells on surface-immobilized albumin-heparin conjugate. *Tissue Engineering.* **4**, 267-79 (1998).

59. Marois,Y., Chakfe,N., Guidoin,R., Duhamel,R.C., Roy,R., Marois,M., King,M.W., & Douville,Y. An albumin-coated polyester arterial graft: in vivo assessment of biocompatibility and healing characteristics. *Biomaterials.* **17**, 3-14 (1996).

60. McGee,G.S., Shuman,T.A., Atkinson,J.B., Weaver,F.A., & Edwards,W.H. Long-term assessment of a damp-stored, albumin-coated, knitted vascular graft. *American Surgeon.* **55**, 174-6 (1989).

61. Laemmel,E., Penhoat,J., Warocquier-Clerout,R., & Sigot-Luizard,M.F. Heparin immobilized on proteins usable for arterial prosthesis coating: growth inhibition of smooth-muscle cells. *Journal of Biomedical Materials Research.* **39**, 446-452 (1998).

62. Nojiri,C., Park,K.D., Grainger,D.W., Jacobs,H.A., Okano,T., Koyanagi,H., & Kim,S.W. In vivo nonthrombogenicity of heparin immobilized polymer surfaces. *ASAIO Transactions.* **36**, 168-72 (1990).

63. Leseche,G., Bikfalvi,A., Dupuy,E., Tobelem,G., Andreassian,B., & Caen,J. Prelining of polytetrafluoroethylene grafts with cultured human endothelial cells isolated from varicose veins. *Surgery.* **105**, 36-45 (1989).

64. Oltrona,L., Eisenberg,P.R., Abendschein,D.R., & Rubin,B.G. Efficacy of local inhibition of procoagulant activity associated with small-diameter prosthetic vascular grafts. *Journal of Vascular Surgery.* **24**, 624-31 (1996).

65. Weatherford,D.A., Sackman,J.E., Reddick,T.T., Freeman,M.B., Stevens,S.L., & Goldman,M.H. Vascular endothelial growth factor and heparin in a biologic glue promotes human aortic endothelial cell proliferation with aortic smooth muscle cell inhibition. *Surgery.* **120**, 433-9 (1996).

66. Lambert,A.W., Fox,A.D., Williams,D.J., Horrocks,M., & Budd,J.S. Experience with heparin-bonded collagen-coated grafts for infrainguinal bypass.[see comment]. *Cardiovascular Surgery. 7(5):491-4,* (1999).

67. Walpoth,B.H., Rogulenko,R., Tikhvinskaia,E., Gogolewski,S., Schaffner,T., Hess,O.M., & Althaus,U. Improvement of patency rate in heparin-coated small synthetic vascular grafts. *Circulation. 98(19 Suppl):II319-23; discussion II324,* (1998).

68. Greisler,H.P., Tattersall,C.W., Henderson,S.C., Cabusao,E.A., Garfield,J.D., & Kim,D.U. Polypropylene small-diameter vascular grafts. *Journal of Biomedical Materials Research.* **26**, 1383-94 (1992).

69. Gray,J.L., Kang,S.S., Zenni,G.C., Kim,D.U., Kim,P.I., Burgess,W.H., Drohan,W., Winkles,J.A., Haudenschild,C.C., & Greisler,H.P. FGF-1 affixation stimulates ePTFE endothelialization without intimal hyperplasia. *Journal of Surgical Research.* **57**, 596-612 (1994).

70. Wissink,M.J., Beernink,R., Poot,A.A., Engbers,G.H., Beugeling,T., van Aken,W.G., & Feijen,J. Improved endothelialization of vascular grafts by local release of growth factor from heparinized collagen matrices. *Journal of Controlled Release.* **64**, 103-14 (2000).

71. Williams,S.K. Endothelial cell transplantation. *Cell Transplantation.* **4**, 401-410 (1995).

72. Cines,D.B., Pollak,E.S., Buck,C.A., Loscalzo,J., Zimmerman,G.A., McEver,R.P., Pober,J.S., Wick,T.M., Konkle,B.A., Schwartz,B.S., Barnathan,E.S., McCrae,K.R., Hug,B.A., Schmidt,A.M., & Stern,D.M. Endothelial cells in physiology and in the pathophysiology of vascular disorders. *Blood.* **91**, 3527-3561 (1998).

73. Zilla,P., von Oppell,U., & Deutsch,M. The endothelium: a key to the future. *Journal of Cardiac Surgery.* **8**, 32-60 (1993).

74. Vinard,E., Leseche,G., Andreassian,B., & Costagliola,D. In vitro endothelialization of PTFE vascular grafts: A comparison of various substrates, cell densities, and incubation times. *Annals of Vascular Surgery.* **13**, 141-50 (1999).

75. Shi,Q., Bhattacharya,V., Hong-De Wu,M., & Sauvage,L.R. Utilizing granulocyte colony-stimulating factor to enhance vascular graft endothelialization from circulating blood cells. *Annals of Vascular Surgery.* **16**, 314-320 (2002).

76. Dixit,P., Hern-Anderson,D., Ranieri,J., & Schmidt,C.E. Vascular graft endothelialization: comparative analysis of canine and human endothelial cell migration on natural biomaterials. *Journal of Biomedical Materials Research.* **56**, 545-55 (2001).

77. McMillan,R., Meeks,B., Bensebaa,F., Deslandes,Y., & Sheardown,H. Cell adhesion peptide modification of gold-coated polyurethanes for vascular endothelial cell adhesion. *Journal of Biomedical Materials Research.* **54**, 272-83 (2001).

78. Budd,J.S., Allen,K.E., Bell,P.R., & James,R.F. The effect of varying fibronectin concentration on the attachment of endothelial cells to polytetrafluoroethylene vascular grafts. *Journal of Vascular Surgery.* **12**, 126-30 (1990).

79. Pompe,T., Kobe,F., Salchert,K., Jorgensen,B., Oswald,J., & Werner,C. Fibronectin anchorage to polymer substrates controls the initial phase of endothelial cell adhesion. *Journal of Biomedical Materials Research. Part A. 67(2):647-57,* (2003).

80. Foxall,T.L., Auger,K.R., Callow,A.D., & Libby,P. Adult human endothelial cell coverage of small-caliber Dacron and polytetrafluoroethylene vascular prostheses in vitro. *Journal of Surgical Research.* **41**, 158-72 (1986).

81. Sapienza,P., di Marzo,L., Cucina,A., Corvino,V., Mingoli,A., Giustiniani,Q., Ziparo,E., & Cavallaro,A. Release of PDGF-BB and bFGF by human endothelial cells seeded on expanded polytetrafluoroethylene vascular grafts. *Journal of Surgical Research.* **75**, 24-9 (1998).

82. Mooradian,D.L., Trescony,P., Keeney,K., & Furcht,L.T. Effect of glow discharge surface modification of plasma TFE vascular graft material on fibronectin and laminin retention and endothelial cell adhesion. *Journal of Surgical Research.* **53**, 74-81 (1992).

83. Hubbell,J.A., Massia,S.P., & Drumheller,P.D. Surface-grafted cell-binding peptides in tissue engineering of the vascular graft. *Annals of the New York Academy of Sciences.* **665**, 253-8 (1992).

84. Boateng,S.Y., Lateef,S.S., Mosley,W., Hartman,T.J., Hanley,L., & Russell,B. RGD and YIGSR synthetic peptides facilitate cellular adhesion identical to that of laminin and fibronectin but alter the physiology of neonatal cardiac myocytes. *American Journal of Physiology - Cell Physiology. 288(1):C30-8,* (2005).

85. Ozaki,C.K., Phaneuf,M.D., Hong,S.L., Quist,W.C., & LoGerfo,F.W. Glycoconjugate mediated endothelial cell adhesion to Dacron polyester film. *Journal of Vascular Surgery.* **18**, 486-94 (1993).

86. Massia,S.P. & Hubbell,J.A. An RGD spacing of 440 nm is sufficient for integrin alpha V beta 3-mediated fibroblast spreading and 140 nm for focal contact and stress fiber formation. *Journal of Cell Biology. 114(5):1089-100,* (1991).

87. Massia,S.P., Rao,S.S., & Hubbell,J.A. Covalently immobilized laminin peptide Tyr-Ile-Gly-Ser-Arg (YIGSR) supports cell spreading and co-localization of the 67-kilodalton laminin receptor with alpha-actinin and vinculin. *Journal of Biological Chemistry. 268(11):8053-9,* (1993).

88. Vogel,V. & Baneyx,G. The tissue engineeting puzzle: a molecular perspective.. *Annual Review of Biomedical Engineering. 5:441-63,* (2003).

89. Pankov,R. & Yamada,K.M. Fibronectin at a glance. *Journal of Cell Science. 115(Pt* 3861-3863 (2002).

90. Kreis,T. & Vale,R. Guidebook to the Extracellular Matrix and Adhesion Proteins. (Oxford University Press,1993).

91. Hynes,R.O. Integrins: a family of cell surface receptors. *Cell. 48(4):549-54,* (1987).

92. Shyy,J.Y. & Chien,S. Role of integrins in endothelial mechanosensing of shear stress. *Circulation Research. 91(9):769-75,* (2002).

93. Burridge,K., Fath,K., Kelly,T., Nuckolls,G., & Turner,C. Focal adhesions: transmembrane junctions between the extracellular matrix and the cytoskeleton. *Annual Review of Cell Biology. 4:487-525,* (1988).

94. Yamada,K.M. & Geiger,B. Molecular interactions in cell adhesion complexes. *Current Opinion in Cell Biology. 9(1):76-85,* (1997).

95. Ruegg,C. & Mariotti,A. Vascular integrins: pleiotropic adhesion and signaling molecules in vascular homeostasis and angiogenesis. *Cellular & Molecular Life Sciences. 60(6):1135-57,* (2003).

96. Dekker,A., Poot,A.A., van Mourik,J.A., Workel,M.P., Beugeling,T., Bantjes,A., Feijen,J., & van Aken,W.G. Improved adhesion and proliferation of human endothelial cells on polyethylene precoated with monoclonal antibodies directed against cell membrane antigens and extracellular matrix proteins. *Thrombosis & Haemostasis.* **66**, 715-24 (1991).

97. Truskey,G.A. & Pirone,J.S. The effect of fluid shear stress upon cell adhesion to fibronectin-treated surfaces. *Journal of Biomedical Materials Research. 24(10):1333-53,* (1990).

98. Burmeister,J.S., Vrany,J.D., Reichert,W.M., & Truskey,G.A. Effect of fibronectin amount and conformation on the strength of endothelial cell adhesion to HEMA/EMA copolymers. *Journal of Biomedical Materials Research.* **30**, 13-22 (1996).

99. Wigod,M.D. & Klitzman,B. Quantification of in vitro endothelial cell adhesion to vascular graft material. *Journal of Biomedical Materials Research.* **27**, 1057-62 (1993).

100. Anderson,J.S., Price,T.M., Hanson,S.R., & Harker,L.A. In vitro endothelialization of small-caliber vascular grafts. *Surgery.* **101**, 577-86 (1987).

101. Li,J.M., Menconi,M.J., Wheeler,H.B., Rohrer,M.J., Klassen,V.A., Ansell,J.E., & Appel,M.C. Precoating expanded polytetrafluoroethylene grafts alters production of endothelial cell-derived thrombomodulators. *Journal of Vascular Surgery.* **15**, 1010-7 (1992).

102. Kaehler,J., Zilla,P., Fasol,R., Deutsch,M., & Kadletz,M. Precoating substrate and surface configuration determine adherence and spreading of seeded endothelial cells on polytetrafluoroethylene grafts. *Journal of Vascular Surgery. 9(4):535-41,* (1989).

103. Bhat,V.D., Klitzman,B., Koger,K., Truskey,G.A., & Reichert,W.M. Improving endothelial cell adhesion to vascular graft surfaces: clinical need and strategies. *Journal of Biomaterials Science, Polymer Edition.* **9**, 1117-35 (1998).

104. Anamelechi,C.C., Truskey,G.A., & Reichert,W.M. Mylar and Teflon-AF as cell culture substrates for studying endothelial cell adhesion. *Biomaterials. 26(34):6887-96,* (2005).

105. Chan,B.P., Chilkoti,A., Reichert,W.M., & Truskey,G.A. Effect of streptavidin affinity mutants on the integrin- independent adhesion of biotinylated endothelial cells. *Biomaterials* **24**, 559-570 (2003).

106. Brown,M.A., Wallace,C.S., Anamelechi,C.C., Clermont,E., Reichert,W.M., & Truskey,G.A. The use of mild trypsinization conditions in the detachment of endothelial cells to promote subsequent endothelialization on synthetic surfaces. *Biomaterials. 28(27):3928-35,* (2007).

107. Grainger,D.W., Pavon-Djavid,G., Migonney,V., & Josefowicz,M. Assessment of fibronectin conformation adsorbed to polytetrafluoroethylene surfaces from serum protein mixtures and correlation to support of cell attachment in culture. *Journal of Biomaterials Science, Polymer Edition. 14(9):973-88,* (2003).

108. Schraa,A.J., Kok,R.J., Berendsen,A.D., Moorlag,H.E., Bos,E.J., Meijer,D.K.F., de Leij,L.F.M.H., & Molema,G. Endothelial cells internalize and degrade RGD-modified proteins developed for tumor vasculature targeting. *Journal of Controlled Release* **83**, 241-251 (2002).

109. Thomson,G.J., Vohra,R.K., Carr,M.H., & Walker,M.G. Adult human endothelial cell seeding using expanded polytetrafluoroethylene vascular grafts: a comparison of four substrates. *Surgery.* **109**, 20-7 (1991).

110. Vadgama,P. Surfaces and interfaces for biomaterials. (2005).

111. Mathur,A.B., Chan,B.P., Truskey,G.A., & Reichert,W.M. High-affinity augmentation of endothelial cell attachment: long-term effects on focal contact and actin filament formation. *Journal of Biomedical Materials Research. Part A. 66(4):729-37,* (2003).

112. Crist,B. Handbook of Monochromatic XPS Spectra. (Wiley, Chichester, New York,2000).

113. Brandup,J., Immergut,E., & Grulke,E. Polymer Handbook. (Wiley, New York,1999).

114. Bhat,V.D., Truskey,G.A., & Reichert,W.M. Using avidin-mediated binding to enhance initial endothelial cell attachment and spreading. *Journal of Biomedical Materials Research.* **40**, 57-65 (1998).

115. Andrade,J. in Surface and Interfacial Aspects of Biomedical Polymers 105-191 (1985).

116. Jenney,C.R. & Anderson,J.M. Adsorbed serum proteins responsible for surface dependent human macrophage behavior. *Journal of Biomedical Materials Research. 49(4):435-47,* (2000).

117. Baugh,L. & Vogel,V. Structural changes of fibronectin adsorbed to model surfaces probed by fluorescence resonance energy transfer. *Journal of Biomedical Materials Research. Part A. 69(3):525-34,* (2004).

118. Haynes,C.A. & Norde,W. Structures and Stabilities of Adsorbed Proteins. *Journal of Colloid and Interface Science* **169**, 313-328 (1995).

119. Bergkvist,M., Carlsson,J., & Oscarsson,S. Surface-dependent conformations of human plasma fibronectin adsorbed to silica, mica, and hydrophobic surfaces, studied with use of Atomic Force Microscopy. *Journal of Biomedical Materials Research. Part A. 64(2):349-56,* (2003).

120. Huebsch,J.B., Fields,G.B., Triebes,T.G., & Mooradian,D.L. Photoreactive analog of peptide FN-C/H-V from the carboxy-terminal heparin-binding domains of fibronectin supports endothelial cell adhesion and spreading on biomaterial surfaces. *Journal of Biomedical Materials Research.* **31**, 555-67 (1996).

121. Kikuchi,A., Taira,H., Tsuruta,T., Hayashi,M., & Kataoka,K. Adsorbed serum protein mediated adhesion and growth behavior of bovine aortic endothelial cells on polyamine graft copolymer surfaces. *Journal of Biomaterials Science, Polymer Edition. 8(2):77-90,* (1996).

122. Danen,E.H. & Yamada,K.M. Fibronectin, integrins, and growth control. *Journal of Cellular Physiology. 189(1):1-13,* (2001).

123. Wilson,C.J., Clegg,R.E., Leavesley,D.I., & Pearcy,M.J. Mediation of biomaterial-cell interactions by adsorbed proteins: a review. *Tissue Engineering. 11(1-2):1-18,* -Feb (2005).

124. Alberts,B., Lewis,J., Raff,M., Roberts,K., & Watson,J. Molecular Biology of the Cell, 2nd Ed. (1989).

125. Tsai,W.B. & Wang,M.C. Effects of an avidin-biotin binding system on chondrocyte adhesion and growth on biodegradable polymers. *Macromolecular Bioscience. 5(3):214-21,* (2005).

126. Kojima,N., Matsuo,T., & Sakai,Y. Rapid hepatic cell attachment onto biodegradable polymer surfaces without toxicity using an avidin-biotin binding system. *Biomaterials. 27(28):4904-10,* (2006).

127. Hoya,K., Guterman,L.R., Miskolczi,L., & Hopkins,L.N. A novel intravascular drug delivery method using endothelial biotinylation and avidin-biotin binding. *Drug Delivery. 8(4):215-22,* -Dec (2001).

128. McDevitt,T.C., Nelson,K.E., & Stayton,P.S. Constrained cell recognition peptides engineered into streptavidin. *Biotechnology Progress. 15(3):391-6,* -Jun (1999).

129. Smith,J.T., Tomfohr,J.K., Wells,M.C., Beebe,T.P., Jr., Kepler,T.B., & Reichert,W.M. Measurement of cell migration on surface-bound fibronectin gradients. *Langmuir.* 8279-8286 (2004).

130. Koenig,A.L., Gambillara,V., & Grainger,D.W. Correlating fibronectin adsorption with endothelial cell adhesion and signaling on polymer substrates. *Journal of Biomedical Materials Research. Part A. 64(1):20-37,* (2003).

131. Becquemin,J.P., Riff,Y., Kovarsky,S., Ardaillou,N., & Benhaien-Sigaux,N. Evaluation of a polyester collagen-coated heparin bonded vascular graft. *Journal of Cardiovascular Surgery.* **38**, 7-14 (1997).

132. Shimada,T., Nishibe,T., Miura,H., Hazama,K., Kato,H., Kudo,F., Murashita,T., & Okuda,Y. Improved healing of small-caliber, long-fibril expanded polytetrafluoroethylene vascular grafts by covalent bonding of fibronectin. *Surgery Today. 34(12):1025-30,* (2004).

133. Fujita,K. & Silver,J. Surprising lability of biotin-streptavidin bond during transcription of biotinylated DNA bound to paramagnetic streptavidin beads. *Biotechniques. 14(4):608-17,* (1993).

134. Jung,L.S., Nelson,K.E., Stayton,P.S., & Campbell,C.T. Binding and dissociation kinetics of wild-type and mutant streptavidins on mixed biotin-containing alkylthiolate monolayers. *Langmuir* **16**, 9421-9432 (2000).

135. Yang,N., Su,X., Tjong,V., & Knoll,W. Evaluation of two- and three-dimensional streptavidin binding platforms for surface plasmon resonance spectroscopy studies of DNA hybridization and protein-DNA binding. *Biosensors and Bioelectronics* **22**, 2700-2706 (2007).

136. Huang,S.C., Stump,M.D., Weiss,R., & Caldwell,K.D. Binding of Biotinylated DNA to Streptavidin-Coated Polystyrene Latex: Effects of Chain Length and Particle Size. *Analytical Biochemistry* **237**, 115-122 (1996).

137. Jones,M.L. & Kurzban,G.P. Noncooperativity of biotin binding to tetrameric streptavidin. *Biochemistry. 34(37):11750-6,* (1995).

138. Anamelechi,C.C., Clermont,E.E., Brown,M.A., Truskey,G.A., & Reichert,W.M. Streptavidin binding and endothelial cell adhesion to biotinylated fibronectin. *Langmuir. 23(25):12583-8,* (2007).

139. Gao,B., Curtis,T.M., Blumenstock,F.A., Minnear,F.L., & Saba,T.M. Increased recycling of (alpha)5(beta)1 integrins by lung endothelial cells in response to tumor necrosis factor. *J Cell Sci* **113**, 247-257 (2000).

140. Caswell,P.T. & Norman,J.C. Integrin trafficking and the control of cell migration. *Traffic. 7(1):14-21,* (2006).

141. Bordenave,L., Remy-Zolghadri,M., Fernandez,P., Bareille,R., & Midy,D. Clinical performance of vascular grafts lined with endothelial cells. *Endothelium.* **6**, 267-75 (1999).

142. Nelson,K.E., Gamble,L., Jung,L.S., Boeckl,M.S., Naeemi,E., Golledge,S.L., Sasaki,T., Castner,D.G., Campbell,C.T., & Stayton,P.S. Surface characterization of mixed self-assembled monolayers designed for streptavidin immobilization. *Langmuir* **17**, 2807-2816 (2001).

143. Wolz,C., Pohlmann-Dietze,P., Steinhuber,A., Chien,Y.T., Manna,A., van Wamel,W., & Cheung,A. Agr-independent regulation of fibronectin-binding protein(s) by the regulatory locus sar in Staphylococcus aureus. *Molecular Microbiology. 36(1):230-43,* (2000).

144. Talamas-Rohana,P., Rosales-Encina,J.L., Gutierrez,M.C., & Hernandez,V.I. Identification and partial purification of an Entamoeba histolytica membrane protein that binds fibronectin. *Archives of Medical Research. 23(2):119-23,* (1992).

145. Bhat,V.D., Truskey,G.A., & Reichert,W.M. Fibronectin and avidin-biotin as a heterogeneous ligand system for enhanced endothelial cell adhesion. *Journal of Biomedical Materials Research. 41(3):377-85,* (1998).

146. Romer,L.H., Birukov,K.G., & Garcia,J.G. Focal adhesions: paradigm for a signaling nexus. *Circulation Research. 98(5):606-16,* (2006).

147. Garcia,A.J., Vega,M.D., & Boettiger,D. Modulation of cell proliferation and differentiation through substrate-dependent changes in fibronectin conformation. *Molecular Biology of the Cell. 10(3):785-98,* (1999).

148. Preissner,K.T. Structure and biological role of vitronectin. *Annual Review of Cell Biology. 7:275-310,* (1991).

149. Petrie,T.A., Capadona,J.R., Reyes,C.D., & Garcia,A.J. Integrin specificity and enhanced cellular activities associated with surfaces presenting a recombinant fibronectin fragment compared to RGD supports. *Biomaterials. 27(31):5459-70,* (2006).

150. Keselowsky,B.G., Collard,D.M., & Garcia,A.J. Integrin binding specificity regulates biomaterial surface chemistry effects on cell differentiation. *Proceedings of the National Academy of Sciences of the United States of America. 102(17):5953-7,* (2005).

151. Cavalcanti-Adam,E.A., Volberg,T., Micoulet,A., Kessler,H., Geiger,B., & Spatz,J.P. Cell Spreading and Focal Adhesion Dynamics Are Regulated by Spacing of Integrin Ligands. *Biophys. J.* **92**, 2964-2974 (2007).

152. Coussen,F., Choquet,D., Sheetz,M.P., & Erickson,H.P. Trimers of the fibronectin cell adhesion domain localize to actin filament bundles and undergo rearward translocation. *Journal of Cell Science. 115(Pt 12):2581-90,* (2002).

153. Miyamoto,S., Akiyama,S.K., & Yamada,K.M. Synergistic roles for receptor occupancy and aggregation in integrin transmembrane function. *Science. 267(5199):883-5,* (1995).

154. Zamir,E. & Geiger,B. Molecular complexity and dynamics of cell-matrix adhesions.[comment]. [Review] [75 refs]. *Journal of Cell Science. 114(Pt* 3583-3590 (1920).

155. Zamir,E., Katz,M., Posen,Y., Erez,N., Yamada,K.M., Katz,B.Z., Lin,S., Lin,D.C., Bershadsky,A., Kam,Z., & Geiger,B. Dynamics and segregation of cell-matrix adhesions in cultured fibroblasts. *Nature Cell Biology. 2(4):191-6,* (2000).

156. Danen,E.H., Sonneveld,P., Brakebusch,C., Fassler,R., & Sonnenberg,A. The fibronectin-binding integrins alpha5beta1 and alphavbeta3 differentially modulate RhoA-GTP loading, organization of cell matrix adhesions, and fibronectin fibrillogenesis. *Journal of Cell Biology. 159(6):1071-86,* (2002).

157. Munn,L.L., Melder,R.J., & Jain,R.K. Analysis of cell flux in the parallel plate flow chamber: implications for cell capture studies.[erratum appears in Biophys J 1996 Apr;70(4):2033]. *Biophysical Journal. 67(2):889-95,* (1994).

158. Hocking,D.C., Sottile,J., & McKeown-Longo,P.J. Activation of Distinct alpha 5beta 1-mediated Signaling Pathways by Fibronectin's Cell Adhesion and Matrix Assembly Domains. *J. Cell Biol.* **141**, 241-253 (1998).

159. Ochsenhirt,S.E., Kokkoli,E., McCarthy,J.B., & Tirrell,M. Effect of RGD secondary structure and the synergy site PHSRN on cell adhesion, spreading and specific integrin engagement. *Biomaterials. 27(20):3863-74,* (2006).

160. Helmlinger,G., Geiger,R.V., Schreck,S., & Nerem,R.M. Effects of pulsatile flow on cultured vascular endothelial cell morphology. *Journal of Biomechanical Engineering. 113(2):123-31,* (1991).

161. Feugier,P., Black,R.A., Hunt,J.A., & How,T.V. Attachment, morphology and adherence of human endothelial cells to vascular prosthesis materials under the action of shear stress. *Biomaterials. 26(13):1457-66,* (2005).

162. Malek,A.M. & Izumo,S. Control of endothelial cell gene expression by flow. *Journal of Biomechanics. 28(12):1515-28,* (1995).

163. Hsu,S.h., Tsai,I.j., Lin,D.j., & Chen,D.C. The effect of dynamic culture conditions on endothelial cell seeding and retention on small diameter polyurethane vascular grafts. *Medical Engineering & Physics* **27**, 267-272 (2005).

164. Bordenave,L., Fernandez,P., Remy-Zolghadri,M., Villars,S., Daculsi,R., & Midy,D. In vitro endothelialized ePTFE prostheses: clinical update 20 years after the first realization. *Clinical Hemorheology & Microcirculation. 33(3):227-34,* (2005).

165. Soletti,L., Nieponice,A., Guan,J., Stankus,J.J., Wagner,W.R., & Vorp,D.A. A seeding device for tissue engineered tubular structures. *Biomaterials. 27(28):4863-70,* (2006).

166. Nasseri,B.A., Pomerantseva,I., Kaazempur-Mofrad,M.R., Sutherland,F.W., Perry,T., Ochoa,E., Thompson,C.A., Mayer,J.E., Jr., Oesterle,S.N., & Vacanti,J.P. Dynamic rotational seeding and cell culture system for vascular tube formation. *Tissue Engineering. 9(2):291-9,* (2003).

CHARLES C. ANAMELECHI

BIRTHDAY: July 17, 1978

BIRTH PLACE: Imo State, Nigeria

EDUCATION

DUKE UNIVERSITY, Durham, NC
Candidate for Doctor of Philosophy, Biomedical Engineering, expected May 2008.

DUKE UNIVERSITY, Durham, NC
Master of Science, Biomedical Engineering, "In Vitro Optimization of Cell Seeding Methods to Improve Patency of Synthetic Vascular Grafts"

HOWARD UNIVERSITY, Washington, DC
Bachelor of Science, Chemistry, with minor in Mathematics and Allied Health, May 2001. Magna Cum Laude, Phi Beta Kappa.

SELECTED PUBLICATIONS and PEER REVIEWED ABSTRACTS with PRESENTATIONS

C.C. Anamelechi, E. Clermont, M.A. Brown, G.A. Truskey, and W.M. Reichert. Streptavidin Binding and Endothelial Cell Adhesion to Biotinylated Fibronectin. *Langmuir Vol. 23 Is. 25 (2007) 12583-12588*

M.A. Brown, C.S. Wallace, C.C. Anamelechi, E. Clermont, W.M. Reichert, and G.A. Truskey. The Use of Mild Trypsinization Conditions in the Detachment of Endothelial Cells to Promote Subsequent Endothelialization on Synthetic Surfaces. *Biomaterials 28 (2007) 3928-3935*

C.C. Anamelechi (Presenter), E. Clermont, G.A. Truskey, and W.M. Reichert. Endothelial Cell Adhesion on Teflon-AF using Biotin Functionalized Fibronectin. Society for Biomaterials Conference, Chicago, IL. April 2007

C.C. Anamelechi (Presenter), E. Clermont, G.A. Truskey, and W.M. Reichert. In Vitro Optimization of Cell Seeding Methods to Improve Endothelial Cell Attachment to Synthetic Vascular Grafts. American Heart Association Conference, Chicago, Ill. Nov. 2006

C. C. Anamelechi (Presenter) and W.M. Reichert. Strength of Fibronectin Adsorption to Polymer Materials. Society for Biomaterials Conference, Pittsburgh, PA. April 2006

C.C. Anamelechi, G.A. Truskey, and W.M. Reichert. Mylar and Teflon-AF as Cell Culture Substrates for Studying Endothelial Cell Adhesion. *Biomaterials 26 (2005) 6887-6896*

C. C. Anamelechi (Presenter), M. Wang, M. Brown, A. Chilkoti, G.A. Truskey, and W.M. Reichert. Biotinylated Fibronectin Used with RGD-SA Streptavidin Incubated Cells Improved Cell Adhesion on ePTFE Vascular Graft Constructs. American Heart Association Conference, Dallas, TX. November 2005

C. C. Anamelechi (Presenter), M. Wang, L. Lee-Houghton, G.A. Truskey, and W.M. Reichert. In Vitro Characterization of Endothelial Cell Adhesion on Teflon-AF. Gordon Research Conference, Plymouth, NH. July 2005

C. C. Anamelechi (Presenter), G.A. Truskey, and W.M. Reichert. Teflon-AF and Mylar as Model Vascular Surfaces for Studying In Vitro Cell Adhesion. Biomedical Engineering Society Annual Conference, Philadelphia, Pa. October 2004

C. C. Anamelechi (Presenter) and W.M. Reichert. Optimizing In Vitro Cellular Adhesion on Polymer Surfaces. Biomedical Engineering Society Annual Conference, Nashville, TN. October 2003

C. C. Anamelechi (Presenter) and W.M. Reichert. Cellular Adhesion to Substrates as a Function of Shear Stress. Society for Biomaterials Conference, Reno, NV. April 2003

INVITED TALKS

C. C. Anamelechi (Presenter), L. Lee-Houghton, G.A. Truskey, and W.M. Reichert. Teflon-AF as a Model Tissue Culture Material for Studying Endothelial Cell Adhesion. Biomedical Engineering Society Conference. Baltimore, MD October 2005

C. C. Anamelechi (Presenter), G.A. Truskey, and W.M. Reichert. Mylar and Teflon-AF as Model Surfaces for Endothelial Cell Adhesion to Synthetic Vascular Grafts. Southeastern Regional Meeting of the American Chemical Society (SERMACS) Nov. 2004

C. C. Anamelechi. Cellular Adhesion on Model Vascular Substrates. Center for Biomolecular and Tissue Engineering (http://bte.egr.duke.edu) February 2004

PROFESSIONAL MEMBERSHIPS

American Chemical Society (2001-2008); Society for Biomaterials (2004-2008); Biomedical Engineering Society (2003-2008); Council for Entrepreneurial Development (2007-2008)